ALTERNATIVE PATHWAYS FOR PYROLYSIS OF CELLULOSE

Fred Shafizadeh

Department of Chemistry, University of Montana
Missoula, Montana 59812

INTRODUCTION

Pyrolysis of biomass involves heterogeneous substrates and complex reactions. The substrate may contain various amounts of cellulose, hemicelluloses, lignin, extractives and inorganics with different thermal properties. The reactions involve alternative pathways and consecutive series, which are affected by pyrolytic conditions including the time and temperature profile, ambient atmosphere and catalysis by inorganic materials. Consequently, composition, yield and rate of formation of the products are highly dependent on the employed substrate and pyrolytic condition. This situation accounts for variation of the results, particularly on kinetic studies, which may range from kinetics of specific chemical reactions to global kinetics or modeling of an entire process. The latter may be based on a rate determining chemical step or even a physical process such as heat or material transfer. Pyrolysis of cellulose illustrates these points. The alternative pathways proposed for pyrolysis of this material is shown below (1,2).

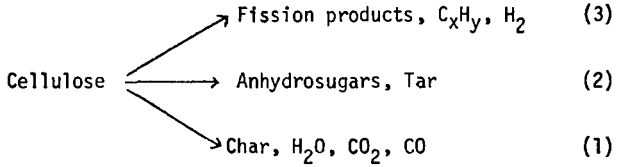

Pyrolysis at temperatures below 300°C involves depolymerization, dehydration, rearrangement and formation of carboxyl and carbonyl groups, evolution of CO and CO_2, development of free radicals and condensation to char. At temperatures above 300°C, these reactions are accompanied by the conversion of the glycosyl units to levoglucosan by transglycosylation. This reaction is preceded by the activation of the molecule, presumably through glass transition, which gives the required conformational flexibility. At still higher temperatures (above 500°C), the glycosyl structure of the levoglucosan or cellulose rapidly breaks down to provide a variety of low molecular weight fission products, including hydrocarbons and hydrogen as well as CO, CO_2 and H_2O obtained at lower temperatures. The pyrolysis products could further react to alter the composition of the pyrolysate. The secondary reaction may proceed in the gas phase as further decomposition of levoglucosan, in the solid phase as the condensation and crosslinking of intermediate chars to highly condensed polycyclic aromatic structures, or by interaction of both phases as gasification of char by reaction with H_2O and CO_2 at high temperatures to produce CO and H_2. In view of all these possibilities the kinetic data are valid only for specific chemical reactions or well defined systems. Generalization could be misleading and controversial, because of major differences in the results obtained under different conditions. These differences are shown in the following examples of pyrolysis of cellulose under different conditions.

KINETICS OF CELLULOSE PYROLYSIS

Global Kinetics

The global kinetics for isothermal evolution of volatile pyrolysis products from purified cotton linter cellulose, within the temperature range of 275-310°C, has been studied in air and nitrogen (3). The Arrhenius plot of the results on first order kinetics is shown in Figure 1. These data gave activation energies of 37 and 17 Kcal/mole in air and nitrogen. Figure 1 indicates a transition at ca. 300°C which reflects the existence of two different pathways. As seen in Figure 2, the rate of pyrolysis measured by weight loss under isothermal conditions, shows an initial period of acceleration and proceeds much faster in air than in inert atmosphere. As the pyrolysis temperature is increased, the initiation period and the differences between pyrolysis under nitrogen and air gradually diminish and disappear at 310°C when pyrolysis by the second pathway takes over.

Kinetics of the lower temperature pathway

The reactions in the first pathway, which dominates at lower temperatures, involve reduction in molecular weight or DP by bond scission, appearance of free radicals, elimination of water, formation of carbonyl, carboxyl and hydroperoxide groups (in air), evolution of carbon monoxide and carbon dioxide, and finally production of a charred residue. These reactions, which contribute to the overall rates of pyrolysis of cellulosic materials, have been individually investigated. Reduction in the degree of polymerization of cellulose on isothermal heating in air or nitrogen at a temperature within the range of 150-190°C has been measured by the viscosity method. The resulting data have been correlated with rates of bond scission and used for calculating the kinetic parameters. These calculations give an activation energy of 21 Kcal/mole for bond scission in air and 27 Kcal/mole in nitrogen, and indicate that at low temperatures a larger number of bonds are broken in air than in nitrogen.

The rates of production of carbon monoxide and carbon dioxide at 170°C are much faster in air than in nitrogen, and furthermore, accelerate on continued heating. It is instructive to compare the initial linear rates for the evolution of these gases with the rates of bond scission obtained for depolymerization at 170°C. As can be seen in Table I the rate of bond scission in air approximately equals the rate of production of carbon dioxide plus carbon monoxide in moles per glucose unit. In nitrogen, however, the rate of bond scission is greater than the rates of carbon monoxide and carbon dioxide evolution combined.

Table I. Initial rates of glycosidic bond scission and carbon monoxide and carbon dioxide formation at 170°C.

Reaction	Rate X 10^5 in N_2 mole/162 gm hr	Rate X 10^5 in air mole/162 gm hr
Bond Scission	2.7	9.0
CO Evolution	0.6	6.4
CO_2 Evolution	0.4	2.1

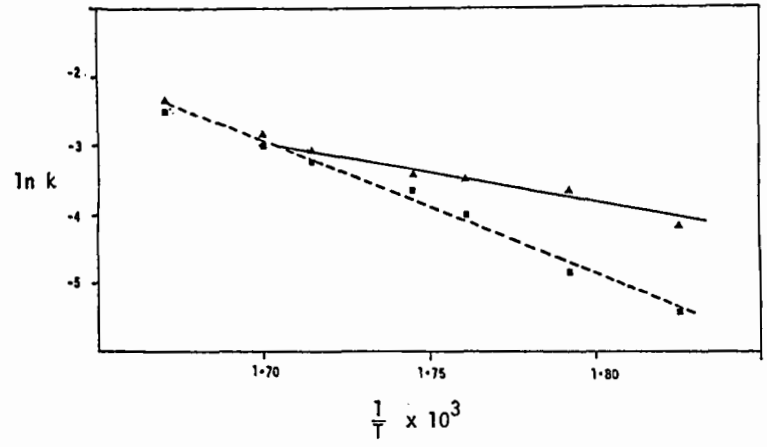

Figure 1. Arrhenius plots for first order reactions in the isothermal degradation of cellulose in air (--■--) and nitrogen (--△--).

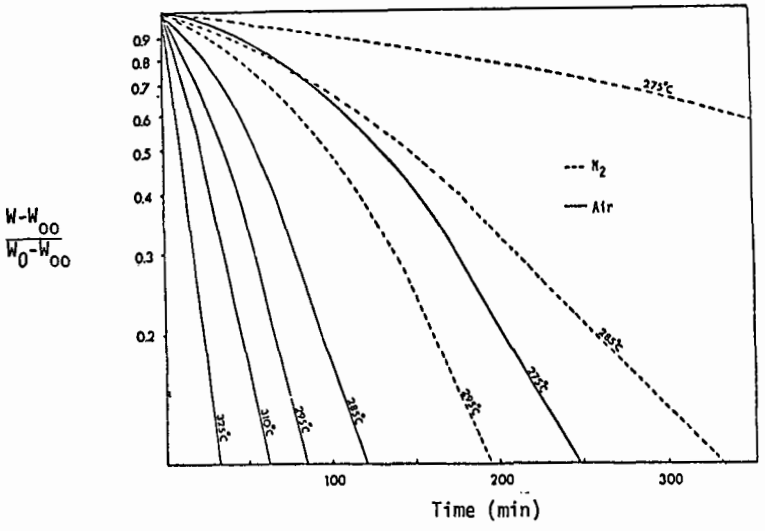

Figure 2. First order plot for the residual cellulose weight (normalized) versus time. Plots at 310°C and 325°C for air and nitrogen are similar.

On heating cellulose in air, hydroperoxide functions are simultaneously formed and decomposed, and their concentration climbs until a steady state is reached. At 170°C the steady state is reached in about 100 min. The decomposition of the hydroperoxide function appeared to follow first-order kinetics with a rate constant of $2.5 \cdot 10^{-2}$ min^{-1} at 170°C. From the steady-state concentration of $3.0 \cdot 10^{-5}$ mole/162 g min, the rate of hydroperoxide decomposition is therefore 7.5×10^{-7} mole/162 g min. When compared with the initial rate of bond scission in air at 170°C (Table I), it is apparent that hydroperoxide formation could make a significant contribution to bond scission.

Kinetics of the intermediate pathway

The primary reaction in this pathway involves depolymerization by transglycosylation forming a tar containing anhydrosugars (levoglucosan and its isomer), randomly linked oligosaccharides and various dehydration and fission products. As the reaction proceeds, the residue contains some glycosyl units that have been detected by CP/MAS ^{13}C-NMR and FTIR, and some char (4). The char is formed partly from direct decomposition of cellulose as discussed earlier and partly by decomposition of the tar. On raising the temperature the tar forming reactions accelerate rapidly and overshadow the production of char. At this time, it should be pointed out that evaporation of levoglucosan and the volatile pyrolysis products is highly endothermic. Thus, the increased oven temperature could raise the rate of heat transfer but not necessarily the temperature of the ablating substrate which is cooled by the heat of evaporation, especially under vacuum. In other words, at the higher temperatures, the pyrolysis process may be controlled by the rate of heat transfer rather than the kinetics of the chemical reaction. Material transport presents another major obstacle to the investigation of chemical kinetics, because if the products of primary reactions are not removed, they can undergo further decomposition reactions. Table II shows the difference between the yield of different pyrolysis products in vacuum, which removes the primary volatile products, and in nitrogen at atmospheric pressure which allows more decomposition of the anhydrosugars. It also shows the effect of inorganic catalysts in changing the nature of the reactions and products.

Table II. Analysis of the pyrolysis products of cellulose at 300°C under nitrogen and vacuum.

Condition	Atm. pressure	1.5 Mm Hg	1.5 Mm Hg, 5% $SbCl_3$
Char	34.2%[a]	17.8%[a]	25.8%[a]
Tar	19.1	55.8	32.5
levoglucosan	3.57	28.1	6.68
1,6-anhydro-β-D-glucofuranose	0.38	5.7	0.91
D-glucose	trace	trace	2.68
hydrolyzable materials	6.08	20.9	11.8

[a]The percentages are based on the original amount of cellulose.

In view of these considerations, the chemical kinetics of cellulose pyrolysis have been investigated within the limited temperature range of 260-340°C and under vacuum in order to obtain chemically meaningful data (5). Under these conditions, the chemical kinetics of cellulose pyrolysis could be represented by the three reaction model shown below.

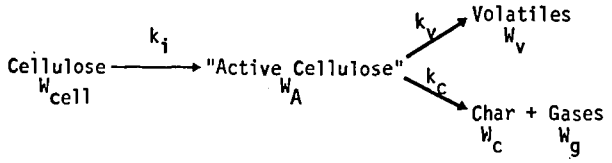

where

$$\frac{-d(W_{cell})}{dt} = k_i[W_{cell}]$$

$$\frac{d(W_A)}{dt} = k_i[W_{cell}] - (k_v + k_c)[W_A]$$

$$\frac{d(W_c)}{dt} = 0.35k_c[W_A]$$

$$k_i = 1.7 \times 10^{21} e^{-(58,000/RT)} \text{ min}^{-1}$$

$$k_v = 1.9 \times 10^{16} e^{-(47,300/RT)} \text{ min}^{-1}$$

$$k_c = 7.9 \times 10^{11} e^{-(36,000/RT)} \text{ min}^{-1}$$

In this model it is assumed that the initiation reactions discussed earlier lead to the formation of an active cellulose, which subsequently decomposes by two competitive first order reactions, one yielding anhydrosugars (transglycosylation products) and the other char and a gaseous fraction.

Partially pyrolyzed cellulose, in addition to the original sugar (glycosyl) units, contains new functionalities formed by dehydration, rearrangement, decarbonylation, decarboxylation and condensation. In the intermediate chars these functionalities include carbonyl, carboxyl, aromatic and aliphatic carbons as analyzed by CP/MAS ^{13}C-NMR (5). After complete pyrolysis of the glycosyl units (5 min at 400°C) a relatively "stable" char is left that contains about 70% aromatic and 27% aliphatic carbons. On heating at 500°C char is converted to a highly condensed and crosslinked material, containing about 90% polycyclic aromatic carbons.

CONCLUSION

Pyrolysis of cellulose proceeds by alternative pathways involving a variety of reactions which provide different products. The kinetics of these reactions are highly dependent on the experimental conditions.

ACKNOWLEDGMENTS

The author is pleased to acknowledge the contributions of Dr. A.G.W. Bradbury, and the support of the National Bureau of Standards and the National Science Foundation.

REFERENCES

1. F. Shafizadeh, Advan. in Carbohydr. Chem., 23, 419 (1968).

2. F. Shafizadeh, J. Anal. and Appl. Pyrol., 3, 283 (1982).

3. F. Shafizadeh and A.G.W. Bradbury, J. Appl. Polym. Sci., 23, 1431 (1979).

4. Y. Sekiguchi, J.S. Frye, and F. Shafizadeh, J. Appl. Polym. Sci., submitted for publication.

5. A.G.W. Bradbury, Y. Sakai, and F. Shafizadeh, J. Appl. Polym. Sci., 23, 3271 (1979).

KINETICS OF THERMAL DEGRADATION OF WOOD AND CELLULOSE BY T.G.A.

COMPARISON OF THE CALCULATION TECHNIQUES

C. VOVELLE, H. MELLOTTEE, J.L. DELFAU

C.N.R.S. - Centre de Recherches sur la Chimie de la Combustion
et des Hautes Températures
45045 ORLEANS CEDEX - FRANCE

INTRODUCTION :

Kinetics of thermal degradation of cellulosic materials has attracted widespread attention due to its importance in two main fields : synthetic fuel production from biomass and fire research. Usually, the results of kinetic studies have been expressed by means of an overall mass loss rate equation :

$$-\frac{dm}{dt} = A\,(m - m_f)^n \exp(-E/RT) \qquad 1)$$

with m = mass of material at time t, m_f = final mass, T = temperature, A = preexponential factor, n = reaction order, A = activation energy and R = perfect gas constant.

Several reviews (1), (2), (3) have pointed out that there is a great scatter in the values measured for the kinetic parameters : A, n and E. In particular, activation energies reported for wood are very often lower than those obtained for cellulose.

Recently (4), we have performed thermogravimetric analysis of cellulose and several kinds of woods and we have shown that this discrepancy was mainly related to the use of an overall equation to represent thermal degradation of wood. By calculating the mass variations by means of a simulation model allowing several reactions to be taken into account, we have reproduced with a good precision the experimental thermograms. For wood, in nitrogen, this agreement between experiments and calculations was obtained with a two-step degradation mechanism. The first step starts around 520 K and corresponds to the degradation of the mixture hemicellulose + lignin. The second step is observed around 620 K and is due to the pyrolysis of cellulose.

It is highly interesting to notice that for this second step of wood pyrolysis, the values of the kinetic parameters obtained with pure cellulose could be used.

The methods usually proposed for determining kinetic parameters from thermogravimetric analysis curves are based on the assumption that the mass loss rate can be interpreted by means of an overall equation. In view of the results that we obtained for wood, it was interesting to study how these methods could be applied to a two-step degradation mechanism and compare the precision of the results obtained with different methods. In this paper, we have reported kinetic calculations performed with the most commonly used techniques : FREEMAN and CARROLL (5), maximum point (6), ratio method (7), COATS and REDFERN (8) and BROIDO (9). These calculation techniques have been applied to thermograms measured for pure cellulose and three kinds of woods : fir, poplar and oak, the experiments having been performed under nitrogen.

EXPERIMENTAL :

A SETARAM thermobalance has been used. This apparatus allows simultaneous

TGA and DTA measurements. It is worth specifying that due to DTA requirements, the thermocouple used to measure the sample temperature was surrounded by the platinum sample holder, so that there is a good coupling between temperature measured by the thermocouple and the sample temperature.

A nitrogen flow rate equals to 120 ml/min has been used, and the heating were respectively : 16.2°C/min (cellulose), 12.9°C/min (oak), 13.0°C/min (fir) and 23.2°C/min (poplar). All the experiments have been performed with initial mass close to 25 mg.

Mass and temperature versus time curves were digitized by means of a H.P. plotter. Transformation and smoothing of the data to mass versus temperature curves and derivative calculations were performed by a H.P. 1000 computer.

RESULTS AND DISCUSSION :

We have plotted on figure 1 the thermograms obtained with cellulose and the three kinds of woods. Usually, from these curves, a conversion factor is defined by :

$$Y = \frac{m_o - m}{m_o - m_f} \qquad 2)$$

with : m = mass remaining at time t, m_o = initial mass and m_f = final mass.

The overall kinetic equation is expressed in term of this conversion factor :

$$\frac{dY}{dt} = A\,(1 - Y)^n \exp(-E/RT) \qquad 3)$$

or by using the heating rate : $\beta = dT/dt$

$$\frac{dY}{dT} = \frac{A}{\beta}\,(1 - Y)^n \exp(-E/RT) \qquad 4)$$

To use this equation for wood, it is necessary to define a conversion factor specific to each step of the degradation mechanism. If the step s is assumed to be observed between an initial value of the mass : $(m_o)_s$ and a final value $(m_f)_s$, this conversion factor is defined by :

$$Y_s = \frac{(m_o)_s - m}{(m_o)_s - (m_f)_s} \qquad 5)$$

These boundary values play an important role, since the variation of Y_s over a given temperature range can be modified by changing the values used for $(m_o)_s$ and $(m_f)_s$ and it can be considered that five kinetic parameters are needed to specify the thermal degradation : A, n, E, $(m_o)_s$ and $(m_f)_s$.

In order to get starting values for these boundary values of the mass, we have used the results obtained in the previous study carried out with the simulation model (4). These results have been reported in table I. When performing these calculations, the following assumptions had been made :

- wood is composed in equal proportion of cellulose and a so called "second component"
- for each component, several reactions can be observed, each reaction occurring between an initial value α_o and a final value α_f of the mass ratio $\alpha = m_k/(m_o)_k$ with m_k = mass of component k at time t and $(m_o)_k$ = initial mass of component k.

From the values reported in table I, it can be seen that the first step in the thermal degradation of wood, starting around 520K corresponds to the pyrolysis of the so-called second component, the pyrolysis of cellulose being responsible

for the second step observed at higher temperature. In fact, these two steps are not really successive and a progressive replacement of the first one by the second is rather observed. Owing to this overlapping, it seemed preferable to not use the intermediate part of the thermograms and in the following we have considered that:

- At the beginning of the first step, only the pyrolysis of the second component is observed. Assuming that this component represents 50% of the initial mass of wood and with the values of a_f reported in table I, the boundary values for the first step are equal to m_o and .7 m_o.

- Kinetic parameters of the second step can be calculated accurately only when the pyrolysis of the other component is achieved, so that the initial value of the mass is .7 m_o, while, from the values of a_f it is found that the final value is close to .33 m_o.

In fact , these values have been allowed to vary slightly in order to optimize the results.

In the following we have described the results obtained by applying successively the different methods.

FREEMAN and CARROLL method :

By taking the logarithm of both sides of equation 4 and differentiating with respect to temperature, the following expression is obtained :

$$\frac{d \log (d Y/dT)}{d \log (1 - Y)} = n - \frac{E}{2.3\ R} \frac{d (1/T)}{d \log (1-Y)} \qquad 6)$$

By plotting the left hand side versus $\frac{d (1/T)}{d \log (1-Y)}$ a straight line must be obtained, with a slope equals to E/2.3 R and an intercept equals to n. The preexponential factor A is calculated thereafter by means of equation 4.

To illustrate the precision which can be expected when using this method, we have plotted the results obtained respectively for the first step and the second step of fir pyrolysis on figures 2 and 3. It can be seen on figure 2 that the points corresponding to the lowest values of $d(1/T)/d \log(1 -Y)$ tends to be outside of the straight line, this deviation being due to the beginning of the occurrence of the second step. However, on the main temperature range of each step, the linear relationship is fairly well verified.

The values obtained for the second step of wood pyrolysis and for cellulose pyrolysis (table II) are in good agreement with the values that we calculated previously with the simulation model (table I). For the first step, on the other hand, the activation energies obtained for fir and oak are slightly higher than those calculated previously and some discrepancies are observed in the values of the order of reaction.

It is mainly interesting to notice that these calculations confirm that the kinetic parameters of the second step of wood pyrolysis keep the value obtained with pure cellulose.

A second remark can be done concerning the method of calculation. Due to the properties of logarithms and derivatives, the results are independent of the value chosen for $(m_o)_s$ and only $(m_f)_s$ is playing a rôle. For the second step of wood pyrolysis, the value of $(m_f)_s$ can be known with accuracy since it corresponds to the final value of the mass observed on the thermogram. Therefore, for the second step, the determination of the kinetic parameters by means of this method is not affected by errors resulting of a wrong estimation of the initial value of the mass.

Maximum point method :

From equation 4, the following relationship is obtained between the values

of the parameters corresponding to the maximum conversion rate :

$$E = n \frac{R\ T_m^2}{(1-Y_m)} \left(\frac{dY}{dT}\right)_m \qquad 7)$$

where T_m, Y_m and $(dY/dT)_m$ represent respectively the values of the temperature, the conversion factor and the derivative of the conversion factor at the point where the conversion rate is maximum.

The order of reaction is calculated by using one of the following expressions :

$$n = (1 - Y_m)^{(1-n)} \quad \text{if} \quad n \neq 1 \qquad 8)$$

$$n = 1 \text{ if } (1- Y_m) = 1/e \qquad 9)$$

with e = basis of neperien logarithm.

The preexponential factor is calculated from equation 4.

This method cannot be applied to the first step of wood pyrolysis, since, due to the overlapping with the second step, there is no maximum in the conversion rate vs temperature curve.

The values obtained for cellulose and the second step of wood pyrolysis are reported in table III.

It can be observed that the kinetic parameters determined for wood are still very close to those calculated for pure cellulose.

However, in addition to its limitation concerning the treatment of the first step of wood pyrolysis, this method suffers a second disadvantage related to its accuracy. A small error in the estimation of the temperature corresponding to the maximum conversion rate entrains a large variation in the values of Y_m . This is illustrated by the following values measured for fir :

T K	635	636	637
$(dY/dT)\ K^{-1}$	$2.77\ 10^{-2}$	$2.85\ 10^{-2}$	$2.82\ 10^{-2}$
Y_m	.612	.644	.672

Moreover, this method is directly dependent on the values chosen for $(m_o)_s$ and $(m_f)_s$ and it can be seen that if the values of n, A and E obtained for poplar are close to the values calculated with the other methods, the value used for $(m_o)_s$ seems abnormally elevated.

Ratio method :

This method has been formulated by MICHELSON and EINHORN (7). If equation 4 is written for two values of the temperature T_i and T_j, the following expression can be derived :

$$\log \frac{(dY/dT)_j}{(dY/dT)_i} = n \log \frac{(1- Y_j)}{(1- Y_i)} + \frac{E}{2.3\ R} \frac{T_j - T_i}{T_i\ T_j} \qquad 10)$$

where the subscripts i and j mean that the quantities have been measured at temperatures T_i and T_j.

If this calculation is repeated for couples of temperature such that the ratio $r = (1-Y_j)/(1-Y_i)$ remains constant, the plot of the left hand side versus $T_j - T_i/T_i\ T_j$ must be a straight line of slope equal to E/2.3 R. The order of reaction is calculated from the value of the intercept.

Values obtained by applying this method (table IV) are in close agreement with those determined with the FREEMAN and CARROLL method for pure cellulose as well as for the two steps of wood pyrolysis.

It is important to notice that the rôle played by the boundary values $(m_o)_s$ and $(m_f)_s$ in the calculation of the conversion factor is reduced to a minimum when to ratio method is used. Calculation of the order of reaction involves only $(m_f)_s$ while, for the activation energy, the values are totally independent of $(m_o)_s$ and $(m_f)_s$ since these two quantities vanish when the left hand side of equation 10 is calculated. This method is therefore particularly convenient for the kinetics of wood pyrolysis, especially for the first step, where, due to the relatively small value of the difference $(m_o)_s - (m_f)_s$, the conversion factor is very sensitive to a small change in the value estimated for $(m_f)_s$.

COATS and REDFERN method :

Equation 4 cannot be integrated directly. However, using an approximation for the integral of the exponential term several expressions can be derived. COATS and REDFERN (8) have obtained :

$$\log \left[\frac{-\log (1-Y)}{T^2}\right] = \log \frac{AR}{\beta E}\left[1 - \frac{2RT}{E}\right] - \frac{E}{2.3\ RT} \quad \text{if } n = 1 \qquad 11)$$

$$\text{and} \quad \log \left[\frac{1-(1-Y)^{(1-n)}}{T^2\ (1-n)}\right] = \log \frac{AR}{\beta E}\left[1 - \frac{2RT}{E}\right] - \frac{E}{2.3\ RT} \quad \text{if } n \neq 1 \qquad 12)$$

The first term in the right hand side is sensibly constant in the temperature range used in the calculations so that a plot of the left hand side of one of the two equations versus 1/T must be a straight line of slope $- E/2.3\ R$. The order of reaction is not calculated directly. In fact, the calculations have to be performed using several values of n in order to retain the value leading to the best linear relationship.

Values calculated with this method are reported in table V.

It can be observed that the values obtained for the activation energy of the second step of wood pyrolysis tend to be lower than the values calculated for pure cellulose. With poplar, it has been necessary to increase the ratio $(m_o)_2 / m_o$ up to .82 in order to obtain a straight line. This value is abnormally elevated even if it lead to satisfactorily results with the maximum point method.

BROIDO method :

Using a different assumption for performing the integration of equation 4, BROIDO derived the following expression, valid only for a first order reaction

$$\log \left(\log \frac{1}{1-Y}\right) = - \frac{E}{2.3\ RT} + \text{constant} \qquad 13)$$

In view of the results obtained with the other methods for the order of reaction, it has not been possible to apply the BROIDO method to both steps of wood pyrolysis (table VI).

This method and the COATS-REDFERN method, often called integral methods are very sensitive to the values chosen for $(m_o)_s$ and $(m_f)_s$ when calculating the conversion factor. This is illustrated by the three curves corresponding to different values of $(m_o)_s$ for the second step of fir pyrolysis (figure 4).

CONCLUSION :

An examination of the results obtained for cellulose pyrolysis in nitrogen

shows that the five techniques of kinetic calculations lead to results very similar : the mass loss rate can be interpreted in term of one reaction of first order of activation energy close to 250 kJ/mole.

For wood pyrolysis, we have distinguished two steps in the thermograms. By calculating a specific conversion factor for each step it has been possible to apply the same calculation techniques. However, calculation of this specific conversion factor introduces an error related to the estimation of the mass range over which each step is observed. Owing to this fact, the accuracy of the different calculation techniques is directly related to the degree at which the boundary values $(m_o)_s$ and $(m_f)_s$ are involved. From this point of view, the FREEMAN and CARROLL method and the ratio method are the most suitable. It is interesting to notice that these two techniques have confirmed that kinetic parameters of the second step of wood pyrolysis, corresponding to the maximum mass loss rate, have the same values than those obtained for pure cellulose.

REFERENCES :

1 - ROBERTS, A.F., Comb. and Flame 14, 261-272 (1970)

2 - WELKER, J.R., J. Fire Flammability 1, (1970), 12.

3 - ANTAL, M.J., FRIEDMAN, H.L., ROGERS, F.E., Comb. Sci. and Technol. (1980), Vol. 24, 141-152.

4 - VOVELLE, C., MELLOTTEE, H., and DELBOURGO, R., Nineteenth Symposium (International) on Combustion, The Combustion Institute, to be published

5 - FREEMAN, E.S., and CARROLL, B., J. Phys. Chem. 62, (1958), 394.

6 - FUOSS, R.M., SALVER, I.O., and WILSON, H.S., J. Polym. Sci. A2, (1964), 3147.

7 - MICHELSON, R.W., and EINHORN, I.N., Thermochimica Acta, 1, (1970), 147-158.

8 - COATS, A.W., and REDFERN, J.P., Nature, Vol. 201, (1964), 68-69.

9 - BROIDO, A., J. Polymer Sci.,7,(1969) p. 1761.

Fig. 1 : Thermograms obtained in nitrogen (120 ml/min)

——— cellulose (16.2°C/min)

▪▪▪▪▪▪▪▪ fir (13.0°C/min)

▪—▪—▪— poplar (23.2°C/min)

—▪—▪— oak (12.9°C/min)

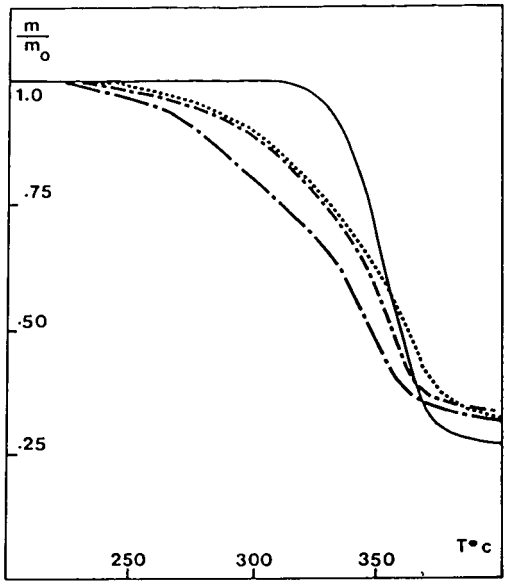

Fig. 2 : FREEMAN and CARROLL method.
First step of fir thermal degradation

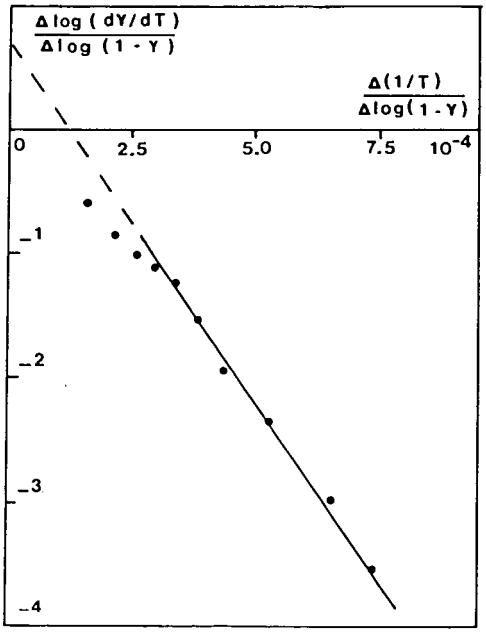

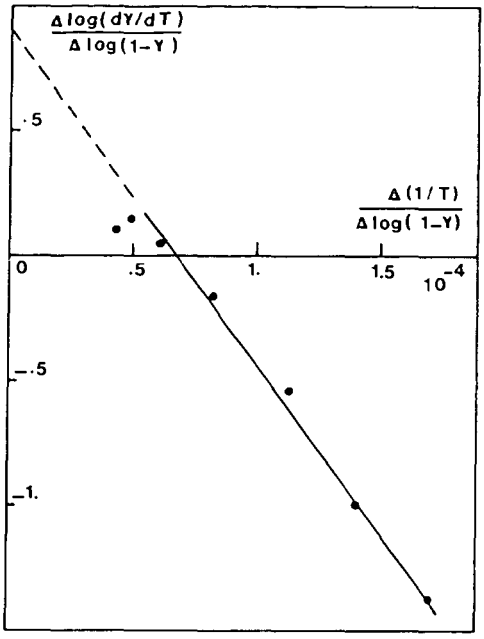

Fig. 3 : FREEMAN and CARROLL method.
Second step of fir thermal degradation

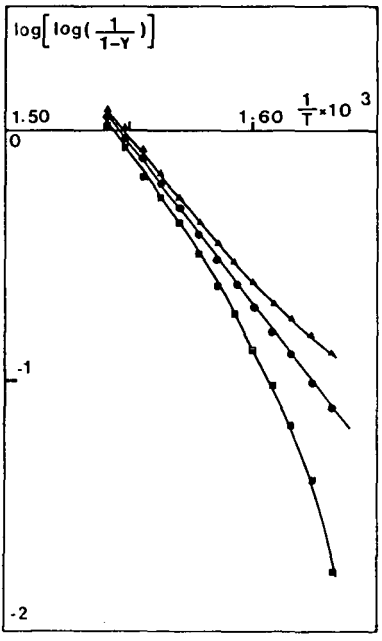

Fig. 4 : BROIDO method.
Second step of fir thermal degradation

▲ $\frac{(m_o)_2}{m_o} = .7$

● $\frac{(m_o)_2}{m_o} = .75$

■ $\frac{(m_o)_2}{m_o} = .8$

material		n	$A(s^{-1})$	E(kJ/mole)	α_o	α_f
cellulose		1	$1.\ 10^{19}$	250	1	.29
fir	50% cellulose	1	$4.\ 10^{18}$	250	1	.27
	50% 2nd component	1	$1.3\ 10^{5}$	84	1	.40
oak	50% cellulose	1	$1.4\ 10^{19}$	250	1	.27
	50% 2nd component	1	$2.6\ 10^{5}$	84	1	.40
poplar	50% cellulose	1	$1.5\ 10^{19}$	250	1	.30
	50% 2nd component	1	$2.2\ 10^{5}$	84	1	.40

Table I : kinetic parameters obtained in a previous study (4) by means of a simulation model

material		n	$A(s^{-1})$	E(kJ/mole)	$\frac{(m_o)_s}{m_o}$	$\frac{(m_f)_s}{m_o}$
cellulose		1.1	$1.\ 10^{18}$	238	1	.26
fir	1st step	.7	$3.4\ 10^{7}$	109	1	.75
	2nd step	.9	$1.4\ 10^{19}$	257	.75	.33
oak	1st step	1	$1.5\ 10^{7}$	100	1	.73
	2nd step	1.4	$3.\ 10^{19}$	253	.73	.33
poplar	1st step	.25	$4.3\ 10^{4}$	76	1	.71
	2nd step	1.1	$3.9\ 10^{19}$	255	.71	.34

Table II : kinetic parameters calculated with the FREEMAN and CARROLL method

material	$1-Y_m$	T_m (K)	n	$A\ (s^{-1})$	E (kJ/mole)	$\frac{(m_o)_s}{m_o}$	$\frac{(m_f)_s}{m_o}$
cellulose	.368	630	1	$2.3\ 10^{18}$	243	1	.26
fir	.356	636	.93	$5.8\ 10^{18}$	252	.75	.33
oak	.430	619	1.4	$6.5\ 10^{20}$	269	.73	.33
poplar	.380	626	1.07	$7.7\ 10^{17}$	234	.82	.34

Table III : kinetic parameters calculated with the maximum point method

material		r	n	A (s^{-1})	E (kJ/mole)	$\frac{(m_f)_s}{m_o}$
cellulose		1.5	1.1	$2.9\ 10^{17}$	232	.26
fir	1st step	1.2	.7	$5.2\ 10^{7}$	111	.75
	2nd step	2	.91	$4.6\ 10^{18}$	250	.33
oak	1st step	1.2	.99	$1.5\ 10^{7}$	100	.73
	2nd step	2	1.3	$1.1\ 10^{19}$	248	.33
poplar	1st step	1.25	.3	$2.\ 10^{4}$	72	.71
	2nd step	2	1.12	$1.7\ 10^{18}$	238	.34

Table IV : kinetic parameters calculated with the ratio method

material		n	A (s^{-1})	E (kJ/mole)	$\frac{(m_o)_s}{m_o}$	$\frac{(m_f)_s}{m_o}$
cellulose		1.1	$1.1\ 10^{20}$	263	1	.26
fir	1st step	.7	$9.9\ 10^{6}$	104	1	.75
	2nd step	1	$6.3\ 10^{17}$	239	.75	.33
oak	1st step	1	$5.9\ 10^{7}$	106	1	.73
	2nd step	1.4	$1.\ 10^{16}$	211	.79	.33
poplar	1st step	.3	$1.8\ 10^{5}$	83	1	.71
	2nd step	1	$3.\ 10^{15}$	205	.82	.34

Table V : kinetic parameters calculated with the COATS-REDFERN method

material		n	A (s^{-1})	E (kJ/mole)	$\frac{(m_o)_s}{m_o}$	$\frac{(m_f)_s}{m_o}$
cellulose		1	$5.\ 10^{19}$	259	1	.26
fir	2nd step	1	$9.1\ 10^{18}$	254	.75	.33
oak	1st step	1	$5.5\ 10^{8}$	117	1	.73
poplar	2nd step	1	$4.8\ 10^{16}$	220	.82	.34

Table VI: kinetic parameters calculated with the BROIDO method

The Effect of Pressure on the Pyrolysis of Newsprint

Ravindra K. Agrawal and Richard J. McCluskey

Department of Chemical Engineering, Clarkson College, Potsdam, New York 13676

Introduction

There is national concern over the disposal of solid municipal waste. Several pyrolysis plants designed to convert such waste into useful products have proven uneconomical. To help provide a stronger data base for improved pyrolysis processes, we have been studying the thermal chemistry of newsprint, the principle cellulosic material in urban waste. Previously, we have reported on the rate of degradation at low pressure, where secondary reactions of pyrolysis products are negligible (1). This paper discusses the influence of ambient pressure on newsprint pyrolysed at 340°C.

Since a dilute acid wash pre-treatment has been shown to significantly alter product yields from newsprint pyrolysis (2), we have examined both untreated and 1% HCl washed newsprint.

Pyrolysis of any lignocellulosic material gives a host of different products which are usually classified as either chars, tars, or gases depending upon their volatility. Chars are carbonaceous products, such as charcoal, that are not volatile. Tars are relatively high molecular weight compounds that are volatile only at pyrolysis temperatures; and gases are those products having readily measureable vapor pressures at room temperature.

Several investigators have shown, using a variety of cellulosic materials, ranging from cotton cellulose to wood, that pyrolysis in nitrogen at atmospheric pressure results in lower tar yields and greater gas and char formation than pyrolysis in a strong vacuum (3 , 4). This difference in yields has been interpreted as due to secondary decomposition of tar molecules whose ability to escape from the reacting substrate is reduced at higher pressures. While the effect of ambient pressure on pyrolysis yields is qualitatively understood, there exists little quantitative information that allows mathematical modeling of this phenomena and, thereby, a clear link between low pressure pyrolysis experiments, used to study fundamental reaction kinetics, and industrial pyrolysis processes carried out at atmospheric pressure.

Experimental Procedures

A sketch of our experimental apparatus is shown in Figure 1. Since a detailed account of our procedures is provided in reference (1), only a brief outline will be given here.

100 mg samples of dry, shredded newsprint are weighed into a small aluminum foil boat. The boat is sealed into a cool end of the reactor and a vacuum is drawn on the system. If we are examining the effects of ambient pressure, nitrogen is bled slowly into the system. Then the pyrolysis chamber is brought to a temperature slightly above that of pyrolysis. Next, power is reduced to that necessary for maintaining pyrolysis temperature and the sample boat is quickly brought to the center of the pyrolysis zone by means of a hand held magnet. Sample temperature is continuously monitored by a thermocouple embedded in the newsprint.

After a set time period, the boat is quickly withdrawn from the pyrolysis chamber, the cold traps are sealed off, and the reactor is allowed to cool.

The weight of residue in the sample boat is measured, and the tar products are rinsed off the cool glass walls of the reactor's side arms into tared vials. In this manner we can measure the weights of residue and tar as a function of pyrolysis time and pressure.

Theory

Our basic assumptions are that secondary decomposition of tar molecules is negligible in pyrolysis experiments below one torr, and that, ΔW_t, the difference between W_t, the weight of tar obtained below one torr, and W_t', the weight of tar formed at higher pressure, is a direct measure of the amount of secondary reaction.

A tar molecule may undergo two types of secondary reactions, decomposition to char and gases and repolymerization with the substrate. If each type of reaction is homogeneous and first order in tar, the rate of secondary reaction is

$$\frac{d\,\Delta W_t}{dt} = (k_d + k_r)\, W_t'' \qquad 1)$$

where k_d and k_r are the rate constants for decomposition and repolymerization, respectively, and W_t'' is the weight of tar molecules within the heated newsprint.

Diffusion coefficients in low pressure gases are inversely proportional to pressure. Therefore, if the tars rate of escape from the newsprint is taken as proportional to the amount of tar in the newsprint and inversely proportional to pressure, then

$$\frac{d\,W_t'}{dt} = \frac{\alpha}{P}\, W_t'' \qquad 2)$$

where α is the escape rate per unit weight per unit pressure.

If k_d, k_r and α are independent of time, then the ratio of equations 1 and 2 implies that for any time interval during which the amount of repolymerized tar is unimportant relative to the amount of unreacted newsprint

$$\frac{\Delta W_t}{W_t'} = \frac{(k_d + k_r)}{\alpha}\, P \qquad 3)$$

Similarly, when reaction of repolymerized tar is unimportant, the fractional conversion to char via secondary decomposition may be expressed

$$\frac{\Delta R}{\Delta W_t} = \frac{f_d k_d + k_r}{k_d + k_r} \qquad 4)$$

For longer pyrolysis times, when the fate of repolymerized tar molecules must be considered

$$\frac{\Delta R}{\Delta W_t} = \frac{f_d k_d + f_r k_r}{k_d + k_r} \qquad 5)$$

where ΔR is the difference in the weight of residue (char) between higher and very low pressure pyrolyses, f_d is the weight fraction of any tar molecule undergoing secondary decomposition that becomes char, and f_r is the average weight of char resulting from repolymerization of one tar molecule. If the repolymerization reaction disrupts the tar molecule's ring structure, the repolymerized compound may be predisposed to form char and gases.

An interesting parameter to consider is the ratio of the amount of tar escaping from the substrate during any given time interval at higher pressure to the amount of tar formed in the same time interval at very low pressure. If all repolymerized material eventually decomposes to char and gases, then this ratio is

$$\frac{W_t'}{W_t} = \frac{\alpha/P}{(\alpha/P) + k_d + k_r} \qquad 6)$$

If a repolymerized tar molecule can be regenerated, then this ratio will be larger than the value predicted by equation 6. However, should the breakdown to char of the repolymerized material induce or catalyze substrate conversion to char, then the W_t'/W_t ratio will be less than predicted by equation 6 .

Results

The influence of ambient pressure on pyrolysis yields is illustrated in Figure 2. The weight of tar products and the weight of sample residue is plotted versus time, comparing 700 torr and below one torr pyrolyses of 100 mg of acid washed newsprint at 340°C. The ultimate tar yield at 700 torr is 34 % less than at very low pressure, while the final weight of residue (char) is 32 % greater at 700 torr. Notice that at both pressures there is an initial rapid generation of tar.

In our previous paper we noted that the thermal degradation of newsprint occurs in two stages: a fast initial degradation, that can be modeled as a zeroth order reaction; and a subsequent, slower degradation that is first order in remaining newsprint. At 340°C, the rapid, early degradation is over within three minutes of the sample's entry into the pyrolysis zone. This initial reaction accounts for 68 % of the ultimate tar production. As seen in Figure 2, the remaining 32 % of the tar is produced largely during the next sixty minutes of pyrolysis, while the degradation reaction follows a first order rate law.

Table 2 gives data describing the secondary decomposition during the first three minutes of pyrolysis. The fractional extent of secondary tar decomposition and $\Delta R/\Delta W_t$ are listed for both acid washed and untreated newsprint. For each substrate, the extent of secondary decomposition increases uniformly with ambient pressure. The change in the sample residue is nearly a constant fraction of the change in weight of recovered tar. $\Delta R/\Delta W_t$ is not a function of ambient pressure.

The ratio of the amount of secondary reaction to the amount of recovered tar is plotted versus pressure in Figure 3, for the initial degradation of both acid washed and untreated newsprint. As predicted by equation 3 , the data are well fit by a straight line passing through the origin. Linear least square fits to the data that are constrained to pass through the origin are included in Figure 3. The slopes of these lines are reported in Table 1 along with their 95% confidence limits. From equation (3), these slopes represent the ratio of the rate of secondary tar reaction to the rate of tar escape per unit pressure. The larger value obtained for the acid washed newsprint suggests that the tars produced from acid washed newsprint are more reactive than the tars arising from untreated newsprint.

As seen from equation 4 , the magnitude of the $\Delta R/\Delta W_t$ ratio depends on two factors, f_d, the fractional char yield during secondary decomposition, and k_d/k_r, the ratio of the rate of decomposition to the rate of repolymerization.

If we arbitrarily adopt a value for f_d of 0.2, the ultimate char yield in low pressure pyrolyses, then the k_d/k_r ratios implied by the R/W_t results are 7.0 and 0.6 for the acid washed and untreated newsprint, respectively. The point is that, irrespective of the f_d value, the repolymerization reactions are relatively more important in the untreated than in the acid washed newsprint.

Insight into the types of secondary reactions that occur at longer pyrolysis times can be gathered from the data in Table 2. At longer times the amount of repolymerized material will no longer be small in regard to the amount of remaining substrate. The ultimate $\Delta R/\Delta W_t$ ratios are given in Table 2 for both acid washed and untreated substrates. These ratios show no pressure dependence, but they are slightly higher than the corresponding ratios at the end of only three minutes pyrolysis time. This suggests that char forming reactions are more prevalent at longer pyrolysis times.

Table 2 also lists the ratio of the amount of tar recovered in higher pressure experiments to the amount of tar formed in low pressure pyrolyses for pyrolysis times greater than three minutes. Also included in Table 2 is the value predicted for this ratio by equation 6 , based on the assumption that all repolymerized material eventually forms either char or gases. Agreement between the experimental and predicted quantities is poor only for the lowest pressures, where the measured values fall below those given by equation 6 . This implies some ability of the repolymerized material to catalyze char formation in the substrate, although the effect is subtle and readily masked at higher loadings of repolymerized tar.

Summary

We have developed a simple model, based upon homogeneous first order reactions, for describing the influence of ambient pressure on newsprint pyrolysis. Values for the relative rates of secondary tar reaction to tar escape per unit pressure have been obtained for acid washed and untreated newsprint. Tars from the acid washed material are more apt to decompose while tars from untreated newsprint have a greater likelihood of repolymerizing and then catalyzing char formation.

References

1. R.K. Agrawal and R.J. McCluskey, J. Appl. Poly. Sci., 27, 367 (1983).
2. F. Shafizadeh, R.H. Furneaux, T.G. Cochran, J.P.Scholl and Y. Sakai, J. Appl. Poly. Sci., 23, 3525 (1979).
3. A. Roberts, Combust. Flame, 14, 261 (1970).
4. F. Shafizadeh, T.G. Cochran and Y. Sakai, AIChE Symp. Ser. No. 184, 75, 24 (1979).

Table 1 - Early Secondary Decomposition Reactions

Pressure (torr)	Acid Washed Newsprint $\frac{\Delta W_t}{W_t\ 3min}$	Acid Washed Newsprint $\frac{\Delta R}{\Delta W_t\ 3min}$	Untreated Newsprint $\frac{\Delta W_t}{W_t\ 3\ min}$	Untreated Newsprint $\frac{\Delta R}{\Delta W_t\ 3\ min}$
100	.072	.33	.026	.80
175	.13	.30	.036	.64
400	.27	.28	.11	.73
700	.35	.29	.18	.73
$\frac{k_d + k_r}{\chi}$ (torr^{-1})	$8.15 \pm .33 \times 10^{-4}$		$3.07 \pm .07 \times 10^{-4}$	

Table 2 - Longer Time Secondary Reaction Data

Pressure (torr)	$\frac{\Delta R}{\Delta W_{t'\infty}}$	$\frac{W_{t'\infty} - W_{t'3}}{W_{t\infty} - W_{t3}}$	$\frac{\chi/P}{\frac{\chi}{P} + k_d + k_r}$	
100	.37	.75	.93	Acid Washed Newsprint
400	.36	.77	.75	
700	.40	.69	.64	
175	.76	.90	.95	Untreated Newsprint
400	.81	.88	.89	
700	.84	.82	.82	

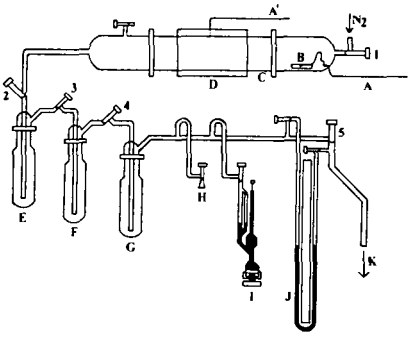

Fig. 1. Experimental apparatus: (A,A') thermocouple wires; (B) sample boat; (C) Pyrex cylinder; (D) insulated, quartz pyrolysis zone; (E, F, G) cold traps; (H) sample port; (I) McLeod gauge; (J) manometer; (K) connection to vacuum pump; (1-5) PTFE valves.

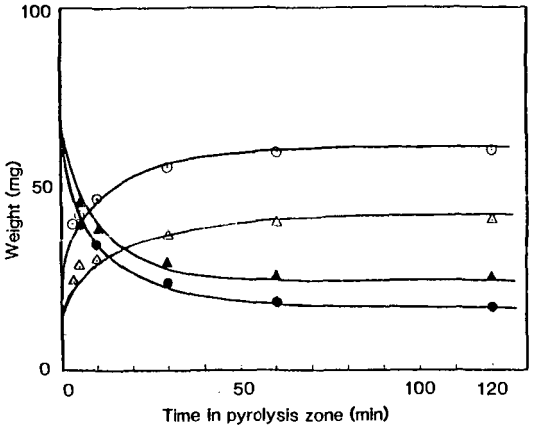

Fig 2. Influence of ambient pressure on pyrolysis yields at 340 C. Open figures represent tars and solids represent residue. Pressures are 1 torr (○) and 700 torr (△).

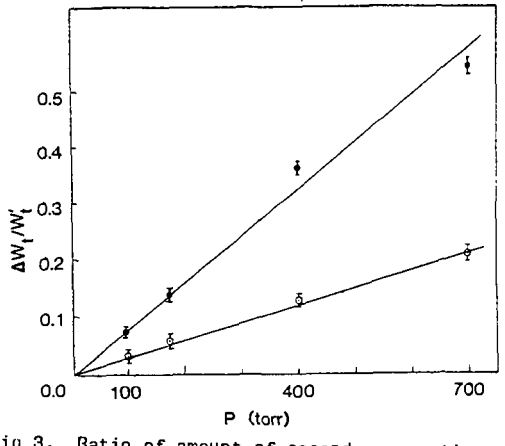

Fig 3. Ratio of amount of secondary reaction to the amount of recovered tars versus pressure. Open figures represent unwashed newsprint and solids represent 1% HCl washed newsprint.

LIGNIN PYROLYSIS IN HEATED GRID APPARATUS: EXPERIMENT AND THEORY

Eitan Avni and Robert W. Coughlin

University of Connecticut, Storrs, CT 06268

Peter R. Solomon and Hsiang Hui King

Advanced Fuel Research, Inc., 87 Church Street, East Hartford, CT 06108

Introduction

The study of lignin pyrolysis has a vitsl importance since all lignin conversion processes, namely; combustion, liquefaction and gasification, are initiated by this step. Lignin, a major component of biomass is a potential source of aromatic chemicals through the pyrolysis process. Important recent reviews of lignin conversion processes have been published by Goldstein (1), Drew (2), Goheen (3) and Coughlin and Avni, et.al., (4).

Very few kinetic studies of lignin pyrolysis have been carried out recently. Gavsiss, et.al., (5) studied the pyrolysis of Kraft lignin using the captive sample technique. At 400-650°C for 10-120 sec, he claimed that a fundamental kinetic description of lignin pyrolysis was not possible at the time. Klein (6) modeled lignin pyrolysis based on its model components and compared his simulations to previously published data (7). In a recent study by Avni, et.al., (8-9), the pyrolysis behavior of Iotech lignin was studied at different ambient pressures and heating rates.

This paper considers the application of a recently developed pyrolysis model of coal pyrolysis (10-12) applied to a heated grid as well as an entrained flow reactor, to the pyrolysis of lignin. Flash pyrolysis as well as slow heating rate pyrolysis was carried out in a heated grid (13), in which on-line, in-situ gas and tar analysis is performed by Fourier Transform Infrared (FT-IR) Spectroscopy. The model has proved to be successful in simulating the results of vacuum flash pyrolysis and slow heating rate pyrolysis for a variety of lignins.

Experimental

Lignin Samples

Seven lignins were used in the study; Table 1 compares the different lignins and their sources. Four of them were received from manufacturers while the last three were extracted in our laboratory. Table 2 shows the elemental composition and methoxy content of the lignins. All lignin samples were dried for 48 hours at 108°C under vacuum before the experiments.

Flash Pyrolysis Experiments

The flash pyrolysis apparatus is illustrated in Fig. 1. It consists of a heated grid pyrolyzer located in the center of a large gas cell with KBr windows to allow FT-IR (Nicolet) analysis (13). The lignin is evenly distributed between two layers of stainless-steel or tungsten screen which is electrically heated. Lignin temperatures of 1800°C and heating rates in excess of 10,000°C/sec for the highest temperatures can be achieved using a tungsten screen. When flash pyrolysis is performed in vacuum, the tar molecules quickly escape the grid and land on the cold glass.

Evolution kinetics for gaseous species are determined with the FT-IR which permits low resolution spectra (8 wavenumbers) to be taken at 80 msec intervals. The low resolution analysis can determine CO, CO_2, H_2O, CH_4, SO_2, CS_2, C_2H_2, C_2H_4, C_3H_6, benzene, and heavy paraffins and olefins. The time-temperature evolution for

each species can be determined from such scans as indicated in Fig. 2 which shows the CO yield as a function of time at several temperatures.

The distribution of major products is determined by weighing the lignin, the char (which remains on the screen) and the tar (which accumulates on a glass tube surrounding the grid) and by quantitative analysis of 0.5 wavenumber, FT-IR spectra of the evolved gas taken at the completion of a run. The high resolution spectra can quantitatively determine all of the above species plus C_2H_6, C_3H_8, C_4H_8, NH_3 and potentially many other species which have not yet been observed. Calibration of the FT-IR was made using pure gases or prepared gas mixtures. Analysis of the solids was performed with the FT-IR and by elemental analysis.

Constant Heating Rate Experiment

Slow constant heating rate experiments with evolved gas analysis by Mass Spectrometry (MS) or Gas Chromatography (GC) has been used by several investigators to study coal (14-17). Gas analysis by FT-IR, as used in the experiments here, offers advantages over GC in speed and over MS in the ability to identify heavy tar materials.

Constant heating rate experiments were performed for lignin using the apparatus shown in Fig. 1. The sample is heated at a constant rate (30°C/min) while gas evolution is monitored by FT-IR. The pyrolysis gas is swept from the cell with a constant flow of nitrogen (700 ml/min) at a presaure of 1 atm.

Pyrolysis Model

The pyrolysis model assumes a lignin structure constisting of substituted phenyl-propane subunits linked by C-O and C-C bonds. During thermal decomposition the relatively weak bonds break, releasing the tar which is comprised of monomers, dimers and trimers of phenyl-propane subunits. The FT-IR spectra of the lignin tar show a remarkable similarity to the parent lignin. Figure 3a-c shows such a comparison. Such similarity has also been observed for pyrolysis of coals and model polymers.

A pyrolysis model should simulate the evolution of tar fragments and competitive cracking of substituted groups and ring clusters to form the light molecular species of the gas. The yield of each gas species should depends on the functional group distribution in the original lignin. At low temperatures there is very little rearrangement of the lignin polymer but there is decomposition of the substituted groups and aliphatic structures resulting in CO_2 release from the carbonyl, H_2O from hydroxyl, hydrocarbon gases from aliphatic and methoxy groups, and CO from weakly bound oxygen groups such as aldehyde groups. At high temperatures there is breaking and rearrangement of the aromatic rings. Late in the pyrolysis, the rearrangment of the lignin subunits permits H_2 to be evolved from the aromatic hydrogen. Additional CO form tightly bound oxygen functionalities. As this process continues the char becomes more graphitic. At high temperatures the FT-IR spectra of lignin char and coal char are remarkably similar, (see Figure 3d) both are highly aromatic. A striking feature of thermal decomposition which was observed for a variety of coals and lignins in the heated grid experiments is that the temperature dependent evolution rate of CO_2 and CO are similar for all lignins and coals while the evolution rates of H_2O, CH_4, paraffins and tar from lignin vary slightly from coal, due to the different bridges between the ring clusters. The rate of evolution of a specie will depend on the nature of the functional group which is its source but appears relatively insensitive to lignin source or extraction processes. The insenitivity of kinetic rates to coal rank has been reported in other investigations (14,18-21).

The mathematical description of the pyrolysis used here has been presented previously (10-12). The model considers the removal of functional groups by a parallel independent evolution of the light species in competition with the tar evolution.

To model these two competing paths with one path yielding a product which is similar in composition to the parent coal, the dry, ash-free (DAF) coal or lignin is

represented as a rectangular area. As shown in Fig. 4a, the Y dimension is divided according to the chemical composition of the coal or lignin. Y°_i represents the initial fraction of a particular component (carboxyl, aromatic hydrogen, etc) and the sum of the Y°_i's equals 1. The evolution of each component into the gas (carbonxyl into CO_2, aromatic hydrogen into H_2, etc) is represented by the first order diminishing of the Y_i dimension, $Y_i = Y^\circ_i \exp(-k_i t)$. The X dimension is divided into a potential tar forming fraction X° and a non-tar forming fraction $1-X^\circ$. The evolution of the tar is represented by the first order diminishing of the X dimension $X = X^\circ \exp(-k_t t)$.

Figure 4-a shows the initial state of the coal. Values for Y° are obtained from elemental and FT-IR analysis and from the heated grid pyrolysis experiments (10,12,22). The value of X° is at present a parameter of the model. It is controlled by the oxygen and aliphatic or hydroaromatic hydrogen content of the lignin and can be influenced by pressure, particle size, bed geometry and the transport properties of the pyrolysis medium.

Figure 4-b shows the initial stage of thermal decomposition during which the volatile components, H_2O, CO-loose and CO_2, evolve from the hydroxyl, ether-loose and carboxyl groups, respectively, along with aliphatics and tar. At a later stage (Fig. 4-c) CO-tight and H_2 are evolved from the ether-tight and aromatic hydrogen. Figure 4-d shows the final state of the char, tar and gas.

Table 3 presents the kinetic rates used in the model and the functional group composition of Iotech Aspen lignin. A distributed activation energy is used for species evolution kinetics. Such models were used by Pitt (23) and by Anthony, et.al. (24) for describing coal weight loss. Weimer and Nagan (14) employed Anthony's model to describe individual species evolution. This model was used in the present study.

Results and Discussion

Figure 5 shows the evolution rates of the major gas species and tar from Iotech lignin at a constant heating rate pyrolysis of 30°C/min. The simulations of the evolution rates, using the parameters in Table 3 agree well with the experimental results. As was mentioned previously, the kinetic rates of CO and CO_2 are similar for coal and lignin. The experimental CO evolution rates (Fig. 6) of several lignins indicate a high temperature tight-CO and show the insensitivity of the evolution rate to the lignin source or the extraction processes used.

The methane evolution rate suggests a tightly and loosely bound precursor. The loose methane is probably from the methoxy group of the phenylpropane subunit. The methoxy content of Iotech lignin is 17.01 weight percent, much higher then any coal methoxy content. Figure 8 compares the experimental evolution rate of methane from Iotech lignin and Pittsburgh Seam coal, the only difference between the two is the loose methane in the lignin. The similarity between the two can be explained in light of the similar FT-IR spectra (see Fig. 3-d) of lignin char and coal char at 500°C and higher temperatures. In both cases the char is highly aromatic relative to the starting materials. The relative ratio of the area under the aliphatic peaks near 2900 cm^{-1} to the aromatic peaks near 800^{-1} decreased drastically in the lignin char at 500°C compared to the ratio in the lignin. In both coal and lignin the residual oxygen appears to be predominantly ether type oxygen. Figure 7 compared the methane evolution rate of several lignins, again the rate is insensitive to the lignin source and extraction process. The ratio of the loose methane to tight methane peaks is changing from one lignin to another. The ratio seems to increase with an increase in the methoxy content of the lignin (see Table 2 for methoxy content).

The predicted tar evolution rate is in excellent agreement with the experimental data. The activation energy used for the simulations of tar evolution (48 kcal/mole $\pm$ 1500 cal/mole) is in a very good agreement with the estimated activation energy of the ether linkage (48 kcal/mole) connecting the phenylypropane subunits. The activation energies have been calculated using the group additivity theory of S. W. Benson (25,26). The DTGA of Iotech lignin confirms the location and shape of the tar rate curve on the temperature scale. The differences in the tar rates between

coal and lignin are due to the weak ether linkages that exist in the lignin between the polymer subunits; such weak linkages do not exist in coal.

Figure 9 shows the gas yield versus pyrolysis time in a flash pyrolysis. The major gas species evolved were CO, CO_2, H_2O and paraffins, at a final static temperature of 500°C for 80 seconds. The simulations of the gas species obtained with the parameters in Table 3 are in good agreemet with the data presented within the experimental errors. The methane evolution in the slow heating rate experiments shows a higher fraction of tight-methane than is observed in the flash pyrolysis. There is no such indication with the rest of the gas species.

Yield of CO versus pyrolysis time in a flash pyrolysis at different temperatures of flash pyrolysis are shown in Fig. 2 where it is evident that the agreeement between theory and experiment is good.

Conclusions

The experiments have shown that lignin pyrolysis kinetics are insensitive to lignin source or extracting process. Theory and experiment agree well for both slow and fast heating rates, using the given model parameters. The lignin parameters of the model are related to the functional group composition of the lignin.

References

1. Goldstein, I.S., Applied Polymer Symposium, 28, 256-267, (1975).
2. Drew, S., AIChE Symposium Series, 181,, Vol. 79, pp. 21-25, (1978).
3. Goheen, D.W., Chapter in Organic Chemicals from Biomass, Ed. by Goldstein, I.S. CRC Press, (1981).
4. Coughlin, R.W., Avni, E. and Sundstrom, D.W., Conversion of Lignin to Useful Chemical Products, Chap., Ed. by Wise, D.L. CRC Press, (1983).
5. Gavalas, G.R., et.al., Ind. Eng. Chem. Prod. Res. Dev., 18, (2), 127, (1979).
6. Klein, M.T. and Kirk, R.S., Preprint, Div. of Fuel Chem., ACS, (1981).
7. Klein, M.T., Sc.D. Thesis, Dept. Chem. Eng.,M.I.T., Cambridge, MA (1981).
8. Avni, E., Devoudzadeh, F. and Coughlin, R.W., International Conference, Fundamentals of Thermochemical Biomass Conversion, October, (1982).
9. Avni, E. and Coughlin, R.W., Presented at AIChE Meeting, Los Angeles, Nov. (1982).
10. Solomon, P.R. and Colket, M.B., 17th Symposium (International) in Combustion, The Combustion Institute, Pittsburgh, PA pp. 131-143, (1979).
11. Solomon, P.R., Prepr., Div. of Fuel Chem., ACS, 2, 24, 179-184, (1979).
12. Solomon, P.R., Fuel 60, 3, (1981).
13. Solomon, P.R., Hamblen, D.G. and Carangelo, R.M., Coal Pyrolysis, AIChE Symposium on Coal Pyrolysis, Nov. (1981).
14. Weimer, R.F. and Nagan, D.Y., ACS Div. of Fuel, Chem. Prepr., 24, (3),
15. Juntgen, H. and van Heek, K.H., Fuel Processing Technology, 2, 261,
16. Fitzgerald, D. and van Krevelen, D.W., Fuel, 38, 17, (1959).
17. Campbell, J.H., Fuel, 57, 217, (1978).
18. Tyler, R.J., Fuel, 59, 218, (1980).
19. Freihaut, J.D., Solomon, P.R. and Seery, D.J., ACS Division of Fuel Chemistry Preprints, 25, Sept. (1980).
20. Suuberg, E.M., Peters, W.A. and Howard, J.B., Ind. Eng. Chem. Process. Des. Devel., 17, 37, (1978).
21. Solomon, P.R. and Hamblen, D.G., Coal Gasification Reactions wtih On-Line In-Situ FT-IR Analysis, 1st Quaterly Report, DOE Contract #DE-AC21-FE05122.
22. Solomon, P.R., Preprints, Div. of Fuel Chem., ACS, 24, 3, 1514, (1979).
23. Pitt, G.J., Fuel, 41, 267, (1962).
24. Anthony, D.B., Howard, J.B., Meissner, H.P. and Hottel, H.G., 15th Symposium (International) on Combustion, p 1303, Aug. 25-31, (1975).
25. Benson, S.W. and Oneal, H.E., Kinetic Data on Gas Phase Unimolecular Reactions, NSRDS-NBS, 21, (1970).
26. Benson, S.W., Thermochemical Kinetics, Wiley, NY, (1978).

TABLE 1

LIGNIN SOURCE

Lignin	Wood	Manufacturer	Pretreatment
Iotech	Aspen	Iotech Corp.	steam explosion
Stake	Aspen	Stake Tech. Ltd.	autohydrolysis
BEC	Aspen	Biological Energy Corp.	---
Indulin	Pine	Westvaco	---
Ethanol	Aspen	b	[a] steam explosion
HCl	Aspen	c	[a] steam explosion
H_2SO_4	Aspen	d	[a] steam explosion

a) The Aspen wood was steam-exploded by Iotech Corp. and extracted in our laboratory.

b) 25 g of wood is mixed with 250 g of 43 Wt% ethanol in water mixture at pH 6. The reaction is carried out in autoclave at 185°C for 1 hour.

c) 25 g of wood was stirred for 4 hours with 500 g conc. HCl at room temperature. After 20 hours water is added and the mixture is filtered and washed with soda solution.

d) 25 g of wood is treated with 250 ml of 72% H_2SO_4 and stirred at room temperature for 2 hours, 2 volumes of water is added and the mixture is filtered. The lignin is reflex for 1 hour in 125 ml 3% H_2SO_4.

TABLE 2

ELEMENTAL COMPOSITION AND METHOXY CONTENT OF LIGNINS

Lignin	Iotech	Indulin	BEC	Stake	Ethanol	HCl	H_2SO_4
C	63.44	64.35	66.84	60.61	65.57	52.33	61.54
H	5.87	5.71	6.09	5.31	5.76	5.75	5.14
O	29.94	27.69	27.04	33.39	28.37	40.08	31.83
S	-	1.3	-	-	-	-	0.5
Mineral	0.75	0.95	0.03	0.69	0.30	0.56	0.99
Methoxyl	17.01	13.95	19.32	12.58	17.41	6.93	10.99

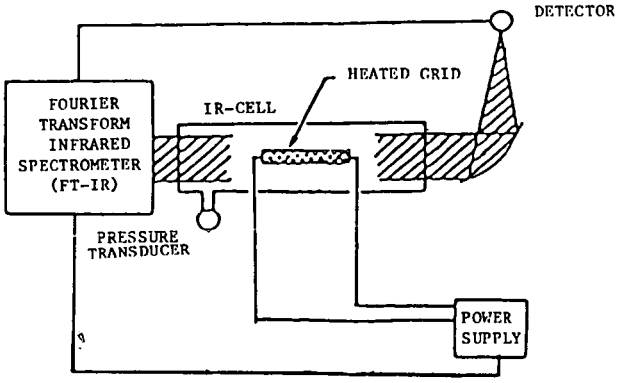

Figure 1. Pyrolysis Apparatus.

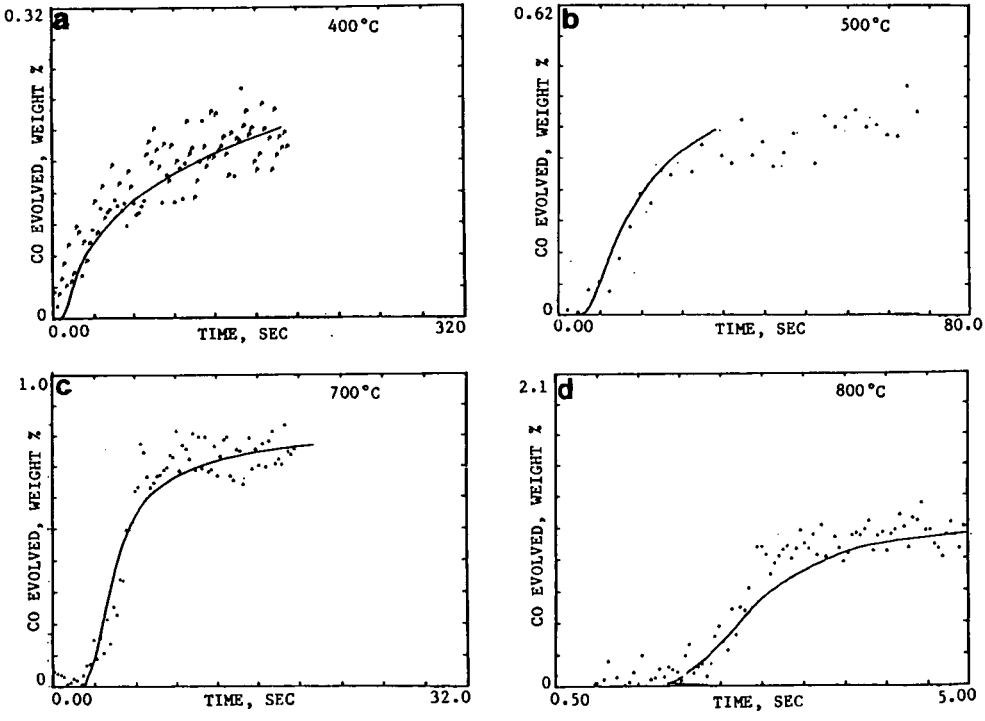

Figure 2. CO Yield from Iotech Lignin at Different Temperatures of Flash Pyrolysis, (points) experiment and (solid line) simulation.

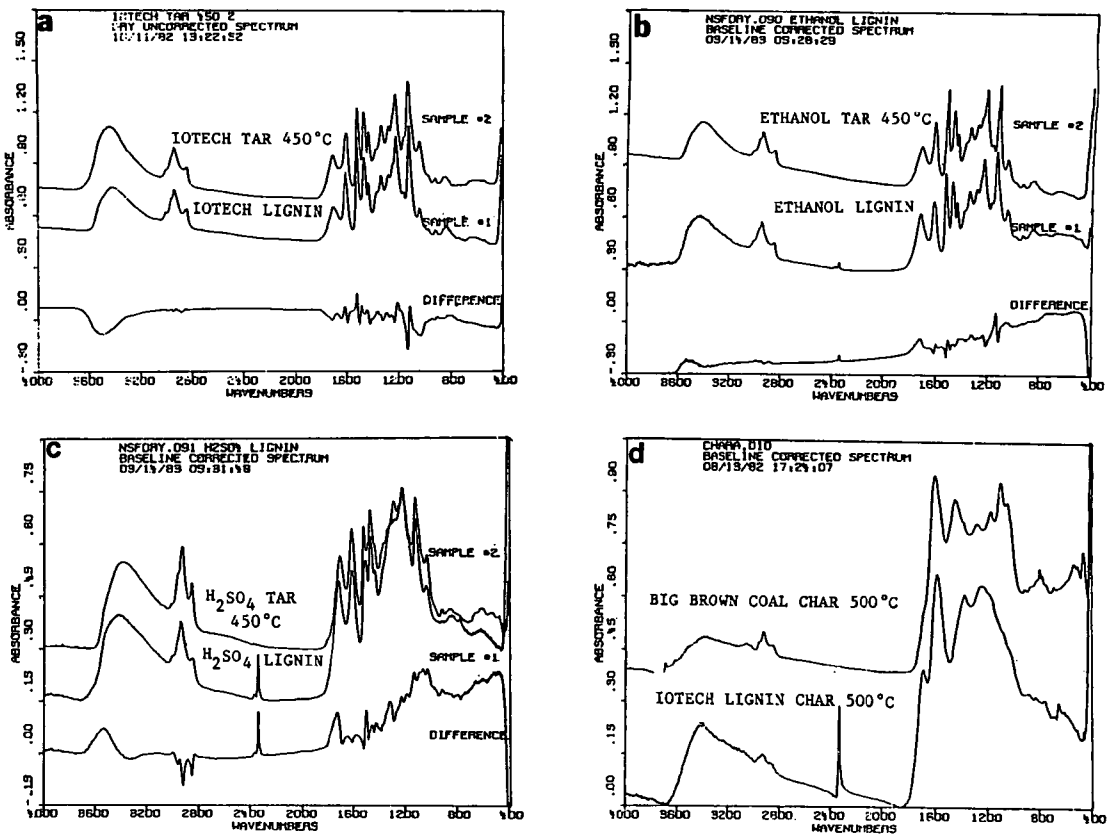

Figure 3. Infrared Spectra showing Comparison of Lignin and Tar as well as Coal Char and Lignin Char.

TABLE 3

Kinetic Rates and Functional Group Compositions

Composition Parameter		Iotech Lignin (WTX DAF)	Kinetic Rate Constants (sec^{-1})
	C	0.634	
	H	0.059	
	N	0.000	
	S(organic)	0.000	
	O	0.307	
		1.000	
Y^o_1	CO_2 - Extra-loose	0.0068	k_1 = 0.10E+15 exp((23900. ± 2500.)/T)
Y^o_2	CO_2 - Loose	0.0036	k_2 = 0.10E+15 exp((27900. ± 1400.)/T)
Y^o_3	CO_2 - Tight	0.0026	k_3 = 0.10E+15 exp((32900. ± 3300.)/T)
Y^o_4	H_2O	0.0654	k_4 = 0.10E+14 exp((23000. ± 2000.)/T)
Y^o_5	CO - Ether Loose	0.0300	k_5 = 0.17E+12 exp((25000. ± 2500.)/T)
Y^o_6	CO - Ether Tight	0.3889	k_6 = 0.10E+16 exp((54900. ± 5000.)/T)
Y^o_7	HCN - Loose	0.0000	k_7 = 0.54E+04 exp((8850. ± 0.)/T)
Y^o_8	HCN - Tight	0.0000	k_8 = 0.70E+08 exp((32000. ± 0.)/T)
Y^o_9	NH_3	0.0000	k_9 = 0.12E+13 exp((27300. ± 2400.)/T)
Y^o_{10}	CH_x-Aliphatic	0.0942	k_{10} = 0.17E+15 exp((30000. ± 1500.)/T)
Y^o_{11}	Methane-loose	0.0049	k_{11} = 0.50E+16 exp((30000. ± 1500.)/T)
Y^o_{12}	Methane-tight	0.0100	k_{12} = 0.20E+14 exp((30000. ± 3000.)/T)
Y^o_{13}	H-Aromatic	0.0130	k_{13} = 0.16E+08 exp((23000. ± 2300.)/T)
Y^o_{14}	C-Non Volatile	0.3804	k_{14} = 0
Y^o_{15}	S-Organic	0.0000	
	Total	1.0000	
X^o	Tar	0.6200	K_T = 0.10E+15 exp((24000. ± 1500.)/T)

Cracking Rates:

Paraffins - Olefins k_{OL} = 0.15E+12 exp((27600.)/T)

Olefin - Acetylene k_{AC} = 0.21E+08 exp((22000.)/T)

*Distributed rates have not yet been determined.

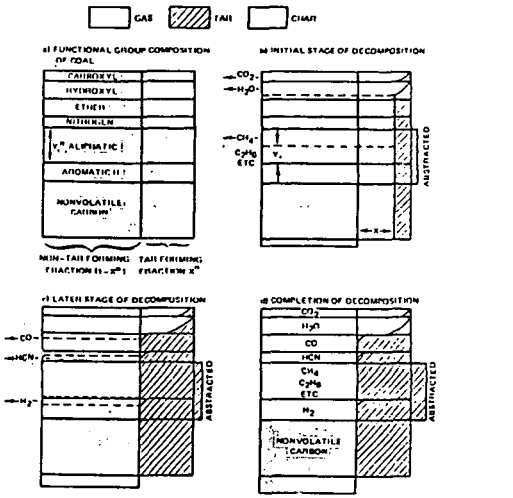

Figure 4. Progress of Thermal Decomposition According to Model. a) Functional Group Composition of Lignin, b) Initial State of Decomposition, c) Later Stage of Decomposition, d) Completion of Decomposition.

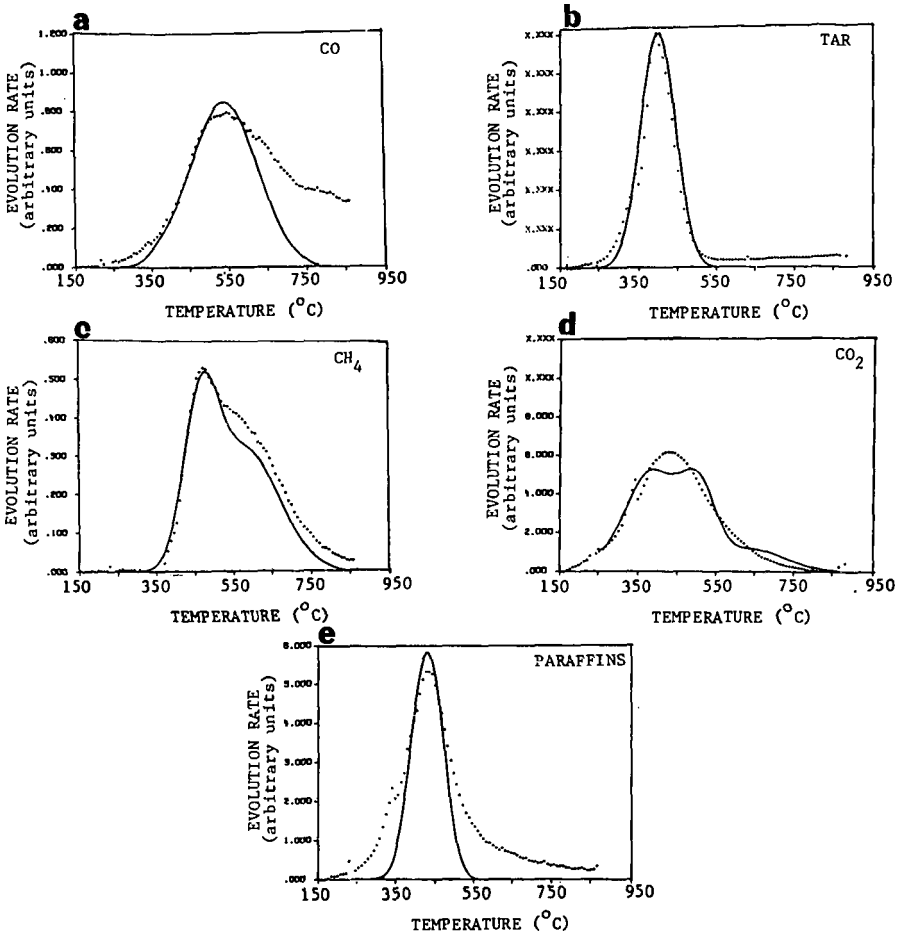

Figure 5. Evolution Rate of Major Volatile Species from Iotech Lignin in a Heating Rate of 30°C/min, Experiment (points) and Simulations (solid line).

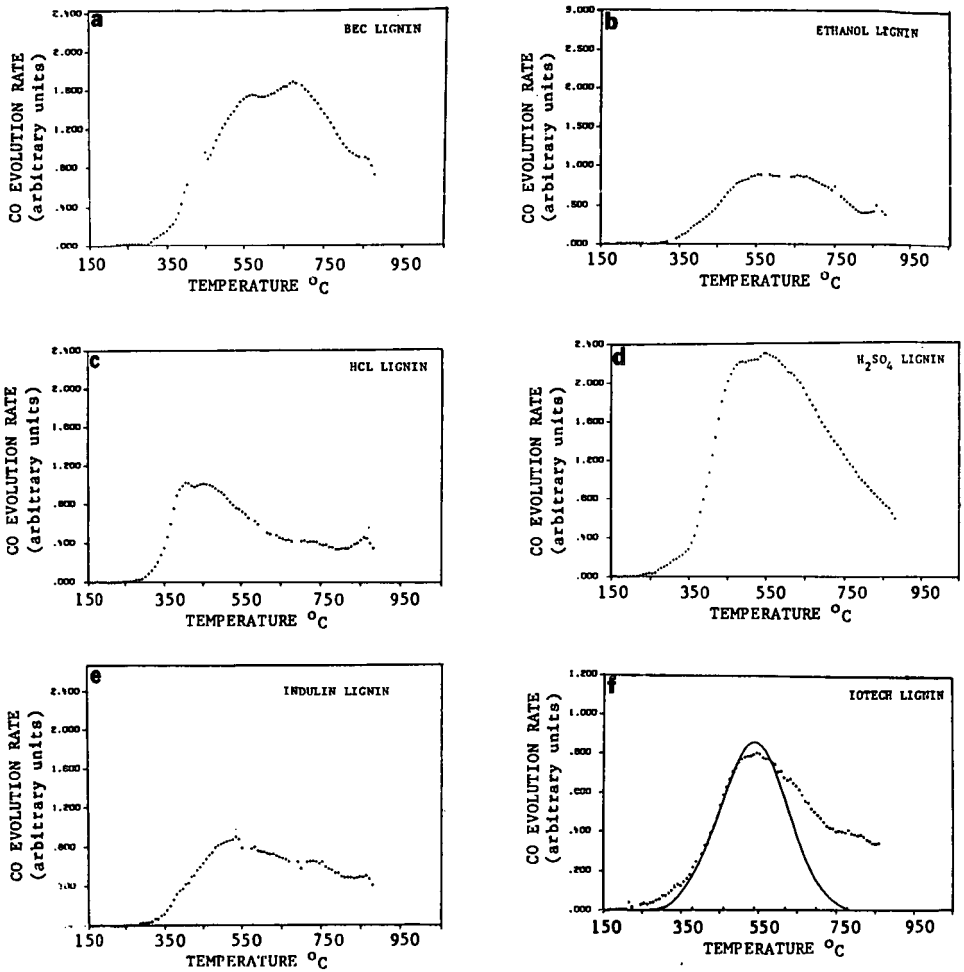

Figure 6. Evolution Rate of CO from Different Lignins at a Heating Rate of 30°C/min, experiment (points) and simulation (solid line).

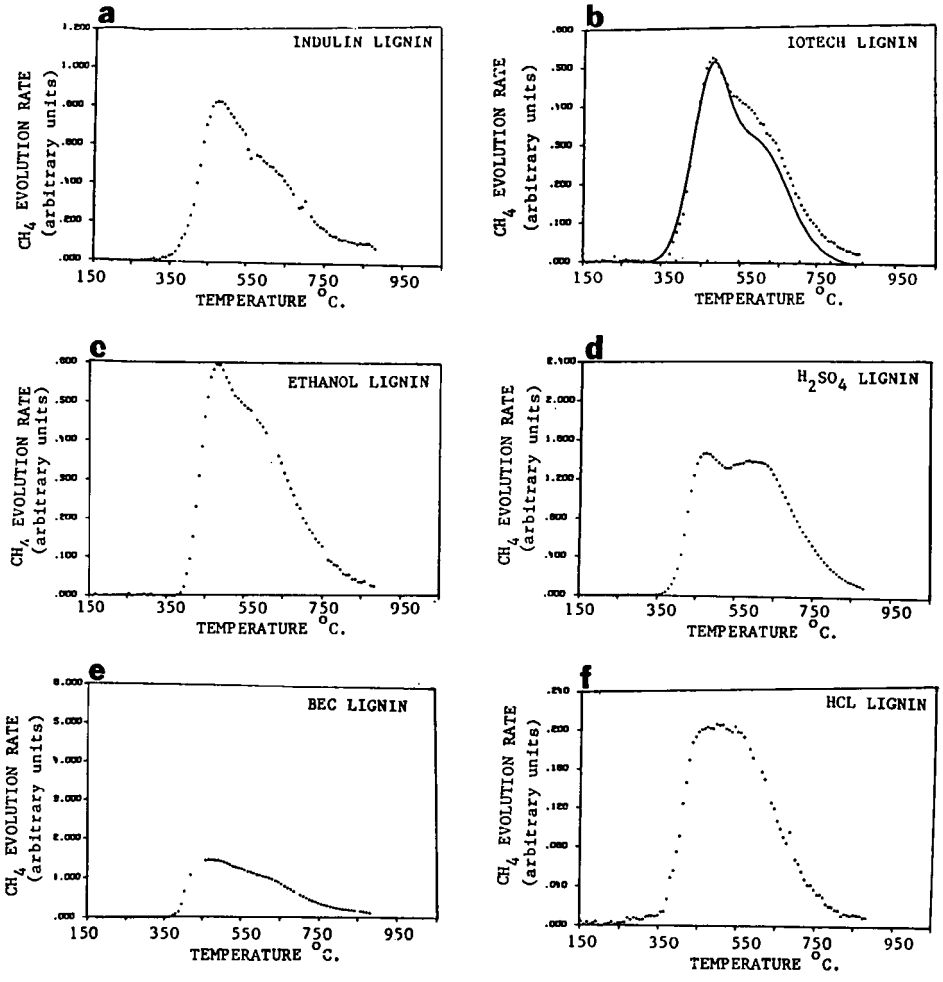

Figure 7. Evolution Rate of Methane from Different Lignins at a Heating Rate of 30°C/min.

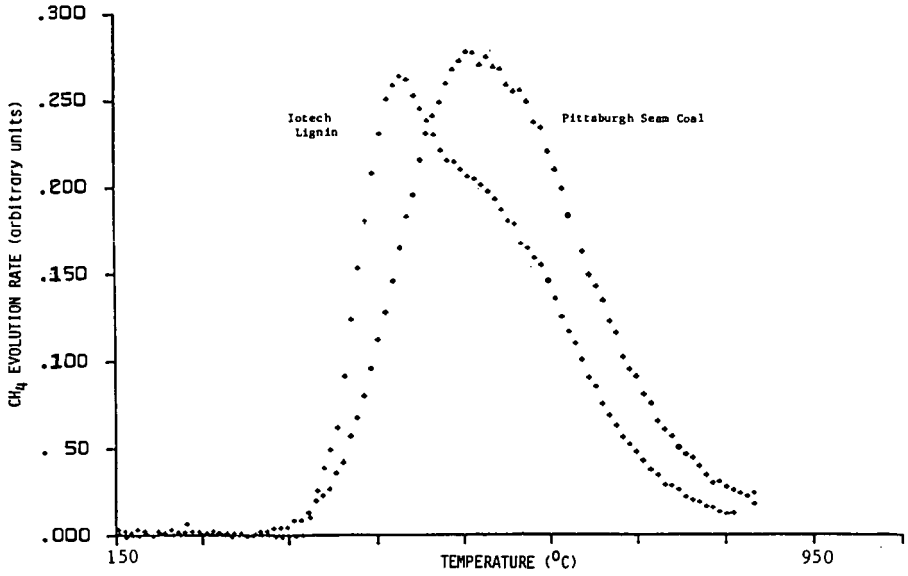

Figure 8. Evolution Rate of Methane from Pittsburgh Seam Coal and Lignin at a Heating Rate of 30°C/min.

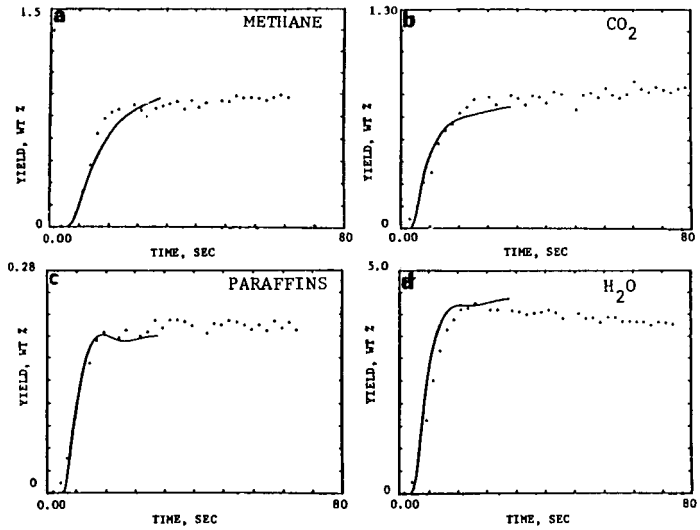

Figure 9. Major Gas Species Versus Time in a Flash Pyrolysis at 500°C, experiment (points) and simulation (solid line).

MODELING TAR COMPOSITION IN LIGNIN PYROLYSIS*

Hsiang-Hui King and Peter R. Solomon

Advanced Fuel Research, 87 Church Street, East Hartford, CT 06108

Eitan Avni and Robert W. Coughlin

University of Connecticut, Storrs, CT 06268

Lignin is an integral constituent in all vascular plants and an important alternative source of fuel and chemical feedstock. Pyrolysis depends strongly on the properties of the substrate and is the initial step in any thermal process. A better understanding of lignin pyrolysis, just as in the case of coal, is essential for developing lignin conversion processes.

Lignin can be viewed as a coploymer consisting of phenylpropane units linked together by carbon-carbon and carbon-oxygen bonds (1). A depolymerization model has been developed recently to predict tar yield and composition for the pyrolysis of model homopolymers which simulate individual structural features of coal (2). In this paper, the depolymerization model is expanded to predict the pyrolysis behavior of a copolymer comprising up to seven different and randomly distributed monomers and applied to simulate the pyrolysis of an Aspen lignin. The effects of pyrolysis temperature and pressure on tar yield are examined. More importantly, this model predicts the molecular weight distributions for pyrolysis tars in detail and the predictions agree reasonably with the experimental results.

EXPERIMENTAL

An alkaline soluble lignin extracted from a steam-exploded Aspen wood was obtained from Iotech Corporation, Canada. The elemental composition is 63.4% C, 5.9% H, 30.0% O (by difference), and 0.7% ash. The pyrolysis experiments, including constant heating rate and flash pyrolysis, were performed in an apparatus which employs an electrically heated grid within an infrared cell to provide on-line, in-situ analysis of evolved products by Fourier Transform Infrared (FT-IR) Spectrometry as presented in Fig. 1. In the constant heating rate experiments the cell was swept by a constant flow (700 ml/sec) of nitrogen gas to keep the cell pressure at 1 atm. In the flash pyrolysis experiments the cell was closed. The FT-IR spectra were recorded on a Nicolet model 7199 FT-IR spectrometer. Both tar and char yields were obtained gravimetrically. The field ionization mass spectrometry (FIMS) and elemental analysis were performed at SRI International and Galbraith Laboratories, respectively.

THEORY FOR POLYMER PYROLYSIS

Thermal depolymerization of macromolecules to produce volatile products requires: 1) cleavage of weak bonds, 2) stabilization of the free radicals by donatable hydrogen atoms, and 3) transport of the products away from the reaction zone. To understand the effect of these three factors, consider first the case in which the donatable hydrogen is unlimited. In pyrolysis, the depolymerization proceeds with the random breaking of weak bonds until the fragments are small enough to vaporize. With unlimited hydrogen, the polymer will decompose completely into volatile products if at least the monomer can be vaporized under the reaction conditions. The actual distribution of monomer, dimer, trimer and higher molecular weight oligomers in the

*Work supported by the National Science Foundation under Contract #CPE-8107453

products will depend in detail on the rate of bond breaking relative to the rate of transport of the fragments formed. Conditions which enhance transport relative to bond breaking will increase the average molecular weight of the volatile products. In cases where donatable hydrogen is limited, the volatile yield will depend on the demand for hydrogen; i.e., the amount of hydrogen employed for stabilization of products which are carried away. For a given polymer, the higher the average molecular weight of the volatile products the fewer the broken bonds requiring stabilization, and the lower the hydrogen demand per weight of volatile product.

The theory combines random cleavage of weak bonds with transport of depolymerization fragments by vaporization and diffusion to predict product yield and composition. The assumptions in this theory include: 1) the bonds between the monomer units in the polymer molecule are the only weak bonds and equally likely to be cleaved; 2) during an infinitesimal period of time the probability of cleaving simultaneously two weak bonds in one molecule is so small that it can be ignored, 3) the melt is homogeneous, i.e., there is no concentration and temperature gradient in the particle; and 4) the particle is spherical and its radius shrinks proportionally to the cubic root of its mass as the reaction proceeds. The theory has been developed for the geometry indicated in Fig. 2, where spherical particles (located within the heated grid), are at the pyrolysis temperature while the temperature of the cell wall, where tar is condensed and collected, is only slightly above room temperature. The particle size and cell diameter are not shown to scale in Fig. 2, the cell diameter is 5 cm and the mean particle size is 0.3 mm.

The theory considers the molecular weight distribution Q_i in the reacting polymer and the molecular weight distribution N_i of the tar, where Q_i and N_i are the molar quantities of the polymeric component with DP = i in the reacting polymer and in the tar. DP (degree of polymerization) is defined as the number of monomer units in a polymer molecule. The rate of change of Q_i is

$$dQ_i/dt = (dF_i/dt) - (dB_i/dt) - (dN_i/dt) \qquad 1)$$

where dF_i/dt is the rate of formation for the component with DP = i from the decomposition of components with DP $>$ i in the reacting polymer, dB_i/dt is the rate of disappearance by decomposition for the component with DP = i in the reacting polymer, and dN_i/dt is the rate of transport of fragments with DP = i from the particle as tar or gas.

In the following paragraphs we develop the equations for the terms on the right hand side of eq. 1.

The terms dF_i/dt and $dB_i dt$ are the rate of creating and distruction of oligomers with DP = i through the cleavage of weak bonds. The cleavage of these weaks bonds is assumed to be a first order process with a rate constant k, i.e., the rate at which bonds break is k times the number of breakable bonds. Since there are (i - 1) weak bonds in the polymeric component with DP = i and the breaking of any one of them will remove that component from the distribution parameter Q_i. The rate of distribution for the component i may be written,

$$dB_i/dt = (i - 1)\ k\ Q_i \qquad 2)$$

The creation of component i can occur by the distribution of all components j with j $>$ i. For each component with DP = j $>$ i in the reacting polymer, there are two ways of breaking weak bonds to form component with DP = i, thus, the rate at which component i is created from component j ia

$$(dF_i/dt)_j = 2\ k\ Q_j \qquad 3)$$

and

$$dF_i/dt = 2k\sum_{j=i+1}^{a} Q_j \qquad 4)$$

where the DP of the starting homopolyer is a.

As illustrated in Fig. 2, there are five weak bonds in the hexamer which decomposes to pentamer plus monomer by cleaving two different bonds, to tetramer plus dimer by cleaving another two different bonds, or to a pair of trimers by cleaving the middle bond. Comparing equations 2 and 4, it is obvious that $(dF_i/dt)_6 = (2/5)(dB_6/dt)$ where i range from 1 to 5.

For component i to leave a particle as tar it must be volatile and be available within the particle (Q_i greater than 0). The maximum possible transport rate for component with DP = i is

$$dN_i/dt = [W/((4/3)\pi r_o^3 d)][dV_i/dt] \qquad 5)$$

$$= [\text{number of particles}][\text{transport rate for component i from each particle}]$$

where w, r_o and d are the starting weight of polymer, the particle radius and the density of the original polymer, respectively. The transport rate for oligomer with DP = i from a particle of radius r_p at any given time is approximately given by the following equation (2)

$$dV_i/dt = 4\pi r_p D_i (P_i/RT)(Q_i/\sum_{m=1}^{a} Q_m) \qquad 6)$$

where D_i and P_i are the diffusion coefficient and the vapor pressure for oligomer with DP = i, R is the gas constant, and T is temperature in K. D_i and P_i can be estimated by the following equations (2,3,7)

$$D_i(T,P) = 1.585M_i^{-0.675}(T/273)^{1.08}(1/P) \quad cm^2/sec \qquad 7)$$

$$P_i = (1.23\times10^5 \text{ atm})\exp(-236M_i^{-0.654}/T) \qquad 8)$$

where M_i is the molecular weight of component i

The tar fraction Y, is defined as

$$Y = (M/Wa)\sum_{i=1}^{a}(iN_i) \qquad 9)$$

where M is the molecular weight of the polymer.

This theory has been expanded to predict the pyrolysis behavior of a copolymer comprising up to seven different and randomly distributed monomers. The expanded theory is not included because of page limit. In each simulation, an activation energy (E) and a frequency factor (A) were given to calculate the rate constant, k, using the following equation

$$k = A \exp(-E/RT) \qquad 10)$$

Other initial inputs include a, M, W, r_o, d, molecular weights of monomers, reaction pressure and the temperature of the particle as a function of time. At time zero,

$$Q_a = W/M$$

$$Q_i = 0 \qquad \text{if } i \neq a$$

and

$$N_i = 0$$

The simulation is carried out by keeping track of Q_i, N_i, Y, k, and r_p at each time step using equations 1 to 9. The time increment is kept very small. All computations were performed on a PDP 11/23 computer.

INPUT INFORMATION

Aspen is a hardwood and its milled wood lignin was reported to contain 57% of guaiacylpropane units and 43% syringylpropane units (4). As indicated by FIMS results for lignin tars presented in Figs. 3a and 4a, in addition to the formation of coniferyl alcohol (MW = 180), 3-guaiacyl-1-propanol (MW = 182), sinapaldehyde (MW = 208) and sinapyl alcohol (MW = 210), other products derived from these compounds with concurrent formation of CO, CO_2, H_2O, CH_4, C_2H_6, etc. were also detected in lignin tars. One of the most probable structures for each molecular weight is presented in Table 1. The compound with MW = 418 is probably dehydrobis-sinapyl alcohol with biphenyl type linkage. Although it is a dilignol, it is treated as a monomer in this simulation because the linkage between the two C_9 units is very stable under the pyrolysis conditions. Therefore, compounds with MW $\leq$ 210 and the compound with MW = 418 are viewed as monomers in this simulation.

Equation 8 was originally used to estimate vapor pressures for hydrocarbons. Since lignin and its tar contain fairly large amounts of oxygen, adjustment in the estimation of vapor pressure is necessary. Boiling points and molecular weights for selected relevant compounds are presented in Table 2. By comparing a pair of compounds, one hydrocarbon and one oxygen-containing compound, with the same boiling point and assuming that compounds with the same boiling point show the same temperature dependence for vapor pressure, adjustments in molecular weights for selected groups are estimated and presented in Table 3. Accordingly, the adjusted molecular weights for the compounds in Table 1 are estimated and used in eq. 8 to estimate the vapor pressure. In this simulation, monomers with very similar molecular weights are treated as one entity and the molecular weights for the seven monomers are included in Table 4. The mole fractions for these compounds are assumed so that theoretical prediction can fit the FIMS result for lignin tar produced at 500°C (Fig. 3a). The monomers with MW = 154, 196 and 210 contain one syringyl group and the monomer with MW = 418 contains two syringyl groups. Thus, guaiacyl to syringyl ratio among these monomers is 40 to 60. This ratio is lower than that reported (4) for the milled wood lignin of Aspen (57% to 43%) and suggests that the bonds connected to syringyl units are more reactive than those to guaiacyl units. The thermally most labile bond in lignin is the α-O-4 bond as shown below

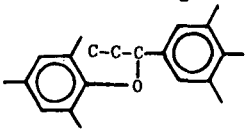

The rate constant for homolysis of the carbon-oxygen bond in benzyl phenyl ether has been reported as $5 \times 10^{14} \exp(-25{,}400/T)$ (5). An alkyl substituent at the benzylic position reduces the activation energy by about 3 Kcal according to some reported activation energies (5). Consequently, the rate constant for lignin pyrolysis is estimated as $10^{14} \exp(-24{,}000/T)$.

A correlation between coal density and elemental composition on a dry mineral matter free (dmmf) basis has been developed (6).

$$D_{He(dmmf)} = 0.023\ C_{dmmf} + 0.0292\ O_{dmmf} - 0.0261\ H_{dmmf} + 0.0225\ S_{org(dmmf)} - 0.765 \quad 11)$$

From this expression, the density for the Aspen lignin used in this study is estimated to be 1.43 g/cm^3. The particle radius of 0.03 mm is used in this simulation. DP of the original polymer, a, is assumed to be 50 and the molecular weight of the original polymer

$$M = 50\ (0.4 \times 180 + 0.6 \times 210) = 9900\ g/mole$$

RESULTS AND DISCUSSION

Fraction of Potentially Depolymerized Bonds (F_{pdb})

The fraction of potentially depolymerized bonds (F_{pdb}) is defined as the fraction of weak bonds whose resulting free radicals can be stabilized by donatable hydrogen atoms. In the pyrolysis of lignin, some weak bonds convert to much stronger bonds, e.g., conversion of carbon-carbon single bond to double bond as a result of hydrogen donation, thus, F_{pdb} is usaully less than one. F_{pdb} depends on the structure of lignin and on the reaction conditions and is one of the most important factors in determining the char yield. F_{pdb} should be regarded as an adjustable parameter in the simulation. In each computer simulation, a certain value is used for F_{pdb}. When x_c becomes equal to F_{pdb} then there will be no additional bond cleavage, i.e., dF_i/dt and dB_i/dt in equation 1 are zeros.

Effect of Reaction Temperature

The molecular weight distribution of tar is determined by the competition between transport and decomposition for all possible components. For a certain component, if transport is much faster than decomposition, it transports away to tar fraction before it decomposes, otherwise, a fraction or all of this component remains on the heated grid and decomposes to smaller components. An increase in temperature accelerates both transport and decomposition, however, the increase in decomposition rate is more significant. Consequently, a higher reaction temperature favors the formation of tar components with higher volatilities or lower molecular weights.

The effect of reaction temperature has been examined experimentally. Pyrolyais experiments of Aspen lignin were performed at 500°C and 650°C. FIMS results for the tar samples are presented in Figs. 3a and 4a. The major products are monolignols and dilignols along with small amounts of trilignols. The number average molecular weight ($\bar{M}_n$) decreases from 388 to 333 as reaction temperature increases from 500°C to 650°C. The yields of dilignols and trilignols at 650°C are less than those at 500°C. Theoretical predictions (assuming $F_{pdb} = 0.5$) presented in Figs. 3b and 4b show the same patterns of molecular weight distributions although the predicted number average molecular weights are smaller than the experimental ones.

Effect of External Pressure

The transport rate decreasea as the external pressure increases at a constant temperature while the decomposition rate is independent of the pressure of inert gas. Consequently, a higher external pressure suppresses the formations of tar components with higher molecular weights. Theoretical prediction at 550°C and 4 atm of inert gas pressure is presented in Fig. 5b. Under 4 atm of nitrogen, only compounds MW $\ll$ 210 are produced in significant amounts. The FIMS spectrum for the tar sample produced under these conditions is presented in Fig. 5a. The predicted reduction in molecular weight is observed but is not as drastic as predicted. The data show a smaller ratio of dimer to monomer and ver little trimer compared to a tar obtained at slightly lower temperature at 2 torr, Fig. 3a. But the theory

predicts no dimers or trimers, suggesting some modifications of the pressure and molecular weight dependence of the diffusion coefficient and vapor pressure, equations 7 and 8, may be required.

A higher external pressure results in a smaller average molecular weight for volatile products and therefore an increased usage of donatable hydrogen per weight of volatile products. Because the donatable hydrogen is limited in lignin pyrolysis, the increased hydrogen usage results in a higher char yield. This effect has been verified experimentally. At 550°C, the char yield increases from 33% to 44% as the pressure of nitrogen increases from 2 torr to 4 atm. Theoretical predictions of the char yields are 44% at 2 torr (assuming $F_{pdb} = 0.5$) and 55% at 4 atm (assuming $F_{pdb} = 0.75$, a smaller value of F_{pdb} leads to an even higher char yield) and agree reasonably with the experimental results.

Constant Heating Rate Experiment

The heating rate for lignin pyrolysis is 30°C/min and the pressure of nitrogen is 1 atm. The time and temperature dependent tar evolution rate, monitored by the baseline scattering in the FT-IR spectra, is presented in Fig. 6. The solid line in Fig. 6 is the theoretical fit and its width is about 1/5 of that for the experimental data. This difference is due to the fact that there are different types of bonds between the C_9 units in lignin and indicates the need to expand this theory to include a distribution of activation energies. In addition, this theory in its present form can not predict the evolutions of gaseous products. The theory described in the following paper has these capabilities. Thus, incorporation of these two theories will provide the much needed tool to predict the behavior of lignin in pyrolysis reactions.

SUMMARY

A depolymerization theory has been developed to predict the molecular weight distributions for lignin tars produced in various pyrolysis reactions. It can also predict the char yield semiquantitatively. Incorporation of this theory with the theory described in the following paper will provide the much needed predicting capability for lignin pyrolysis.

REFERENCES

1. Freudenberg, K. and Neish, A.C. "Constitution and Biosynthesis of Lignin", Springer-Verlag, New York, 1968

2. Solomon, P.R. and King, H.-H. Pyrolysis of Model Polymers: Theory and Experiments, submitted to Fuel

3. Unger, P.E. and Suuberg, E.M. "Eighteenth Symposium (International) on Combustion", The Combustion Institute, Pittsburgh, PA, 1981, p. 1203

4. Sarkanen, K.V. and Hergert, H.L. "Lignins", (Ed. Sarkanen, K.V. and Ludwig, C.H.), Wiley Interscience, New York, 1971, p. 43

5. Stein, S.E. "New Approaches in Coal Chemistry", (Ed. Blaustein, B.D., Bockrath, B.C. and Friedman, S.) Am. Chem. Soc. Symp. Series, 169, Am. Chem. Soc., Washington, DC, 1981, p.97

6. Neavel, R.C., Hippo, E.J., Smith, S.E. and Miller, R.N. Preprints Am. Chem. Soc. Div. Fuel Chem., 1980, 25 (3), 246

7. Perry, R.H. and Chilton, C.H. "Chemical Engineer's Handbook", Fifth Ed., McGraw-Hill, New York, 1973, Section 3

TABLE 1

MONOMERS IN LIGNIN TAR

Molecular Weight	Possible Structure (name)	Adjusted Molecular Weight
138	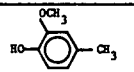 4-methylguaiacol	152
140	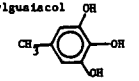 5-methylpyrogallol	252
152	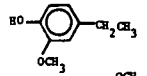 4-ethylguaiacol	176
154	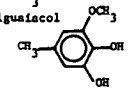 3-methoxy-5-methylcatechol	218
166	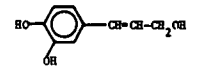 3-(3,4-dihydroxyphenyl)-2-propen-1-ol	278
168	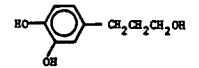 3-(3,4-dihydroxyphenyl)-1-propanol	280
180	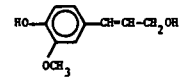 coniferyl alcohol	244

TABLE 1 (continued)

182	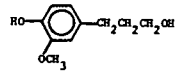 3-guaiacyl-1-propanol	246
194	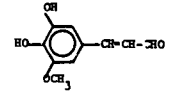 3-(3,4-dihydroxy-5-methoxyphenyl)-2-propenal	272
196	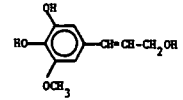 3-(3,4-dihydroxy-5-methoxyphenyl)-2-propen-1-ol	310
208	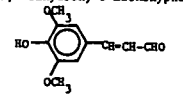 sinapaldehyde	258
210	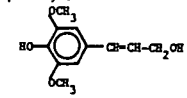 sinapyl alcohol	286
418	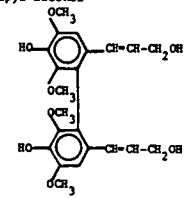 dehydrobis-sinapyl alcohol	570

TABLE 2

BOILING POINTS FOR SELECTED COMPOUNDS

Compound	Structure	Boiling Point (°C)	Molecular Weight
2,6-dimethoxyphenol		261	154
1-phenyloctane	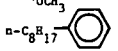	262	190
guaiacol		205	124
1-phenylpentane	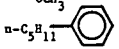	205	148
2-phenylpropionaldehyde	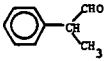	203	134
3-phenyl-1-propanol	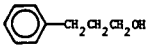	235	136
1-phenylheptane	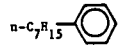	233	176
phenol		181	94
1-phenylbutane	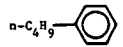	183	134
catechol		245	110

TABLE 3

ADJUSTMENTS IN MOLECULAR WEIGHTS FOR SELECTED GROUP

Group	ΔMW
	36
—OH	40
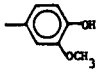	24
—CH=O	14
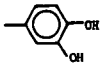	72

TABLE 4

MONOMERS USED IN SIMULATION

Molecular Weight	Adjusted Molecular Weight	Mole Fraction
138	187	0.11
154	206	0.14
168	280	0.185
182	246	0.16
196	291	0.10
210	272	0.155
418	570	0.15

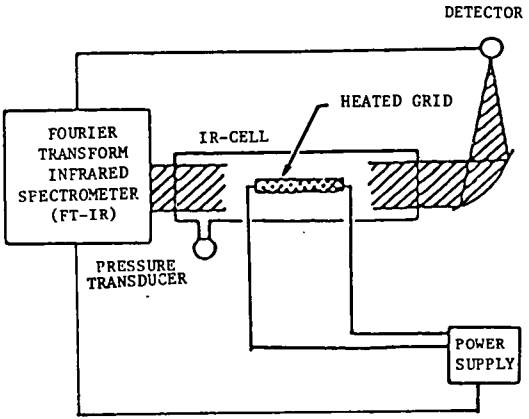

Figure 1. Heated Grid Pyrolysis Apparatus.

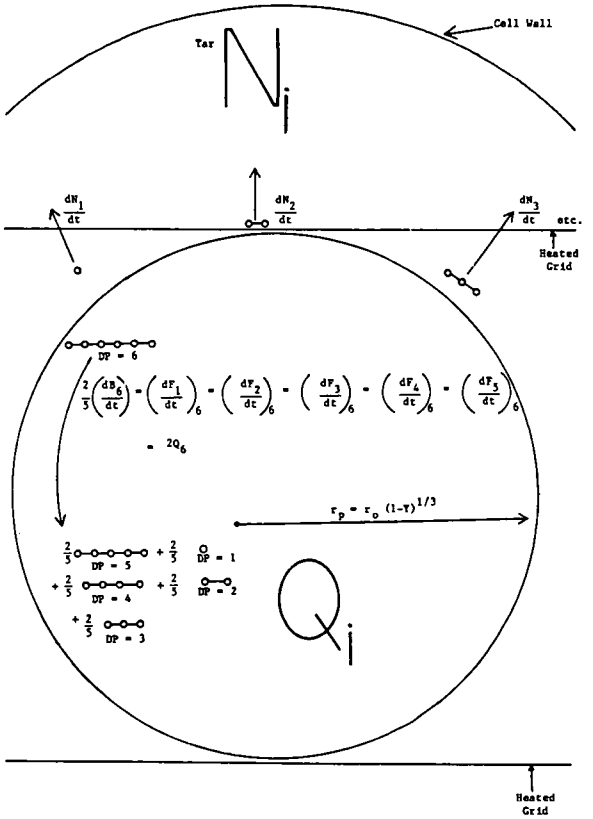

Figure 2. Typical Features Considered in the Depolymerization Theory.

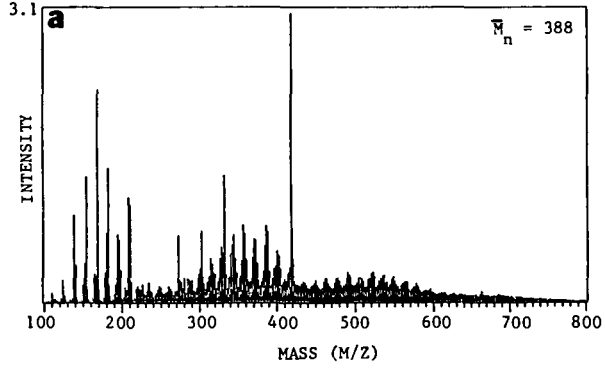

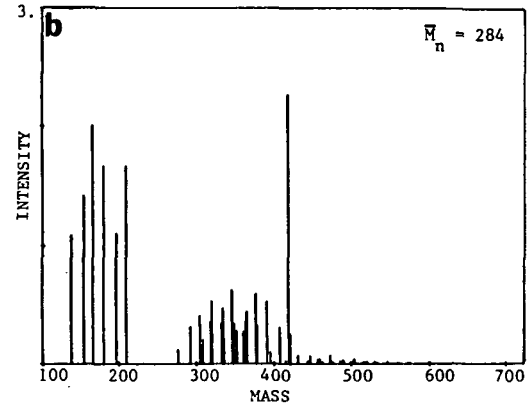

Figure 3. Molecular Weight Distribution for Lignin Tar Produced at 500°C and 2 torr. a) FIMS Result, b) Theoretical Prediction.

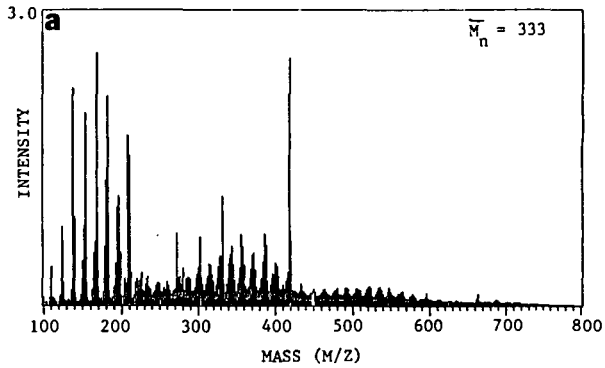

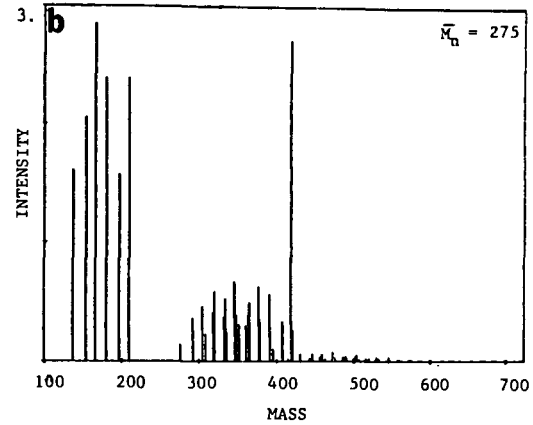

Figure 4. Molecular Weight Distribution for Lignin Tar Produced at 650°C and 2 torr. a) FIMS Result, b) Theoretical Prediction.

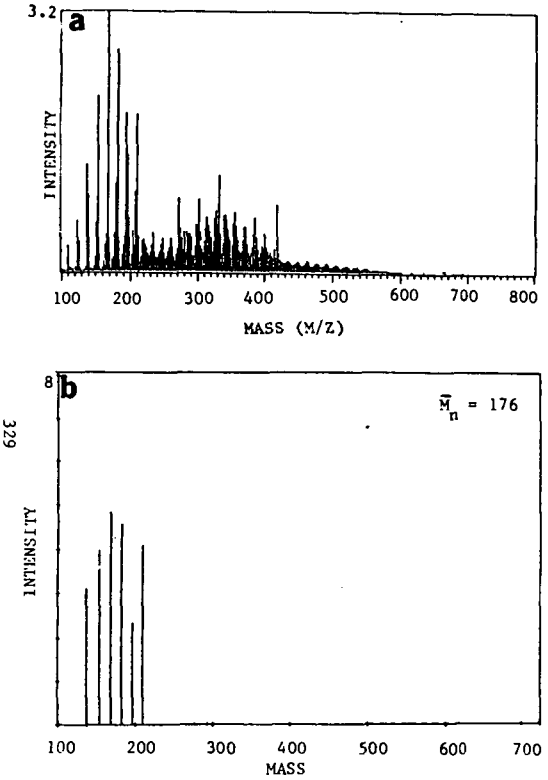

Figure 5. Predicted Molecular Weight Distributions for Lignin Tars Produced at 550°C. a) P = 2 torr, b) P = 4 atm.

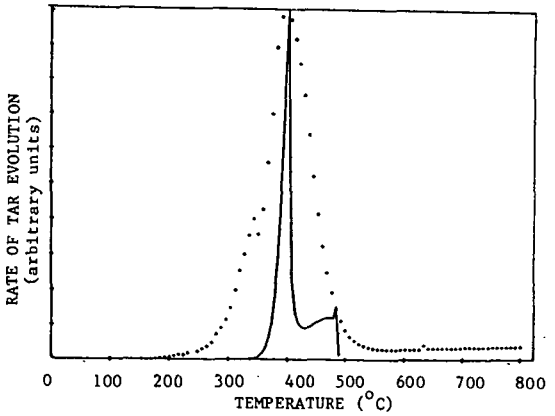

Figure 6. Constant Heating Rate Pyrolysis of Lignin. Heating Rate = 30°C/min. Solid Line is Theoretical Prediction.

MODELING OF PHYSICAL AND CHEMICAL PROCESSES DURING PYROLYSIS OF A LARGE BIOMASS PELLET WITH EXPERIMENTAL VERIFICATION

R. Chan and B.B. Krieger
Dept. of Chemical Engineering, Univ. of Washington
Benson Hall BF-10 Seattle, WA 98195

INTRODUCTION

A desire for optimal energy recovery from biomass has led to furnace simulation (1) and interest in chemicals production has led to biomass gasifier modeling (2). However, global considerations employed in these models give little insight into fundamental physical and chemical processes occuring in individual biomass particles during devolatilization. In previous studies addressing these processes, the emphasis has been on burning times (3), heat transfer rates (4), and weight loss rates (5) rather than detailed prediction of volatiles composition during pyrolysis. Detailed intrinsic kinetics studies of small biomass particles to determine pyrolysis product distribution as a function of temperature and time have been conducted (6,7). However, the results were correlated with Arrhenius type equations using best-fit parameters rather than parameters related to chemical structure. The latter is a difficult task given the diverse physical nature of biomass (8) and the complex molecular structure of the natural polymers of which it is composed (9). Indeed, the effects of particle size and physical microstructure (anisotropy) on devolatilization have not been systematically investigated in experiments, nor modeled using fundamental principles. To what extent the internal geometry of the wood influences the rates of heat and mass transfer, and thus the reaction products' composition, is largely unknown. Of particular importance is the ability to predict the relative proportions of char, tar, and gas (and components therein) that result from a given biomass thermal conversion process and given feedstock.

The goal of this work is to use fundamental considerations to predict changes in biomass pyrolysis product composition. The approach taken is to model a single, well-characterized biomass pellet under varying conditions during pyrolysis. This model can then be used to refine the gasifier and combustor models when a suitable distribution function for the feedstock characteristics is determined. Independent variables are feedstock characteristics (particle size, density, moisture, composition) and thermal conversion process characteristics (heating rate, diluent gas composition). Dependent variables predicted are instantaneous particle temperature and density profiles, gas and tar release rates, and char yields as well as ultimate yields.

For verification of the model, experiments were conducted according to a Box-Behnken design(10). A 1-D model is presented here for comparison with the experiments, and a 2-D model is being developed. Understanding gained from this model will aid in process design for biomass gasification, wood combustor design, as well as aid in fire safety.

BRIEF EXPERIMENTAL DESCRIPTION

The experimental apparatus is described in detail elsewhere (11-13). Briefly, it is a single particle, 1-D reactor. One face of a well-characterized cylinder of wood, compressed sawdust, cellulose, or lignin is heated by a combustion- level radiant heat source (4-12 cal/cm^2-s). As the temperature front at which reaction occurs moves inward, volatile species flow toward the heated face under a slight pressure gradient. The escaping volatiles reduce the incident radiation and the time- dependent magnitude of this effect is

quantified (11). The progress of the temperature front is monitored by 3 thermocouples at 2, 4, and 6 mm from the surface and the surface temperature is measured with an infra red pyrometer. Density profiles along the length of the pellet (integrated over the diameter) are taken via an X-ray technique.

Outflowing volatiles are rapidly quenched by helium and swept to a cold trap where water and tars are collected and analyzed in detail (11) as a time-integrated sample . Uncondensed gases are sampled every 3-15 sec by an automatic gas chromatographic sampling valve which also triggers the X-ray device. Char and gases are also analyzed in detail.

Although the experimental results are intriguing, especially the effects of anisotropy, they are described elsewhere (11). The major emphasis in this preprint is on the formulation and validation of the mathematical model. Other modeling details and aspects such as sensitivity analysis are also presented elsewhere (11,13).

MATHEMATICAL MODEL

An analysis similar to that of Russel, et al (14) was done (11,13) to determine the characteristic times for physical and chemical rate processes in a devolatilizing wood particle. For a 1 cm particle, conduction heat transfer to the interior is two orders of magnitude slower than chemical reaction at high temperature. However, the devolatilization reaction rate is comparable to the heat transfer rate at low temperature. Because the net conduction rate is strongly influenced by reaction product outflow and therefore the reaction rate, a fully unsteady model with variable properties was developed.

Heat Transfer Model

A one dimensional energy balance on the devolatilizing particle is schematically shown in Fig. 1. A time-varying radiant heat flux (Q_1), uniform in the radial direction, heats the face of the particle. Conduction (Q_4) is offset by volatiles outflow (Q_6). The volatiles are assumed to be in thermal equilibrium with the solid behind the reaction front as they flow outward, and are assumed to flow in one direction only[1].

The heats of reaction for wood are not well-known and they have been observed to be functions of particle size (15). In this model, the latent heat of water is treated as a heat of reaction(Q_5), and the heat of the devolatilization reaction (lumped with Q_5) is treated as a parameter using published values as bounds (16).

In the radial direction, the cylinder is considered insulated and impermeable. The heated face boundary condition includes radiation heat loss (Q_3) and convection heat loss (Q_2) which is described using the carrier gas flowrate. The outflowing CO_2 and H_2O absorb the incident radiation. This phenomena is treated using an estimated absorption coefficient for water in the model, and the incident radiation is reduced by an amount corresponding to the instantaneous water outflow.[2] The unheated face is considered impermeable to volatiles owing to the imposed pressure. Radiative (Q_8) and convective heat loss (Q_7) at this surface are treated, however. The film heat transer coefficient at each face was calculated using Nusselt number correlations and the properties and flowrate of helium at conditions of the experiments.

---

[1] It has been verified by Lee, et al, (17).

[2] Experimental verification of the net radiation arriving at the surface during a typical run was accomplished using a Medtherm heat flux gauge. These results were matched to the model using a value for the absorption coefficient which was a best-fit parameter.

For most previous modeling studies, the thermal conductivity and heat capacity of wood were modeled as linear functions of the initial and final (char) values (18) using either the porosity or density change (18-21). It should be observed, however, that these models require a final char density, heat capacity, and conductivity for every case considered, restricting their utility and predetermining the calculated char yield. Additionally, in this study experimental measurements of temperature profiles as a function of time indicated that the thermal conductivity was an order of magnitude higher than would be predicted if it were a function of density alone. Unfortunately, few measurements of wood thermal properties have been made at high temperature because of the attendant chemical reaction. Thermal conductivity was measured for our samples at low temperatures and a model analogous to Birkebak and Ozil (22) was developed to describe a radiation contribution to the temperature variation (11,13). The heat capacity and porosity of wood were described by linear functions of the density(11,13).

Chemical Reaction Model

A schematic of the chemical reactions considered and the lumping scheme for gas, tar, and secondary gases is given in Table 1. Rate coefficients for reactions 1,2 and 4 were taken from Ref. (6). Tar cracking reaction rates (k_5) were taken from Refs. (23) and (24) and alpha and beta are adjustable. The char production rate (k_3) is estimated from the work of Shafizadeh, who has measured the arithmetic sum of char production and gas production (25). In this work k_3 must be viewed as a parameter, and as discussed below, the model is extremely sensitive to its value. Water production by evaporation and dehydration reactions are lumped (k_4) and treated as an activated process. The generation term in the energy equation contains the heat of vaporization of water, since it is larger than the heats of reaction measured for wood (15,16).

Mass Transfer Model

In previous models, with a single reaction step (weight loss kinetics), the product distribution is unaltered by the presence or absence of a finite mass transfer rate (26) since only a lumped gas species is described. The only possible implication of a slow mass transfer step is a delayed appearance of the volatiles. The experimental studies (11) indicated that a mass transfer resistance was not significant for heating parallel to the grain direction. Since the model is one dimensional, anisotropy is not treated and inclusion of a mass transfer resistance at this stage is not warranted. The previous analysis of characteristic times for mass transfer is consistent with this observation and the rather open porous structure of wood. For comparison to experiment, the volatiles mass flux is computed as the instantaneous integral over the pellet length of the local total change in density (11,13).

Numerical Method and Equations

Limited space in the preprint prevents the presentation of the detailed equations. However, earlier versions of the model equations appear in Ref. (11) and the current model will be detailed in a forthcoming publication (13). The coupled partial differential equations for the pellet temperature, and species concentrations are solved in dimensionless form using a GEARB package (Finlayson,1980). For ease of comparison with experimental results, in this paper model predictions are given in dimensional form. The cases of thick pellets heated by high heat flux result in very sharp temperature and reaction fronts which lead to "stiff" systems of equations. Computation times and comments appear in Refs. 11 and 13.

RESULTS AND DISCUSSION

Comparison of the measurements to model predictions of the unsteady temperature profile as a function of time at 3 locations are shown in Fig. 2 for the case of an intermediate heat flux and the thinnest particle, 0.5 cm. The model overpredicts the temperature at short reaction times, but satisfactorily predicts the pseudo-steady temperatures at several depths after 200-300 secs. For other cases, similar overprediction occurs early in the pyrolysis, but the steady state temperatures are in agreement with experiment even for the highest heat flux and thickest particle. Previous studies (5,18) reported only predictions of steady state temperatures. It is felt that refinement of the absorption model for the net radiant heating of the wood surface will enhance agreement of temperature profiles in the early reaction period (11).

Fig. 3 presents the comparison of predicted gas release rate to experimental measurements for the same case as Fig. 2. Only uncondensed gas flux (not tar and water) is presented in the figure. As can be seen both the magnitude and shape of the volatiles release curve agree rather well with experiment. Correction of the temperature overprediction discussed earlier will delay the predicted gas release, in better agreement with experiment.

Extensive comparisons between model and experiment cannot be presented; however, similar agreement to that shown in Figs. 2 and 3 exists for most cases studied by experiment. Numerical difficulties are encountered for the cases with the sharpest fronts, i.e., steepest temperature gradients resulting from high heat flux and thick samples. Oscillations in the temperature and density profiles occur and a refinement of the numerical methods is indicated (27). However, these oscillations have little effect on the prediction of ultimate product distribution. As shown in Table 2, there is satisfactory agreement between predicted and measured gas, tar, and char yield for most cases. Agreement between these values was substantially improved when the experimental mass balance on water was very carefully analyzed and when the moisture release rate in the chemical reaction model and the energy balance was included.

A significant advance resulting from this modeling approach is that it is unnecessary to assume or measure a final value for char yield and thermal properties. Since char deposition is explicitly treated in the chemical reaction model, it is of interest to examine Fig. 4 in which the local density of char is presented as a function of reaction time for a case similar to those previously discussed. There is a slightly greater fraction of char produced when the reaction front is deeper in the sample, owing to the reduced heating rate experienced there. This is consistent with general observations in coal and wood pyrolysis that indicate char yield increases with slower heating. Since no char gasification reactions are currently incorporated into the reaction model, the char deposited near the surface of the sample retains its initial density throughout the reaction period. While it was foreseen that predictions of this nature could be confirmed with the X-ray density profiles, the resolution of this method is not sufficient to confirm this prediction.

The rate coefficient used for the char deposition reaction is estimated from the work of Shafizadeh (25). Behind the reaction front the deposited char insulates the unreacted wood and char thermal conductivity determines the subsequent temperature profile and rate of pyrolysis. Thus, the model is quite sensitive to both the value of the rate coefficient for char deposition as well as the model for the variation of wood and char thermal conductivity with density and temperature. If too little char is predicted, the char density is too low resulting in too slow a pyrolysis. If the char thermal properties are

incorrect as a function of temperature, the reaction can terminate prematurely or runaway can occur. A definite need exists for information on char deposition rates from carbonizing various fuel species (28), as well as on char thermal properties over a wide range of temperatures and porosities.

SUMMARY

A mathematical model of wood pyrolysis has been presented that is in satisfactory agreement with experimental reaction product distributions over a range of conditions of practical importance for gasification and combustion. Both chemical and physical processes are described using fundamental principles. Inclusion of water release and char deposition chemical reactions results in predictions of ultimate product distributions (gas, tar, and char yields) that are in good agreement with experiment and can aid in optimization of processes to maximize or minimize tar production. Predictions of products instantaneously released from a single wood pellet are in fair agreement with experiment. Computational difficulties are encountered for the cases with the steepest temperature gradients.

Previous studies (29) using a complex kinetic mechanism and heat transfer in a wood slab made no comparison to experimental results. Thus, this study provides both a data base (11) and a fundamental modeling approach that will enhance the understanding of the effects of physical properties and processes on the chemistry of devolatilizing biomass. Presentation of sensitivity analyses and further verification comparisons of the model are presented in a forthcoming article (13). Currently, pyrolysis product distribution as a function of particle size can be predicted only for the 1-D case. Extension of the model and experiments to realistic cases using 2-D samples is planned.

ACKNOWLEDGEMENTS

The authors would like to acknowledge the financial support of the Department of Energy, Solar Energy Research Institute. In addition, the helpful suggestions of Prof. Bruce Finlayson are gratefully acknowledged.

LITERATURE CITED

(1) Adams, T.N., Comb. and Flame, 1979, 34, 47-61.
(2) Bacon, D.W. J. Downie, J.C. Hsu, J. Peters, paper presented at "Fundamentals of Thermochemical Biomass Conversion: An Intl. Conference," Solar Energy Research Institute, Estes Park, Colo., Oct. 1982. To be published as a book, 1983.
(3) Phillips, A.M. and H.A. Becker, Comb. and Flame, 1982, 46, 221-251.
(4) Kanury, A.M., and P.L. Blackshear, Jr., Comb. Sci. and Tech., 1970, 18, 339.
(5) Kung, H.C., Comb. and Flame, 1972, 18, 185-195.
(6) Hajaligol,M.R., W.A. Peters, J.B., Howard and J.P. Longwell, Proc. - Specialists Workshop on Fast Pyrolysis of Biomass, Solar Energy Res. Inst., Golden, Colo., 1980.
(7) Iatriadis, B., and G.R. Gavalas, I.E.C. Prod. Res. Dev., 1979, 18, 127.
(8) Bain, R., "Beneficiation of Biomass for Gasification and Combustion", SERI/TR-33-239, A Survey of Biomass Gasification, Vol. II, 1979.
(9) Milne, T., "Pyrolysis - Thermal Behavior of Biomass Below 600 C", SERI/TR-33-239, A Survey of Biomass Gasification, Vol. II, 1979.
(10) Box, G.E.P. and D.W. Behnken, Technometrics, 1960, 2(4), 455.
(11) Chan, W.C.R., Ph.D. Thesis, University of Washington, Dept. Chem. Engrg., 1983.

(12) Chan, W.C.R., and B.B. Krieger, Chemical Reaction Engineering - Boston,, 1982, ACS Symp. Ser. 196, 459.
(13) Chan, W.C.R., and B.B. Krieger, Mathematical Modeling of Biomass Pyrolysis, to be published, 1983.
(14) Russel, W.A., D.A. Saville, and M.I. Greene, AICHE J., 1979, 25, 65.
(15) Roberts, A.F., 13th Symp. (Intl.) on Combustion, Comb. Inst., 1971, 893.
(16) Tang, W.K., Ph.D. Dissertation, University of Wisconsin, 1964.
(17) Lee, C.K., R.F. Chaiken, and J.M. Singer, 16 Symp. on Combustion, Comb. Inst., 1976, 1459.
(18) Kansa, E.J., H.E. Perlee and R.F. Chaiken, Comb. and Flame, 1977, 29 , 311.
(19) Kung, H.C. and A. Kalelkar, Comb. and Flame, 1973, 20, 91.
(20) McClean, J.D., Amer. Soc. of Heat and Vent. Eng. Trans., 1941, 47.
(21) Wong, P.T.Y., For. Prod. J., May, 1964, 195-198.
(22) Birkebak , R.C. and E. Ozil, Studies in Heat Transfer, McGraw-Hill, 1979.
(23) Sakai, T. I.E.C. Prod. Des. Dev., 1971, 10, 305.
(24) Froment, G.F., Chem. Eng. Sci., 1981, 36, 1271-1282.
(25) Shafizadeh, F., personal communications, 1977-1983.
(26) Fan, L., L.S. Fan, K. Tojo and W.P. Walawender, Can. J. Chem. Engrg., 1978, 56, 603.
(27) Finlayson, B.A., Non-Linear Analysis in Chem. Engrg., McGraw-Hill, N.Y., 1981.
(28) MacKay, D. M. and P.V. Roberts, Carbon, 1982, 20(2), 87-94; and 95-104.
(29) Panton, R.L. and J.G. Rittman, 13th Symp. on Combustion, Combustion Institute, 1970, 881.

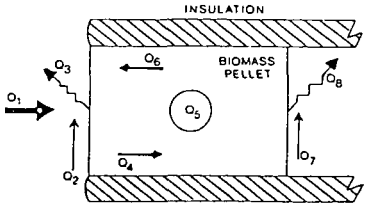

Fig. 1 - Schematic diagram of the heat transfer model.

TABLE 1

CHEMICAL REACTION MODEL

Reaction	Frequency Factor, s^{-1}	E_A, kcal/mol
$S \xrightarrow{1} C_1$	1.3×10^8	33.5
$S \xrightarrow{2} T_1$	2.0×10^8	31.79
$S \xrightarrow{3} C$	1.08×10^7	29.
$M \xrightarrow{4} W$	5.13×10^6	21.
$T_1 \xrightarrow{5} \alpha G_2 + \beta T_2$	1.48×10^6	27.29

Lumped Species Symbol	Identification
S	solid wood
C	char, high molecular weight tar (non-volatile)
M	moisture and chemically bound water in wood
W	vaporized water and released water
C_1	primary gases, e.g., CO_2, some CO, CH_4(?)
T_1	primary tar, e.g., phenols, levoglucosan
G_2	secondary gases, e.g., some CO, C_2H_4, C_2H_2, etc.
T_2	secondary tars, e.g., condensed aromatics (volatile)

α, β are adjustable parameters (stoichiometric coefficients).

TABLE 2
ULTIMATE PRODUCT DISTRIBUTION COMPARISON
EXPERIMENTAL RESULTS AND MODEL PREDICTIONS

1) For L = 0.5 cm, Heat Flux = 4 cal/cm^2-sec.

	Char	Tar*	Gas
Model	21.45	54.78	23.77
Expt.	18.05	62.33	19.63

2) For L = 1.0 cm, Heat Flux = 2 cal/cm^2-sec.

	Char	Tar*	Gas
Model	28.65	58.47	12.88
Expt.	25.12	62.37	12.52

3) For L = 1.5 cm, Heat Flux = 4 cal/cm^2-sec.

	Char	Tar*	Gas
Model	27.49	51.78	20.73
Expt.	22.82	53.98	23.20

* The tar yield includes water produced from the reactions but excludes water from the moisture evaporation.

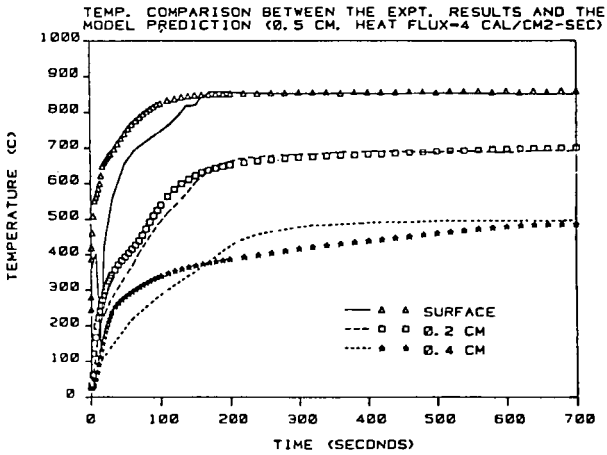

Fig. 2 - Temperature profile comparison - experiment (dashed lines) and model prediction (symbols) - 0.5 cm; ρ = .37 g/cc; initial thermal conductivity = 3.8 x 10^{-4} cal/cm-s-^{o}K

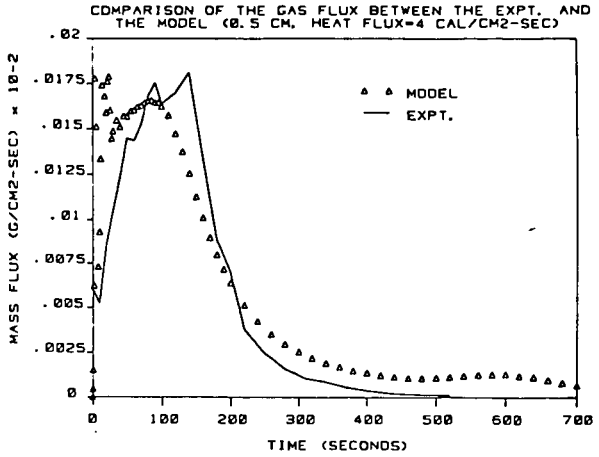

Fig. 3 - Total gas flux comparison - same conditions as Fig. 2

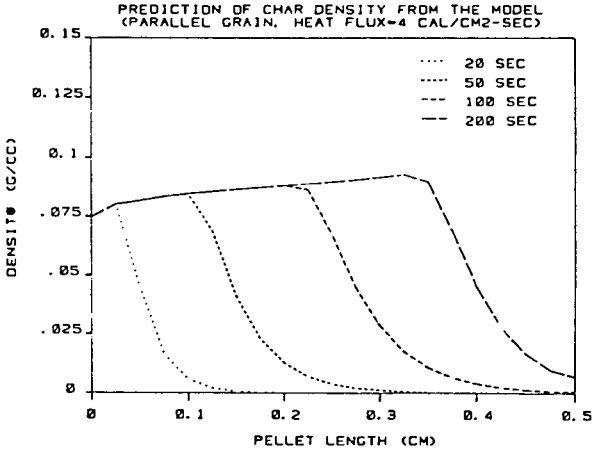

Fig. 4 - Predicted char deposition as a function of time - same conditions as Figs. 2 & 3.

A PHASE-CHANGE APPROACH TO MACRO-PARTICLE PYROLYSIS OF CELLULOSIC MATERIALS.

R. E. DEROSIERS and R. J. LIN

Chemical Engineering Department, Texas Tech University, Lubbock, TX 79409

INTRODUCTION

Biomass is a solid fuel with a high content (approx. 80%) of volatile matter (VM) as defined by standard proximate analyses. As a result, the devolatilization of the material introduced into any thermal conversion device is the most significant process occurring on a mass basis. From the viewpoint of reactor design, it would be convenient to have closed form expressions for the rate of pyrolysis of large particles of cellulosic materials suitable for the convective-heat-transfer environment of the packed or fluidized bed reactor.

The state of knowledge of the fundamental aspects of the pyrolysis "reaction" is advancing rapidly through kinetic studies on small, finely-divided samples in which physical transport considerations are minimized. The Arrhenius rate expressions resulting from these studies are reflective, it is hoped, of the intrinsic chemical reaction rates of pyrolysis processes. The high cost of comminution of feedstock to small mesh sizes however, dictates against the large scale conversion of biomass in this form. Thermal conversion of cellulosic materials in packed or fluidized beds will most likely be accomplished with particle sizes in the range of one to eight cm. With dimensions of that magnitude, the relative rates of chemical and transport processes must be considered.

An indication of the disparity in chemical versus heat transfer rates is afforded by the observation of "advancing front" behavior in the pyrolysis of cylindrical samples of biomass materials (Blackshear, Murty, 1966). The low thermal conductivity and high reactivity of biomass result in a narrow, advancing, reacting zone of pyrolysis. The sharply peaked reaction rate profile results from the depletion of VM in the char and a low temperature level in the virgin solid. The validity of this reaction rate profile is supported by experimental density and temperature profiles. If the reaction rate was slower,

the density profile would be less sharply stepped. The acceleration of the heat transfer rate in the virgin solid would likewise result in a more gradual transition.

Several pyrolysis models have been proposed (Bamford (1946), Roberts (1963), Blackshear (1966), Maa (1973), Lee (1982)) in order to faithfully reproduce the detailed pyrolysis behavior of large samples of cellulosic materials. These usually involve the solution of coupled partial differential equations (PDE's) representing mass, energy, and momentum balances. These models may be classified into two general categories. Volumetric models (Fan, 1978) are the most sophisticated and complex. The rate of decomposition is calculated at the local temperature throughout the solid. Shrinking core models (Maa, 1973) take the advancing front behavior to the limit of an infinitesimally thin reaction zone. In the former case, the reaction is a source term in the conservation equations while in the latter case, the reaction rate appears as a boundary condition. The continuing effort to describe ever more accurately the complicated phenomena of pyrolysis will doubtless give rise to more complex models.

The complexity of the single-particle model used to describe the pyrolysis process will be augmented however, when this model is integrated into the simulation of a gasification reactor. Thus it is our goal to move in the direction of simpler, albeit less precise, models of macro-particle pyrolysis. Consider the computational burden involved in the simulation of a packed-bed reactor. The conservation equations for the bed require an iterative solution because of split boundary conditions. (For example, solid temperature at one terminus, and gas temperature at the other.) For each iteration of the equations for the bed, many evaluations of the reaction rate for the particle must be made. If the evaluation of this rate at each point requires a finite-difference solution of a set of coupled PDE's for the particle, then the calculation time becomes excessive.

The model considered below may be called kinetics-free in that no explicit consideration is given to the rate of pyrolysis. The controlling influence on the rate of decomposition is the heat transfer rate. The progress of the pyrolysis is followed by the rate of advance of a sharp boundary defined as the locus of points at a fixed pyrolysis temperature, T_p. The resulting model is similar in many respects to a phase change problem. In fact, the process may be considered as a change in phase from one solid form (wood) to another (char).

We have been investigating the suitability of such a model in decribing the pyrolysis of 0.5 to 2.5 cm cylindrical samples of natural and densified wood. The objectives of the work are:

1. Develop the proper forms of the relevant equations of change; select an appropriate set of dimensionless variables.
2. Develop efficient numerical schemes to integrate the coupled partial-differential equations and to generate temperature profiles and rate vs time curves.
3. Determine if the model can even crudely reproduce experimental temperature profiles and pyrolysis times without extensive curve fitting. That is, by selecting realistic values of physical parameters, can an a priori calculation produce feasible results.
4. Perform a sensitivity analysis to determine which parameters have the greatest influence on the rate of advance of the pyrolysis front.
5. Determine to what extent the model is capable of faithfully reproducing the details of pyrolysis phenomena even if some parameters must be curve-fitted.

THE PHENOMENA OF PYROLYSIS

Before considering the development of the phase-change model of pyrolysis, it is worthwhile to list some of the more important processes occurring in pyrolysis in order to assess their relevance to any simulation.

Reaction: The primary events of pyrolysis are being intensively studied and it is clear that considering pyrolysis as a single reaction with a fixed product slate is a gross oversimplification. The classification of species as primary and secondary products is far from complete. The expertise to predict in detail even the overall ("final") products of the process is not available. It is not even possible to predict in advance for any feed the precise char yield under different heating rates. It is therefore entirely reasonable to represent pyrolysis crudely as

$$\text{wood} = c\ \text{char} + b\ \text{volatiles}$$

Heat of Reaction: Thermodynamic arguments indicate quite clearly that the overall pyrolysis process is exothermic. TGA studies support this contention. There is some doubt however concerning the amount of char produced by primary and secondary events. The exothermicity is directly proportional to char production. It could be possible for example to have an endothermic primary reaction producing some char and mostly reduced gases such as CO, followed by an exothermic conversion to CO_2 and more carbon at a different location. Since the heat of pyrolysis depends on the spectrum of products, and the spectrum of products depends strongly on the conditions imposed to cause pyrolysis, it is not unreasonable to assume that the primary decomposition is endothermic. Indeed, when carried out under inert atmospheres, some differential scanning calorimetry studies have indicated that this is the case (Muhlenkamp (1975)).

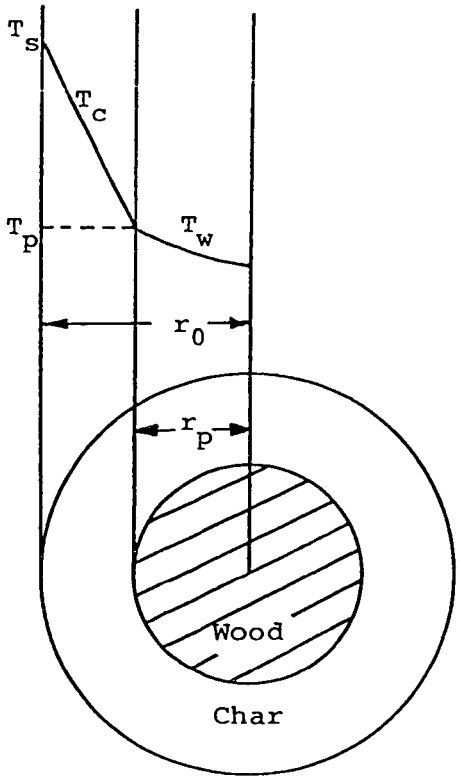

Figure 1: Pyrolysis Scheme of a Single Particle Under the Boundary Condition of First Kind

Reaction Rate: The possibility of representing the rate of decomposition of a mixture of linear polysaccharides and a cross-linked phenylpropane polymer with a single Arrhenius rate expression appears remote. At best it seems likely that a distribution of activation energies would be required. It is assumed below that the rate of decomposition is fast relative to the rate of heat transfer necessary to sustain the pyrolysis.

Geometry: Some shrinkage does occur during pyrolysis as evidenced by checking and pitting of char layers. But this effect will be ignored and constant diameter assumed. Of more importance is the porosity of chars and the resulting effects on density and resistance to gas flow. In this work, the porosity is assumed sufficiently great that the hydrodynamics of gas flow can be ignored. A cylindrical particle geometry has been used in this study.

Gas Flow: A unidirectional, outward flow of non-condensible gases must occur during pyrolysis. But condensible species such as water may be forced inward and result in a net flow towards the cooler, inner region of the cylinder. Water condensing in the layers immediately adjacent to the pyrolysis zone has been proposed by some investigators to explain the delay in the development of the inner temperature profile of samples of pressed cellulose. This inward flow of condensibles has not as yet been considered in the development of the phase-change model but could crudely be accommodated by using a higher effective heat capacity for the unpyrolyzed solid. A better approximation could be made by considering two "phase" changes: in effect, a drying wave and a pyrolysis wave passing through the sample.

THE PHASE CHANGE MODEL OF PYROLYSIS

The simulation of pyrolysis proposed here seeks to avoid the mathematical complexity of the volumetric model as well as the pre-selection of the pyrolysis rate inherent in the steady-state, moving-boundary approach. Maa (1973), for example, uses a kinetic expression for the rate of pyrolysis, but fixes the temperature at which it is evaluated, resulting in a steady state. The pseudo steady-state is probably a reasonable assumption for a large piece of wood (a log or beam) but is probably not valid for a one-cm particle.

To proceed, we make the following assumptions:

1. The pyrolysis reaction may be considered simply as:

   $$\text{Feed} = b\ \text{Gas} + c\ \text{Char}$$

   Here "Gas" refers to all volatile products, and "char" to the completely devolatilized solid. The reaction occurs instantaneously when the solid is raised to a fixed temperature, T_p.
2. Heat is conducted through the char layer to a surface separating char and unpyrolyzed solid. This surface is defined as the locus of points at $T = T_p$. At this surface, the temperature is continuous, but a jump occurs in the temperature gradient, the magnitude of which is determined by the heat of pyrolysis and the thermal properties of the two solids.
3. The temperature of escaping volatiles is always equal to the local char temperature, T_c.

Although not necessary, the following assumptions have been made for convenience in this initial development:

4. Thermal properties (heat capacity, conductivity) and density are assumed constant at an effective or average value.
5. Cylindrical geometry.
6. Specified surface temperature (B.C. of 1st kind).

The mathematical formulation of the model is derived from the equation of change for energy. In the char layer

$$\frac{\partial}{\partial t}(\rho_c c_{pc} T_c) + \frac{\partial}{\partial \underline{r}} \cdot (-k_c \frac{\partial T}{\partial \underline{r}} + \rho_g c_{pg} T_c \underline{u}_g) = 0$$

The third term is the convective flux of gas. A mass balance at any radial location yields an expression for the gas flux.

$$\rho_g u_g = - b \rho_w \frac{r_p}{r} \frac{dr_p}{dt}$$

where r_p is the location of the advancing front. Ordinary conduction occurs in the fresh solid region. (Hereafter referred to as wood.) The system of equations to be solved in each region in cylindrical geometry are

$$\frac{\partial T_c}{\partial t} = \alpha_c \left(\frac{\partial^2 T_c}{\partial r^2} + \frac{1}{r} \frac{\partial T_c}{\partial r} \right) + b \frac{\rho_w}{\rho_c} \frac{c_{pg}}{c_{pc}} \frac{r_p}{r} \frac{dr_p}{dt} \frac{\partial T_c}{\partial r}$$

$$r_p < r < r_o \qquad t > 0$$

With no gas flux in the core:

$$\frac{\partial T_w}{\partial t} = \alpha_w \left(\frac{\partial^2 T_w}{\partial r^2} + \frac{\partial T_w}{r \partial r} \right) \qquad 0 < r < r_p \qquad t > 0$$

$$\text{IC:}\quad T_w = T_i \qquad 0 < r < r_o \qquad t = 0$$

$$\text{BC: (1)}\quad T_c = T_s \qquad r = r_o \qquad t > 0$$

$$\text{(2)}\quad T_c = T_w = T_p \qquad r = r_p \qquad t > 0$$

$$\text{(3)}\quad k_w \frac{\partial T_w}{\partial r} - k_c \frac{\partial T_c}{\partial r} = \rho_w (\Delta H) \frac{dr_p}{dt} \qquad r = r_p \qquad t > 0$$

$$\text{(4)}\quad \frac{\partial T_w}{\partial r} = 0 \qquad r = 0 \qquad t > 0$$

The system of equations is non-linear because of the convective term as well as the third boundary condition (Carslaw, Jaeger, 1959). It is of the same form as a simple phase change problem, with the exception of the convective term. Exact solutions on infinite domains are available (Stefan, 1891; Ockendon and Hodgkins, 1975). Comparable problems on finite geometries are usually solved numerically. Extensive bibliographies are available (Selim, Roberts, 1981; Wilson, et. al., 1978). The numerical procedure developed by Roberts (1981) is used here. This procedure is facilitated by the introduction of the following dimensionless parameters:

$$R = 1 - r/r_o \qquad \tau = \alpha_c \, t/r_o^2$$

$$U = \left(\frac{k_c}{k_w}\right) \frac{T_c - T_p}{T_p - T_i} \qquad V = \frac{T_w - T_p}{T_p - T_i}$$

$$T_s^* = \frac{k_c}{k_w} \frac{T_s - T_p}{T_p - T_i} \qquad T_i^* = \frac{T_i - T_p}{T_p - T_i} = -1$$

$$\alpha^* = \alpha_c / \alpha_w \qquad \Delta H^* = \frac{\alpha_c}{\alpha_w} \frac{\Delta H}{C_{pw}(T_p - T_i)}$$

$$B = 1 + b \frac{\rho_w}{\rho_c} \frac{C_{pg}}{C_{pc}} (R_p - 1) \frac{dR_p}{d\tau}$$

The dimensionless form of the system of equations is

$$\frac{\partial U}{\partial \tau} = \frac{\partial^2 U}{\partial R^2} + \frac{B}{R - 1} \frac{\partial U}{\partial R} \qquad 0 < R < R_p \quad \tau > 0 \qquad (1)$$

$$\frac{\partial V}{\partial \tau} = \frac{1}{\alpha^*} \frac{\partial^2 V}{\partial R^2} + \frac{1}{R - 1} \frac{\partial V}{\partial R} \qquad R_p < R < 1 \quad \tau > 0 \qquad (2)$$

IC $V = -1$ $\qquad 0 < R < 1 \quad \tau = 0 \qquad (3)$

BC $U = T_s^*$ $\qquad R = 0 \quad \tau > 0 \qquad (4)$

$U = V = 0$ $\qquad R = R_p \quad \tau > 0 \qquad (5)$

$$\frac{dR_p}{d\tau} = \left(\frac{\partial V}{\partial R} - \frac{\partial U}{\partial R} \right) \frac{1}{\Delta H^*} \qquad R = R_p \quad \tau > 0 \qquad (6)$$

$$\frac{\partial V}{\partial R} = 0 \qquad R = 1 \quad \tau > 0 \qquad (7)$$

Finite Difference Formulation

The finite difference form of the numerical algorithm requires a finite, non-zero value of R_p. If a fixed surface temperature is imposed with $T_s > T_p$, then the Stefan analytical solution is used to obtain a starting position of the pyrolysis front. A standard explicit finite difference scheme is used to advance through the first time step and a Dufort Frankel scheme (which requires

temperatures at a previous time) is used for all subsequent time steps. If a time dependent surface temperature, beginning with $T_s < T_p$ is imposed, then the numerical integration of the straight-forward conduction problem with no pyrolysis front is implemented until the temperature at a finite value of R reaches T_p, at which time the Dufort Frankel scheme with a moving boundary is begun. Temperatures at points adjacent to either terminus R = 0 or R = 1, or the moving boundary are calculated with the usual approximations. The details are presented below.

In order to approximate the solution of the parabolic partial differential equations, (1) and (2), a network of grid points with equal size in the R-direction and equal size in the time step is established throughout the region $0 < R < 1$, $0 < \tau$.

A DuFort-Frankel scheme (Carnahan, 1969) was chosen to obtain a finite difference solution to the parabolic partial differential equations. Adequate accuracy was obtained with 21 grid points and $\Delta t/(\Delta R)^2 < 0.5$.

The DuFort-Frankel Scheme requires data from two previous time levels. The standard explicit scheme is used as a starting method to provide the required data. Eqs. (1) and (2) expressed in the standard explicit scheme (see Figure 2) are given by

$$\frac{U_{i,j+1} - U_{i,j}}{\Delta\tau} = \frac{U_{i-1,j} - 2U_{i,j} + U_{i+1,j}}{(\Delta R)^2} + \frac{B}{(i\Delta R - 1)} \frac{(U_{i+1,j} - U_{i-1,j})}{2\Delta R} \qquad i = 1,2,\ldots,M-1 \qquad (8)$$

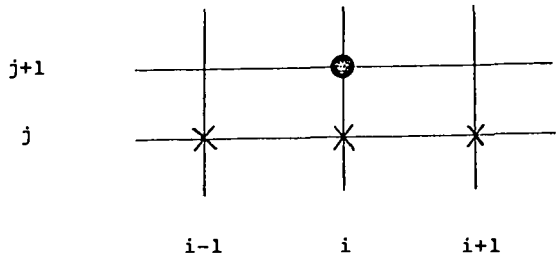

Standard Explicit Scheme

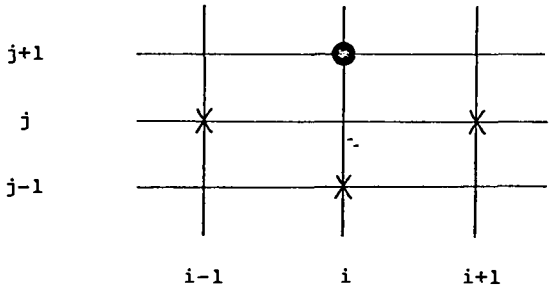

DuFort-Frankel Scheme

Figure 2: Graphic Description of Finite-Difference Scheme.

$$\frac{V_{i,j+1} - V_{i,j}}{\Delta\tau} = \frac{1}{\alpha^*}\frac{V_{i-1,j} - 2V_{i,j} + V_{i+1,j}}{(\Delta R)^2} + \frac{1}{(i\Delta R - 1)}\frac{(V_{i+1,j} - V_{i-1,j})}{2\Delta R} \qquad i = M+2, M+3, \ldots, N-1 \qquad (9)$$

and M indicates the nearest grid point to the left of the pyrolyzing front (see Figure 3). These two equations are rearranged and solved for the unknown terms $U_{i,j+1}$ and $V_{i,j+1}$ to give:

$$U_{i,j+1} = (1 - 2\lambda)U_{i,j} + \lambda\left[\left(1 - \frac{B}{2(i - \frac{1}{R})}\right)U_{i-1,j} + \left(1 + \frac{B}{2(i - \frac{1}{R})}\right)U_{i+1,j}\right] \qquad i = 1,2,\ldots,M-1 \qquad (10)$$

$$V_{i,j+1} = \left(1 - \frac{2\lambda}{\alpha^*}\right)V_{i,j} + \frac{\lambda}{\alpha^*}\left[\left(1 - \frac{1}{2(i - \frac{1}{\Delta R})}\right)V_{i-1,j} + \left(1 + \frac{1}{2(i - \frac{1}{\Delta R})}\right)V_{i+1,j}\right] \qquad i = M+2, M+3, \ldots, N-1 \qquad (11)$$

where $\lambda = \Delta\tau/(\Delta R)^2$.

Expressed in the DuFort-Frankel Scheme, Equations (1), (2) become

$$\frac{U_{i,j+1} - U_{i,j-1}}{2\,\Delta\tau} = \frac{U_{i-1,j} - U_{i,j+1} - U_{i,j-1} + U_{i+1,j}}{(\Delta R)^2} + \frac{B}{(i\Delta R - 1)}\frac{(U_{i+1,j} - U_{i-1,j})}{2\Delta R} \qquad i = 1,2,\ldots,M-1 \qquad (12)$$

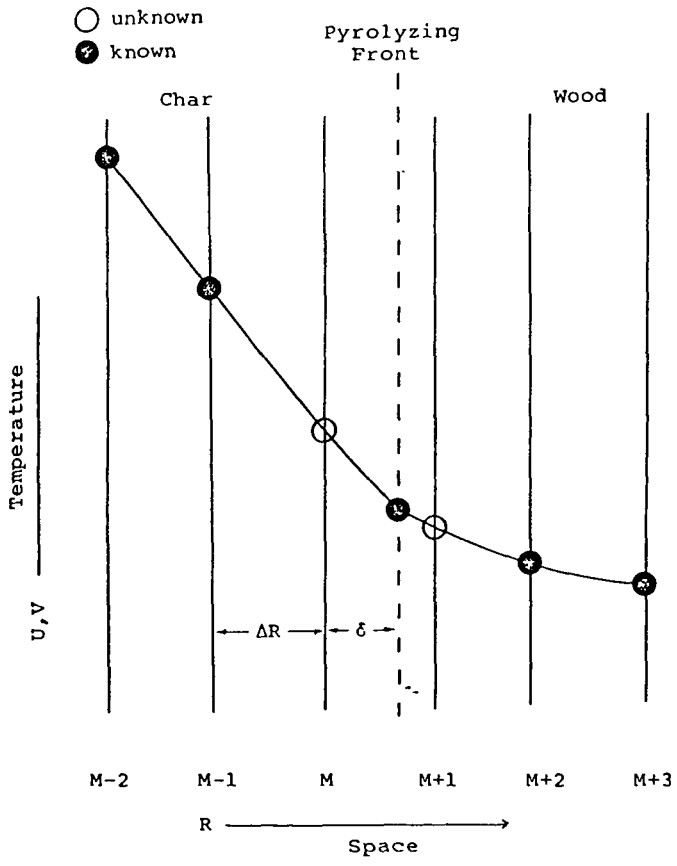

Figure 3: 3-Point Lagrangian Interpolation for the unknow temperature U_M, V_{M+1} Adjacent to the pyrolysis front.

$$\frac{V_{i,j+1} - V_{i,j-1}}{2\Delta\tau} = \frac{1}{\alpha^*} \frac{V_{i-1,j} - V_{i,j+1} - V_{i,j-1} + V_{i+1,j}}{(\Delta R)^2} +$$

$$\frac{1}{(i\Delta R - 1)} \frac{(V_{i+1,j} - V_{i-1,j})}{2\Delta R} \qquad i = M+1, M+2, \ldots, N \qquad (13)$$

Equations (12) and (13) are rearranged and solved for the unknown terms $U_{i,j+1}$, $V_{i,j+1}$ to give

$$U_{i,j+1} = \frac{1 - 2\lambda}{1 + 2\lambda} U_{i,j-1} + \frac{2\lambda}{1 + 2\lambda} \left[\left(1 - \frac{B}{2(i - \frac{1}{\Delta R})}\right) U_{i-1,j} + \left(1 + \frac{1}{2(i - \frac{1}{\Delta R})}\right) U_{i+1,j} \right] \qquad i = 1,2,\ldots,M-1 \qquad (14)$$

$$V_{i,j+1} = \frac{1 - \frac{2\lambda}{\alpha^*}}{1 + \frac{2\lambda}{\alpha^*}} V_{i,j-1} + \frac{\frac{2\lambda}{\alpha^*}}{1 + \frac{2\lambda}{\alpha^*}} \left[\left(1 - \frac{1}{2(i - \frac{1}{\Delta R})}\right) V_{i-1,j} + \left(1 + \frac{1}{2(i - \frac{1}{\Delta R})}\right) V_{i+1,j} \right] \qquad i = M+1, M+2, \ldots, N \qquad (15)$$

The singularity of Equation (2) at R = 1 is prevented by using L'Hopital's rule to yield

$$\frac{\partial V}{\partial \tau} = -\frac{2}{\alpha^*} \frac{\partial^2 V}{\partial R^2} \qquad R = 1 \quad \tau > 0 \qquad (16)$$

This equation written in the standard explicit form is given by

$$\frac{V_{i,j+1} - V_{i,j}}{\Delta\tau} = \frac{2}{\alpha^*} \frac{(V_{i-1,j} - 2V_{i,j} + V_{i+1,j})}{(\Delta R)^2} \qquad (17)$$

and in the Dufort-Frankel Scheme by

$$\frac{V_{i,j+1} - V_{i,j-1}}{2\Delta T} = -\frac{2}{\alpha^*} \frac{(V_{i-1,j} - V_{i,j+1} - V_{i,j-1} + V_{i+1,j})}{(\Delta R)^2} \qquad i = N \qquad (18)$$

Equation (7) can be written in finite-difference form using a central difference approximation to give

$$\frac{V_{N+1,j} - V_{N-1,j}}{2\Delta R} = 0.$$

Combined with Equation (18) this yields an expression for the center-line dimensionless temperature

$$V_{N,j+1} = (1 - \frac{4\lambda}{\alpha^*})V_{N,j} + \frac{4\lambda}{\alpha^*} V_{N-1,j} \qquad R = 1 \qquad (19)$$

in the standard explicit form and

$$V_{N,j+1} = \frac{1 - \frac{4\lambda}{\alpha^*}}{1 + \frac{4\lambda}{\alpha^*}} V_{N,j-1} \quad \frac{\frac{8\lambda}{\alpha^*}}{1 + \frac{4\lambda}{\alpha^*}} V_{N-1,j} \qquad R = 1 \qquad (20)$$

in the DuFort-Frankel Scheme.

Grid Points M, M+1

The temperatures at grid points immediately adjacent to the pyrolyzing front (grid points M and M+1 in Figure 3) cannot be calculated by Equations (10)-(11) and (14)-(15). Instead, a three-point Lagrangian interpolation is used to determine these unknown temperatures.

$$U_{M,j} = \frac{-\delta}{(2\Delta R + \delta)} U_{M-2,j} + \frac{2\delta}{(\Delta R + \delta)} U_{M-1,j} \qquad i = M \qquad (21)$$

$$V_{M+1,j} = \frac{2(\Delta R - \delta)}{(2\Delta R - \delta)} V_{M+2,j} + \frac{(\Delta R - \delta)}{(3\Delta R + \delta)} V_{M+3,j} \qquad i = M+1 \tag{22}$$

Where

$$\delta = R_p - R_M = R_p - M\Delta R$$

Grid Points M = 1,2

When the pyrolyzing front is located within the first grid space, Equation (21) is not required, since the boundary value $U_{0,j}$ is already known.

If the pyrolyzing front is located within the second grid space, Equation (21) cannot be used because the required three points are not available. By assuming that the temperature profile within the char layer is quadratic in R, the derivatives U/τ, U/R, $^2U/R^2$ in equation (1) can be approximated to yield.

$$\frac{U_{2,t+1} - U_{2,t}}{\Delta\tau} = \frac{2}{\Delta R(\Delta R + \delta)} U_{1,t} - \frac{2}{\Delta R(\delta)} U_{2,t+1} - \left(\frac{B}{\Delta R - 1}\right)\left(\frac{\delta}{\Delta R(\Delta R + \delta)}\right)U_{1,t}$$

$$- \left(\frac{\Delta R - \delta}{\Delta R(\delta)}\right)U_{2,t+1} \tag{23}$$

which can be solved for $U_{2,t+1}$

Advancing the Pyrolysis Front

Euler's method (Carnahan, 1969) is used to solve the energy balance across the pyrolyzing surface, Eq. 9. The march of the pyrolysis front is computed from the following finite difference form of Eq. 9.

$$R_p\Big|_{\tau=\tau+\Delta\tau} - R_p\Big|_{\tau} = \Delta R_p = \frac{\Delta\tau}{\Delta H^*}\left(\frac{\partial U}{\partial R} - \frac{\partial V}{\partial R}\right)\Bigg|_{R=R_p},$$

The temperature gradients are approximated by differentiation of the three-point Lagrangian interpolation formulas, Equations (21) and (22), to give

$$\left(\frac{\partial U}{\partial R}\right)_{R=R_p} = \frac{(\Delta R + \delta)}{(2\Delta R + \delta)\Delta R} U_{M-2,j} - \frac{(2\Delta R + \delta)}{(\Delta R + \delta)\Delta R} U_{M-1,j} \tag{24}$$

$$\left(\frac{\partial V}{\partial R}\right)_{R=R_p} = \frac{(3\Delta R - \delta)}{(2\Delta R - \delta)\Delta R} U_{M+2,j} - \frac{(2\Delta R - \delta)}{(3\Delta R - \delta)\Delta R} U_{M+3,j} \tag{25}$$

When the pyrolyzing front is within the first grid space, two point interpolation formulas are used to approximate the temperature gradient in the char layer.

$$\left(\frac{\partial U}{\partial R}\right)_{R=R_p} = -\frac{U_{1,j}}{R_p} \tag{26}$$

When the pyrolyzing front is located within the second grid space, a quadratic polynomial is used to approximate the temperature gradient in the char layer. The gradient at the pyrolyzing front is

$$\left(\frac{\partial U}{\partial R}\right)_{R=R_p} = \frac{-\delta}{\Delta R(\Delta R + \delta)} U_{1,j} - \frac{\Delta R + \delta}{\Delta R(\delta)} U_{2,j} \tag{27}$$

Since the temperature of the unreacted core is so close to the pyrolysis temperature when the pyrolyzing front moves into the last two grid spaces, a two point interpolation formula is used to approximate the temperature gradient in the wood layer. The temperature of the unreacted core is taken equal to the pyrolysis temperature and the temperature gradient in the wood layer at $R = R_p$ becomes equal to zero thereafter.

Since the advance of the front during the last time step may place it beyond R = 1, a three point Lagrangian interpolation formula is used to find the time required for complete the pyrolysis.

$$\tau_p = \frac{(1 - R_{p2})(1 - R_{p3})}{(R_{p1} - R_{p2})(R_{p1} - R_{p3})}\tau_1 + \frac{(1 - R_{p1})(1 - R_{p3})}{(R_{p2} - R_{p1})(R_{p2} - R_{p3})}\tau_2 + \frac{(1 - R_{p1})(1 - R_{p2})}{(R_{p3} - R_{p1})(R_{p3} - R_{p2})}\tau_3$$

Where R_{p1}, R_{p2}, R_{p3} = the last three computed R_p values.

τ_1, τ_2, τ_3 = the three times corresponding to the above values.

SENSITIVITY STUDY

Using the numerical procedures described above, temperature profiles at various times were generated. Sample profiles are illustrated in figure 4. The time required for the pyrolysis front to reach the centerline of the cylinder was defined as t_{pyr}.

The effect of each model parameter on the time required for complete pyrolysis was studied in order to determine its relative importance. A base case was constructed by selecting average values for the parameters (as listed in Table 1) and calculating the pyrolysis time. Values of t_{pyr} were then determined for several cases in which each parameter was varied individually. Sensitivity was defined as $\Delta t_{pyr}/\Delta p$, where Δp is the change in the value of the parameter studied from its base value. A negative sensitivity indicates increasing p will decrease t_{pyr}.

The results of the sensitivity study are summarized in Table 2 and illustrated in Figure 5.

Temperature Profile

With Convection Term.

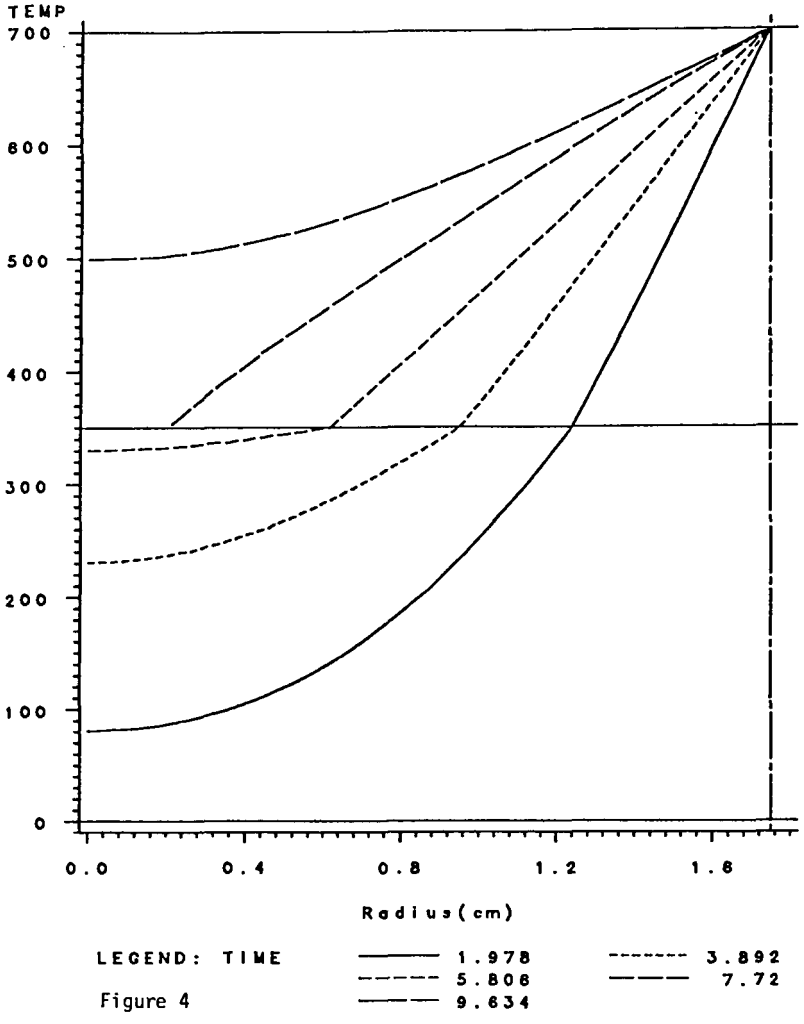

Figure 4

Table 1

Typical Values of Model Parameters Used in Sensitivity Study

ρ_w =	1230.0	Kg/M^3
ρ_c =	$\rho_w(1-b)$	
C_{pw} =	1318.0	Joule/Kg
C_{pc} =	991.6	Joule/Kg
k_w =	0.2000	Joule/M-Sec-K
k_c =	0.20	Joule/M-Sec-K
r_o =	0.01	m
T_s =	700.0	C
T_p =	350.0	C
T_i =	25.0	C
b =	0.7	
ΔH =	368200	Joule/kg of wood

Table 2

Relative Importance of Model Parameters for a Particle 2 cm in Diameter

Parameter	Sensitivity Range	Parameter Range Studied	Relative Importance
r_o	1.5 -- 3.0	0.5 - 2.0 cm	1
T_s	-38.1 -- -0.73	360 - 1050 C	2
k_c	-1.73 -- -0.46	0.1 - 0.4 Joule/M-Sec-K	3
ρ_w	1.0	615 - 2460 (Kg/M^3)	4
T_p	-0.66 -- -1.54	175 - 525 C	5
ΔH	0.5 -- 0.47	184100 - 763640 Joule/Kg	6
C_{pw}	0.28 -- 0.30	659 - 2636 Joule/Kg-K	7
k_w	-0.14 -- -0.07	0.1 - 0.4 Joule/M-Sec-K	8
C_{pg}	0.14 -- 0.13	600 - 2400 Joule/Kg-K	9
C_{pc}	0.07 -- 0.06	495.8 - 1983.2 Joule/Kg-K	10
b	-0.012 -- - 0.027	0.3 - 0.9	11
T_i	-0.0144 -- -0.015	0 - 300 C	12

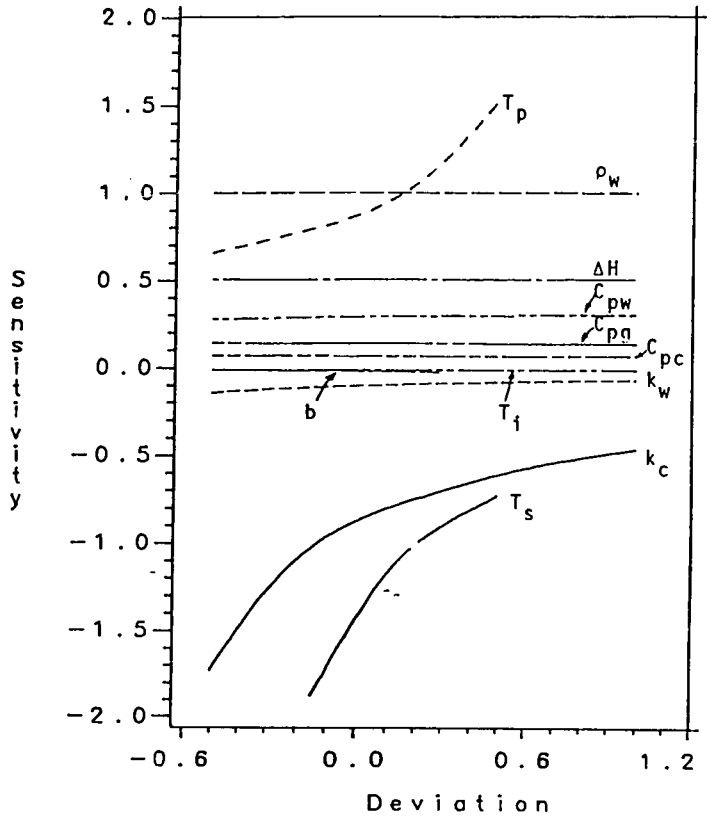

Figure 5 : Sensitivity of Model Parameters for a Particle of 2cm in Diameter

Particle Size and Density (r_o, ρ_w)

As expected, the pyrolysis time varied approximately quadratically with r (cylindrical geometry) and linearly with ρ_w indicating that for the size range studied, t_{pyr} is proportional to the mass of the sample.

Characteristic Temperatures (T_s, T_p, T_i)

For a particle 2 cm diameter, the imposed surface temperature has the greatest effect of all parameters in the determining pyrolysis time. When T_s is 525, 700, 875°C, the corresponding pyrolysis times are 8.8, 5.6, and 4.3 minutes. The pyrolysis temperature has a moderate influence on t_{pyr} when varied over a physically meaningful range. When T_p is varied from 263 to 350°C, t_{pyr} increases from 4.5 to 5.6 minutes. The initial temperature, T_i, has a negligible effect. The sensitivities of these parameters are illustrated in Figure 5. Plots of front position vs. time for a wide range of the parameters T_s, T_p, and T_i appear in Figures 6, 7, and 8.

Thermal Conductivities (k_c, k_w)

Due to the nature of the model, the thermal conductivity of the char is the most sensitive of all the physical properties considered. The thermal conductivity of the virgin solid however, has a negligible influence on the time required for complete pyrolysis. The comparison is best illustrated by the front position vs. time plots when the above parameters are varied (Figures 9, 10).

When k_c is varied from .1 to .4 J/msK t_{pyr} varies from 10 to 3 minutes. Over the same range of values for k_w, t_{pyr} varies from 6 to 5.2 minutes.

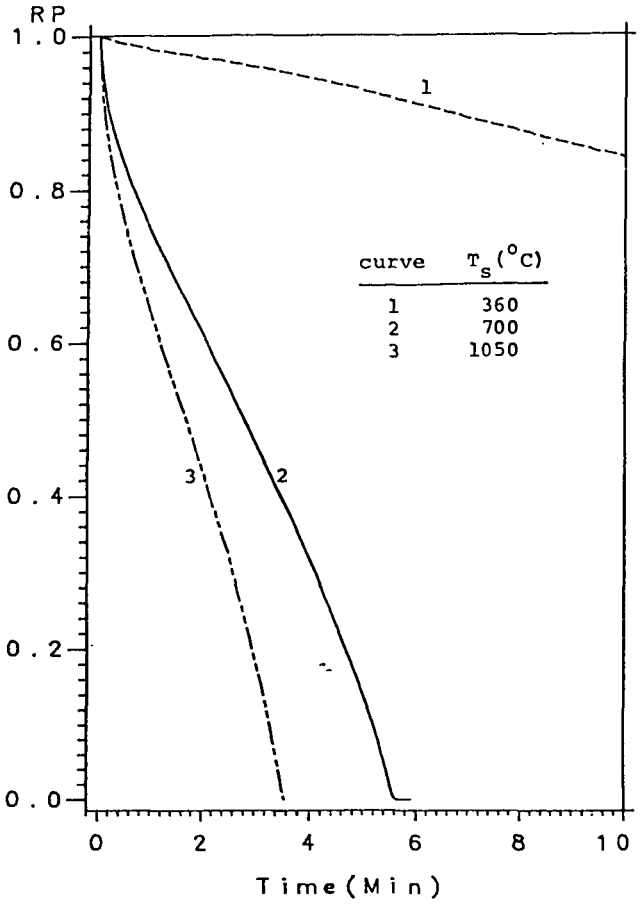

Figure 6: Pyrolyzing Front vs. Time curves at Three Surface Temperatures for a Particle of 2 cm Diameter

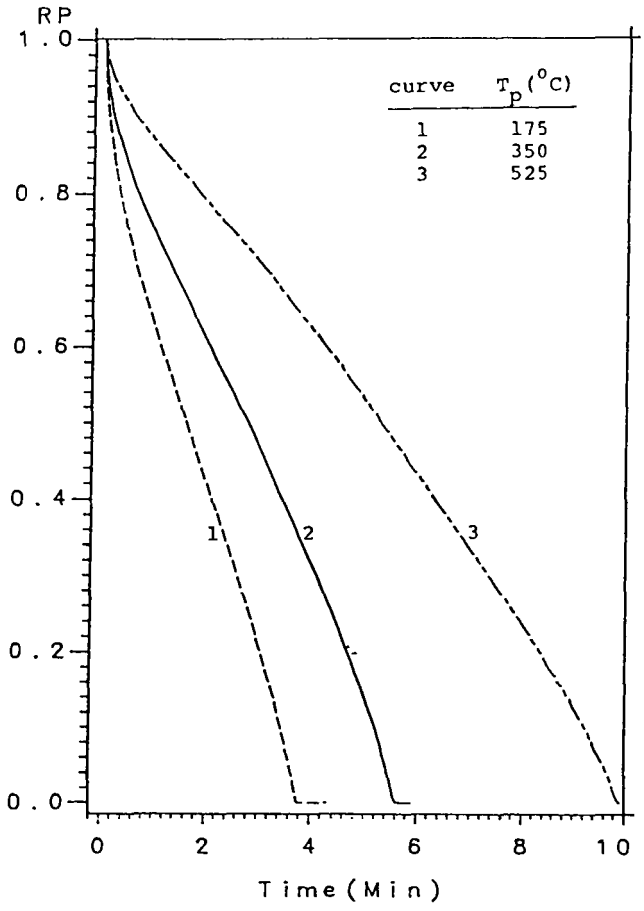

Figure 7 : Pyrolyzing Front vs. Time curves at Three Pyrolysis Temperatures for a Particle of 2 cm Diameter

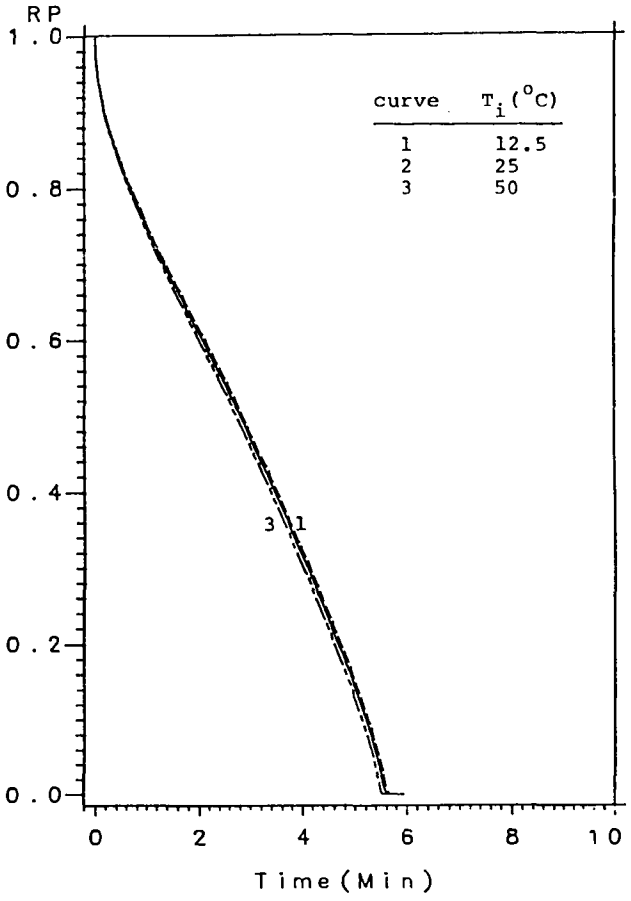

Figure 8: Pyrolyzing Front vs. Time Curves at Three Values of Initial Temperatures for a Particle of 1 cm Radius

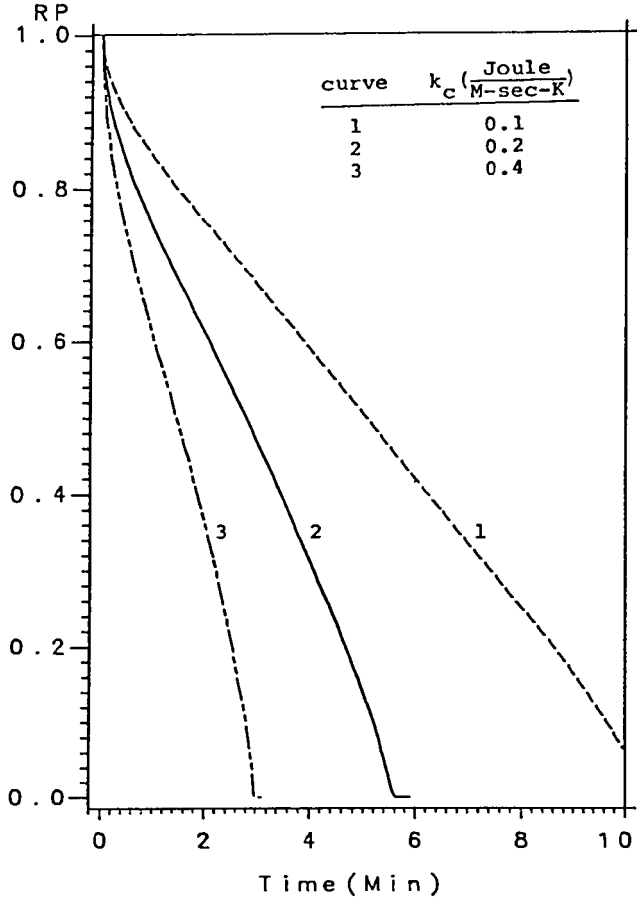

Figure 9 : Pyrolyzing Front vs. Time Curves at Three Values of Char Thermal Conductivity for a Particle of 1 cm Radius

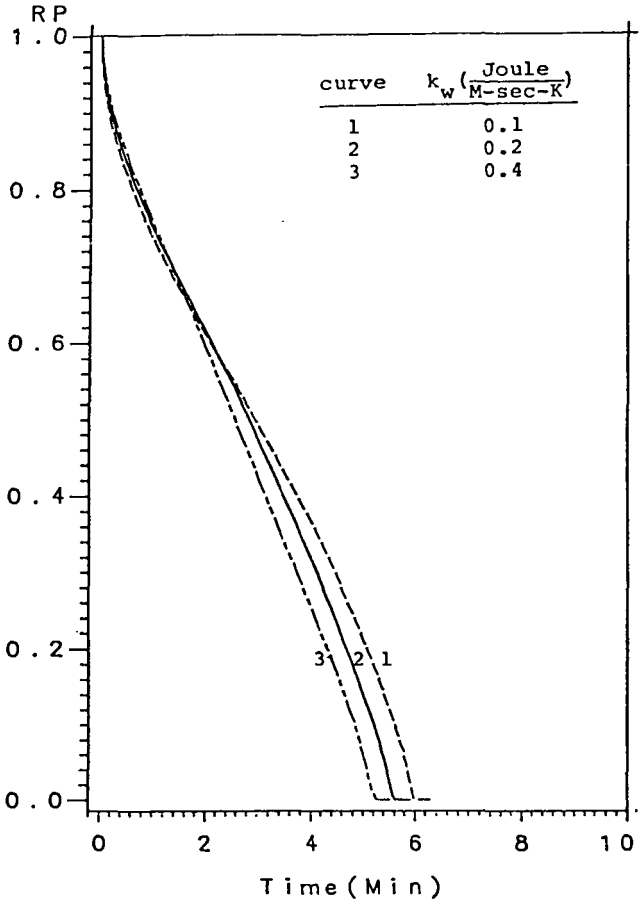

Figure 10: Pyrolyzing Front vs. Time Curves at Three Values of Thermal conductivity of Wood for a Particle of 1 cm Radius

Heat Capacities (C_{pc}, C_{pw})

The heat capacity of the unpyrolyzed solid, C_{pw}, has a greater influence on the rate of pyrolysis than the corresponding property for the resultant char, C_{pc}. The comparison is most directly illustrated in Figures 11 and 12.

Stoichiometric Coefficient (b)

When the stoichiometric coefficient of the gaseous product in the reaction

wood = b gas + c char

is varied over a wide range, there is virtually no change in the time required for pyrolysis (see Figure 13). It appears that the changing density of the char $\rho_c = \rho_w(1-b)$ counteracts the effect of the convective term in the energy balance.

Heat of Pyrolysis (H)

As illustrated in Figure 14, when the endothermic heat of primary pyrolysis varied from 184.1 to 736.4 J/g, the pyrolysis time increased from 4.2 to 8.4 minutes.

Summary

The results of any simulation using the phase-change model of pyrolysis are most significantly affected by the values of pyrolysis temperature, char thermal conductivity, and heat of pyrolysis.

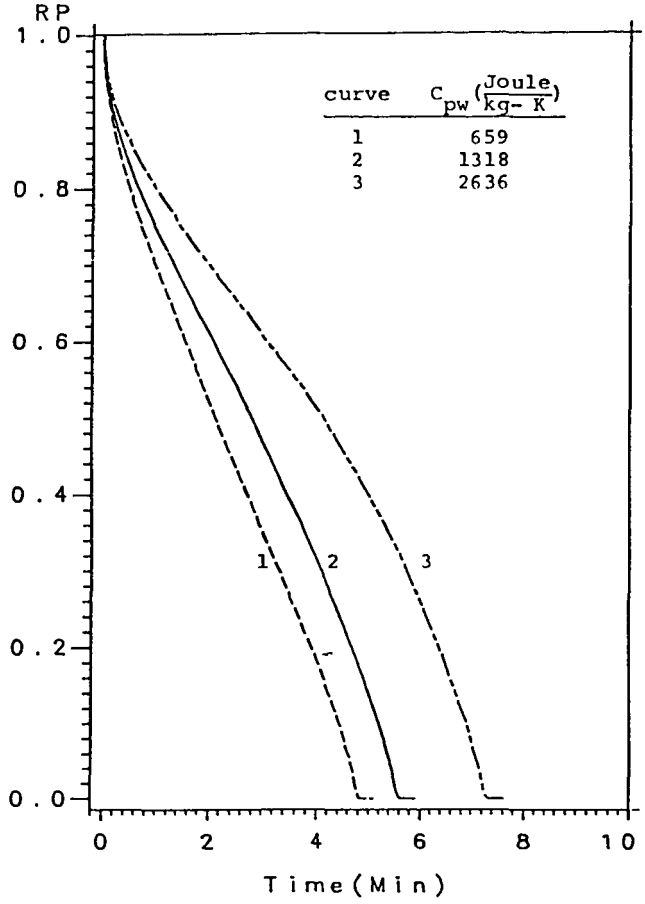

Figure 11: Pyrolyzing Front vs. Time Curves at Three Values of Heat Capacity of Wood for a Particle of 1 cm Radius

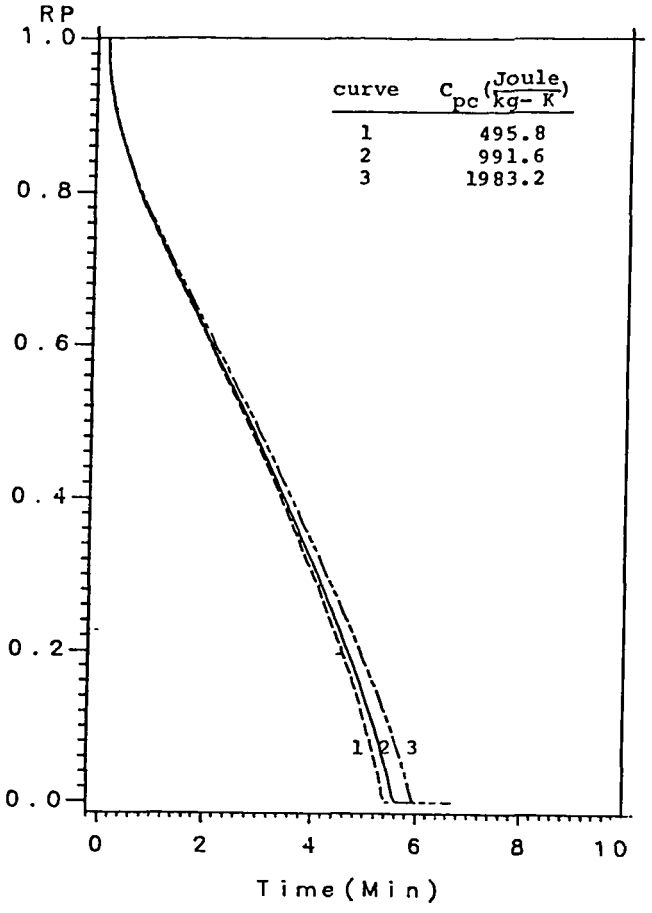

Figure 12: Pyrolyzing Front vs. Time Curves at Three Values of Heat Capacity of Char for a Particle of 1 cm Radius

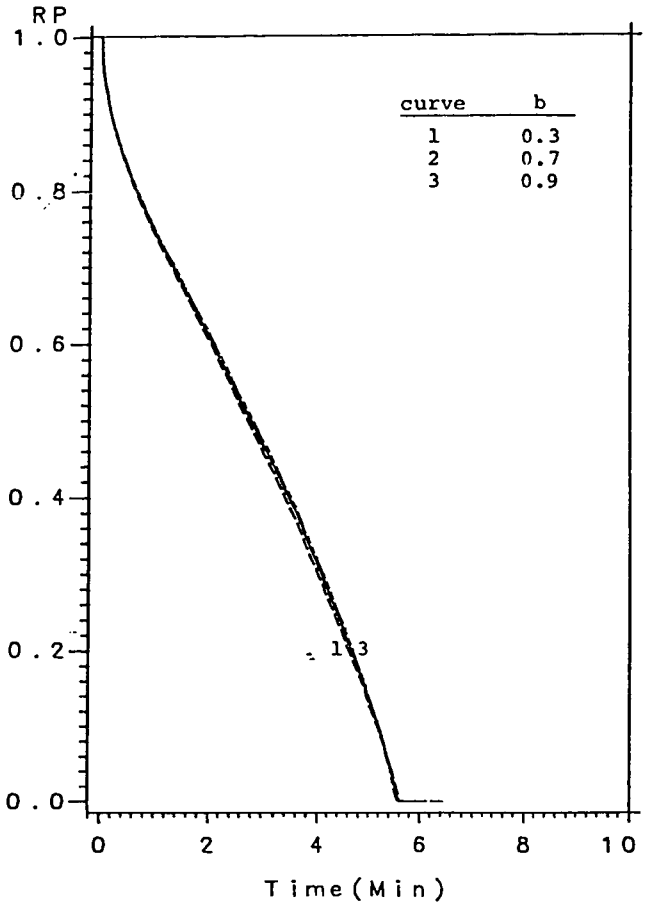

Figure 13: Pyrolyzing Front vs. Time Curves at Three Values of Stoichiometric Coefficient of Pyrolysis Gas for a Particle of 1 cm Radius

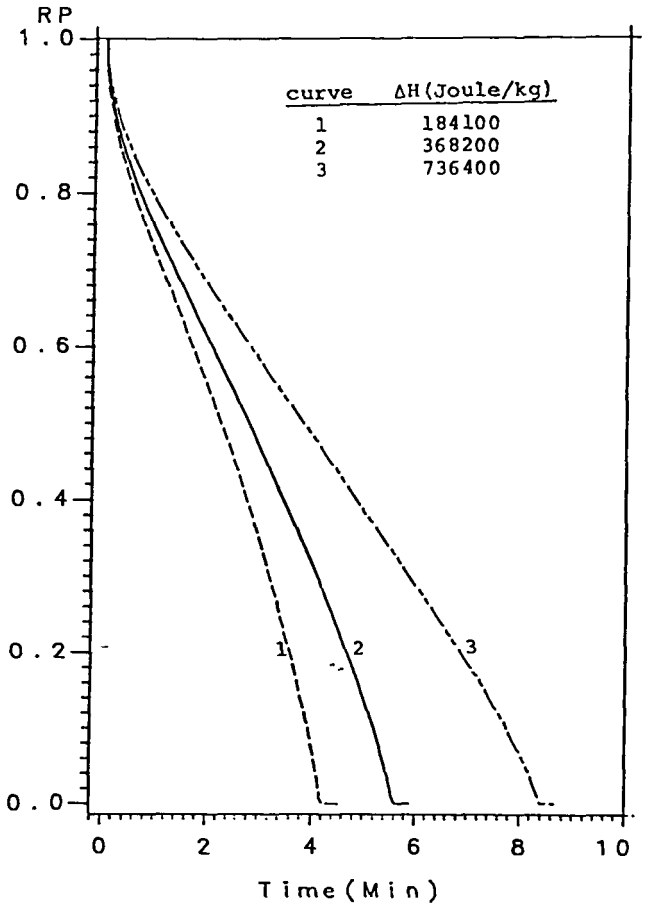

Figure 14: Pyrolyzing Front vs. Time Curves at Three Values of Heat of Pyrolysis for a Particle of 1 cm Radius

SINGLE PARTICLE SIMULATIONS

Up to the present time we have investigated only the case of a boundary condition of the first kind, in which the surface temperature is specified. The more useful case of a convective boundary condition (B.C. of 3rd kind) is currently under study. The choice to study the former problem was made on the basis of available experimental data. Investigators performing pyrolysis experiments on single particles usually measure and report surface temperature.

In one experiment (Kanury, 1966) a cylindrical specimen 1.75 cm in radius of pressed α-cellulose was placed in an externally-heated, rotating copper tube. Temperature profiles were recorded by thermocouples embedded at various radii. Measured surface and centerline temperatures are plotted in Figure 15. Using the parameters listed in Table 3 and the measured surface temperature as a boundary condition, the centerline temperature was calculated using the phase-change model. The calculated profile is also plotted in Figure 15.

The experimental profile displays plateaus at 120°C and 380°C corresponding to drying and pyrolysis temperatures. The calculated profile cannot reproduce the drying plateau because no phase change corresponding to drying was incorporated in the model. The plateau corresponding to pyrolysis however, was clearly observed. The measured surface temperature after complete pyrolysis was erratic because the thermocouple at the surface was not tightly bonded to the char.

In a second experiment (Roberts and Clough, 1963) the weight loss history of a 1 cm (radius) beech cylinder was recorded during pyrolysis in a nitrogen atmosphere. Using the parameters in Table 4 and the measured surface temperature, the weight vs. time curve was calculated. The results are shown in Figure 16. The heating rate of the oven used in the experiment was 20°C/min. Since the model predicts no weight loss until the surface temperature reaches the assumed

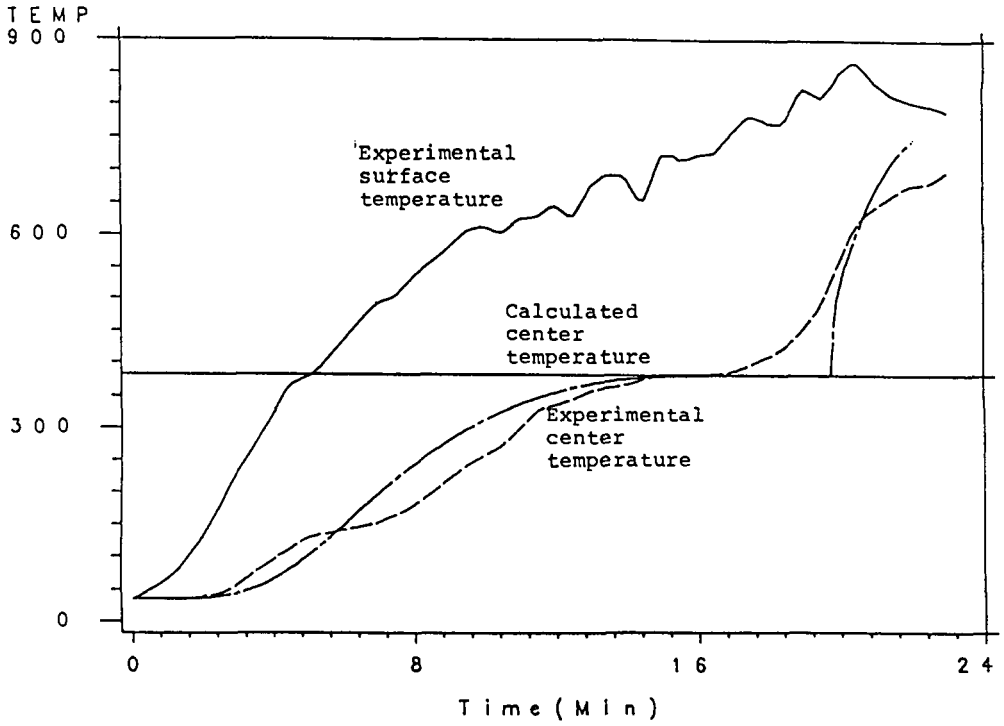

Figure 15 : Comparison between Experimental and Calculated Temperature History.

Table 3

Parameters and Properties Used to Simulate Kannry's Experiment

ρ_w	= 605	(Kg/M^3)
ρ_c	= (1-b) $_w$	(Kg/M^3)
k_w	= 0.14	(Joule/M-Sec-K)
k_c	= 0.06	(Joule/M-Sec-K)
C_{pc}	= 991.6	(Joule/Kg-K)
C_{pw}	= 1318.0	(Joule/Kg-K)
C_{pg}	= 1200	(Joule/Kg-K)
b	= 0.80	
H	= 100000	(Joule/Kg)
T_p	= 382	C
T_i	= 35	C

Table 4

Representative Values of Parameters and Properties Used in Model Calculation for Beech Cylinder

ρ_w	= 600.0	(Kg/M^3)
ρ_c	= (1-b) ρ_w	(Kg/M^3)
k_w	= 0.14	(Joule/M-Sec-K)
k_c	= 0.04	(Joule/M-Sec-K)
C_{pw}	= 1318.0	(Joule/M-Sec-K)
C_{pc}	= 991.6	(Joule/Kg-K)
C_{pg}	= 1200.0	(Joule/Kg-K)
b	= 0.61	
ΔH	= 100000	(Joule/Kg)
T_p	= 290	C
T_i	= 25	C

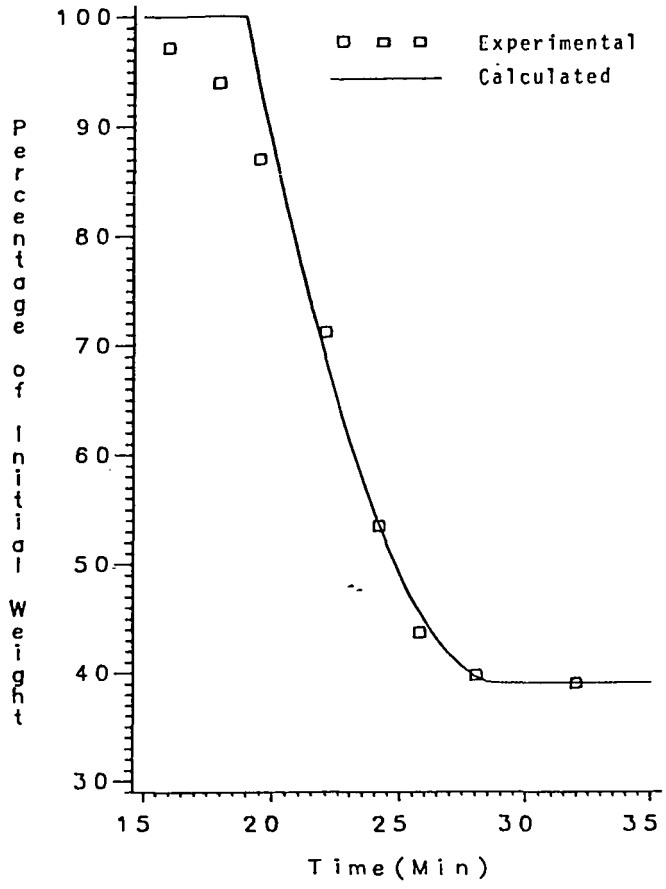

Figure 16: Comparison between Calculated and Experimental Weight/Time Curves for a Pyrolyzing Beech Cylinder.

pyrolysis temperature, it cannot reproduce that portion of the measured curve corresponding to low temperature pyrolysis.

PYROLYSIS ZONE OF A PACKED-BED GASIFIER

In order to simulate the pyrolysis zone of a packed-bed gasifier, the reactor was treated conceptually as two ideal reactors: one, a char combustor/gasifier and the second, a feed pyrolyzer. The gas temperature and flowrate exiting the gasification zone were used as input parameters for the pyrolysis simulation. The other boundary conditions were the offgas and feed temperatures.

The pyrolysis reaction is

$$\text{Feed} \longrightarrow \text{Char} + \text{Oil} + H_2O + \text{Gas}$$

The reaction is driven by the sensible heat in the char-derived gases from the combustion zone. The char-derived gas is considered inert and the offgas composition is obtained by simply mixing the char-derived gas flow with the volatile products of the pyrolysis reaction. The temperature of the gas, which is assumed to be the same as the surface temperature of the solid pellets, is used as the boundary condition of the kinetics-free model. We also assume that the pyrolysis portion of the reactor is characterized by plug flow, with no important radial gradients of mass or temperature.

Material balances were taken over the gas and solid phases.

$$dG_g/dZ = R_g \qquad dG_s/dZ = R_s$$

The energy balance was taken as

$$\frac{d}{dZ}(G_g C_{pg} T_g) = Q_s a + R_s \quad H_2$$

The generation terms are the flux ($Q_s a$) into the pellets and $R_s \Delta H_2$, the exothermic heat of reaction of the volatiles, both based on unit volume of reactor. ΔH_2 is the difference between the exothermic heat of the overall pryolysis reaction and the endothermic heat of the primary pyrolysis step used in the phase change model.

A Runge Kutta method was used to integrate the system of equations. An axial temperature profile for the bed was assumed. This profile was used in the phase change model to calculate the reaction rate and heat flux as a function of time. The velocity of the solid phase was constant (no particle shrinkage) so time was proportional to distance along the bed. The bed temperature was calculated and the process repeated until the boundary conditions were satisfied.

For the conditions listed in Table 5, the calculated profile illustrated in Figure 17 was obtained.

FUTURE WORK

A convective boundary condition (B.C. of 3rd kind) using effective heat transfer coefficients will be investigated. The heat transfer correlations for particles in packed beds will be modified to account for the escape of volatiles from the surface of the char. Single particle experiments are being planned in which the convective environment (gas temperature and velocity) of the sample will be controlled. Gas temperatures can be measured more easily than solid surface temperatures. In addition, packed-bed experiments with thermocouple-studded samples are planned.

Table 5

Operating Conditions for the Test Run on the Biomass Gasifier

Wood Pellett Feed Rate (Kg/Hour)	15.8
Air Feed Rate (Kg/Hour)	9.678
Steam Feed Rate (Kg/Hour)	1.941

Parameters of Char and Wood Pellets Used to Simulate the Test Run of the Biomass Gasifier

ρ_w	= 1230.0	Kg/M^3
ρ_c	$= \rho_w(1-b)$	Kg/M^3
C_{pw}	= 1318.0	Joule/Kg
C_{pc}	= 991.6	Joule/Kg
k_w	= 0.03	Joule/M-Sec-K
k_c	= 0.005	Joule/M-Sec-K
r_o	= 0.003175	m
T_p	= 300.0	C
T_i	= 25.0	C
b	= 0.8	
ΔH	= 62760	Joule/Kg of wood
ΔH_2	= -368200	Joule/Kg of wood

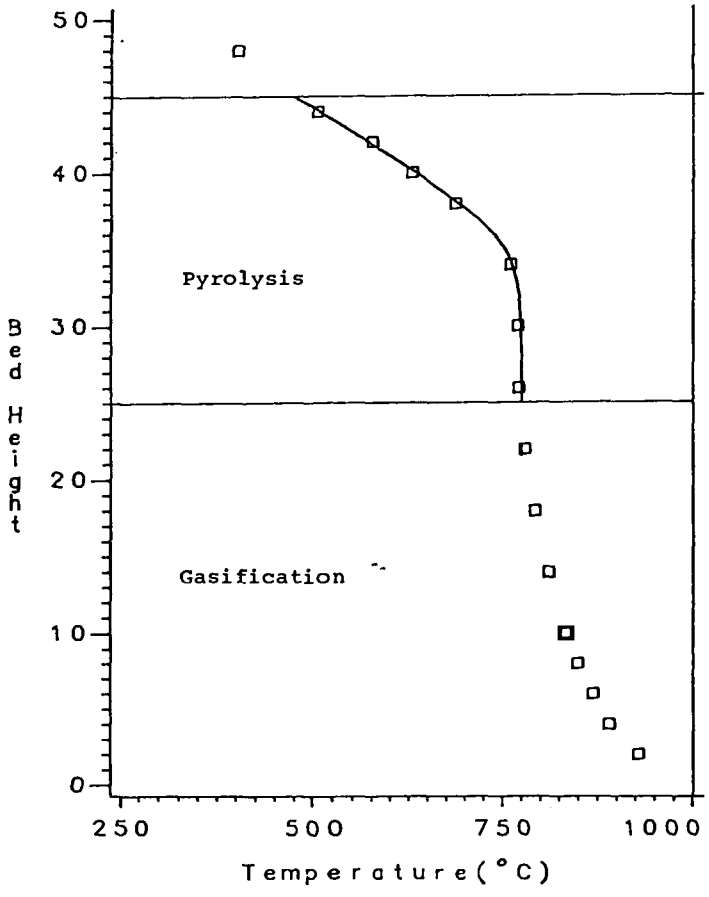

Figure 17: Comparison Between Calculated and Experimental Temperature Profiles in a Packed-Bed Gasifier.

Nomenclature

α	Thermal diffusivity
b	Stoichiometric coefficient of char in the pyrolysis reaction
B	Dimensionless parameter arising from the convective term in the char layer
c_p	Heat capacity
	Distance of pyrolyzing front from nearest grid point in the char layer
k	Thermal conductivity
M	Index of grid point in the char layer nearest the pyrolyzing front
N	Number of grid points
	Density
r	Radial position (r = 0 at center)
r_o	Cylinder radius at surface
R	Dimensionless radial distance (R = 0 at surface, R = 1 at center)
T	Temperature
	Dimensionless time
U,V	Dimensionless temperature
u_g	Velocity of exiting volatiles

Subscripts:

w	Wood layer, virgin solid
c	Char layer
p	Pyrolysis
s	Surface
g	Gas

References

Ackendon, J. R.; Hodgkins, W. R., Moving Boundary Problems in Heat Flow and Diffusion, Clarendon Press, Oxford (1975).

Bamford, C. H., Crank, J. and Malan, D. H., "The Combustion of Wood, Part I," Proc. of Cambridge Phil. Soc., 42, 166-184 (1946).

Carnahan, B., Luther, H. A., Wilkes, J. O., Applied Numerical Method, John Wiley and Sons, New York (1969).

Carslaw, H. S., Jaeger, J. C., Conduction of Heat in Solids, Oxford University Press, London (1959).

Fan, L. S., Fan, L. T., Tojo, K., Walawender, W. P., "Volume Reaction Model for Pyrolysis of a Single Solid Particle Accompanied by a Complex Reaction," Can. J. of Chem. Engr., 56, 603-609 (1978).

Maa, Sheng-Shyong P., "Influence of Particle Size and Environmental Condition on High Temperature Pyrolysis of the Cellulosic Material--I (Theoretical)," Combustion Science and Technology, 7, 257-269 (1973).

Muhlenkamp, S. P., "Pyrolysis of Living Wildland Fuels," Ph.D. Dissertation, University of Oklahoma, Norman, Oklahoma (1975).

Murty, K. A., Blackshear, P. L., "An X-Ray Photographic Study of the Reaction Kinetics of O-Cellulose Decomposition," Pyrodynamics, 4, 285-298 (1966).

Murty, K. A., "An Evaluation of The Physico-Chemical Factors Influencing the Burning Rate of Cellulosic Fuels and a Comprehensive Model for Solid Fuel Pyrolysis and Combustion," Ph.D. Dissertation, University of Minnesota (1969).

Roberts, A. F., Clough, G., "Thermal Decomposition of Wood in an Inert Atmosphere," Ninth Symposium (International) on Combustion, 158-166 (1963).

Roberts, D. L., "Numerical Solution of Heat Conduction Problem with a Change of Phase," Master Thesis, Texas Tech University (1981).

Stefan, Ann. Phys. u. Chem., N.F., 42, 269 (1891).

Wilson, D. G., Solomon, A. D., Boggs, P. T., Moving Boundary Problems, Academic Press (1978).

EXPERIMENTAL MEASUREMENT OF ABLATION RATE OF WOOD PIECES, UNDERGOING FAST PYROLYSIS BY CONTACT WITH A HEATED WALL.

J. LEDE, J. PANAGOPOULOS and J. VILLERMAUX

Laboratoire des Sciences du Génie Chimique, CNRS-ENSIC, 1 rue Grandville 54042 NANCY (France)

1. INTRODUCTION

The conventional pyrolysis of biomass yields about equal amounts of gases, char and tar. When pyrolysis is carried out in severe heating conditions, the reaction products can be almost entirely gaseous and contain significant amounts of light unsaturated hydrocarbons. Authors involved in such research, generally recommend several types of conditions : small wood particles, high temperatures, high heating rates, high heat fluxes, etc. Few of them [1,3,5,6] have associated the idea of ablation regime, to the observation of the fast pyrolysis reaction. Actually, the apparent rate of reaction is a function of two competitive processes within the wood particle : the rate of heat transfer and the rate of chemical decomposition of wood itself. If chemical processes are very fast, the heat transfer is rate controlling: this is the so called ablation regime characterized by a thin superficial layer of reacting wood). Such a regime can be represented by the rate at which the reacting layer moves towards the cold unreacted core of the piece of wood (ablation rate v) and the thickness of this reacting layer (e).

2. EXPERIMENTAL SET UP (Fig. 1)

The experimental system consists in a stainless steel disks (diameter: 7.5×10^{-2} m) spinning at a constant velocity (of the order of 1 $m.s^{-1}$) and heated by four gas burners located under the disk. The mean temperature is measured with a thermocouple pressed on the upper face. Rods of beech wood (2,3,4,6 and 10×10^{-3} m diameter) are vertically applied on the hot surface under known and variable pressures. A jet of argon is directed towards the contact surface in order to prevent spontaneous inflammation in air. No significant rise of wood temperature and no subsequent reaction is observed when the spinning disk is not heated. This eliminates the possibility of frictional heating effects. The experiments reported here are carried out in conditions of independence of reaction rate upon disk velocity. It is to be noticed that no change in the apparent rate was observed when a notched disk was used. The reaction produces gases and liquids undergoing further gasification on the disk surface. The presence of intersticial fluid between wood and steel acts as a kind of lubricant making the frictional contacts smoother.

The apparent rate of reaction **v** is obtained by direct measurement of the time required for a known length of rod to be consumed. The thickness of the ablation layer e is estimated by microscopic measurement of the extent of the uniformly darkened zone near the surface.

3. EXPERIMENTAL RESULTS

The variations of v and e were studied as a function of disk temperature (T_W), rod diameter (d), and pressure (P) under which the rods were pressed onto the disk. The pressure was controlled by placing known weights on the upper part of the rod (Fig. 1).

3.1. Variations of e with v

Fig. 2 shows some typical values of e as a function of **v** for T_W = 873 K and $d = 3 \times 10^{-3}$ m. The large dispersion of points is explained by the difficulty of measurement of e:: wood is a very heterogeneous material and the boundary between fresh and partially reacted wood cannot be defined with accuracy. This boundary is also blurred by capillary migration of strongly coloured liquid between the grains

of the wood (this liquid is mainly water couloured by traces of tar). Despite this lack of accuracy, Fig. 2 shows that the ablation thickness roughly decreases as ablation rate increases. For high values of v, e is two small to be accurately measured (extreme ablation conditions).

3.2. Variations of v with P

A logarithmic plot of v against P shows that v can be represented by a simple relationship

$$v = a\,P^{\beta} \qquad 1)$$

The accuracy of experiments is not sufficient to detect any influence of d. This shows that fast pyrolysis can be carried out with large pieces of wood and not only with small particles, as often stated in the literature. From figure 3 a straight line fitting yields the following β values: $\beta = 0.99$ ($T_w = 873$ K), $\beta = 0.97$ ($T_w = 973$ K), $\beta = 1.02$ ($T_w = 1073$ K), $\beta = 1.01$ ($T_w = 1173$ K). Therefore, we may adopt a linear dependence $v = aP$.

Fig. 3 also shows that under high temperature and pressure, the ablation rate becomes very high and may exceed 3×10^{-2} m s^{-1} in agreement with other determinations [1]. In these conditions, the apparent massic rate of wood consumption reaches 0.24 kg hr^{-1} ($d = 2 \times 10^{-3}$ m) and 6 kg hr^{-1} ($d = 10^{-2}$ m).

4. INTERPRETATION AND DISCUSSION OF RESULTS

4.1. Signification of a

In the same manner as the ablation reaction is controlled by heat transfer inside the wood, it will be supposed that the reaction is also limited by heat transfer from the disk to the surface of wood. The variations of v will be attributed to the variations of the heat flux with T_w and P. It will be also assumed that the temperature T_d of the surface of pyrolyzing wood is constant whatever the experimental conditions. In these conditions :

$$\phi = h(T_w - T_d) = v\,\rho\,C_p(T_d - T_o) + \rho v \Delta H \qquad 2)$$

It is difficult to select an accurate value for the reaction enthalpy ΔH. Direct measurements [7] by rapid pyrolysis of wood have given values close to zero around 773 K. Reed et al. [2] proposed a model assuming that the reaction occurs in several steps: the wood is first sensibly heated without any transformation up to the reaction temperature where it is depolymerized to yield a solid which subsequently melts before vaporizing. If the tars are mechanically wiped away the heat input corresponds to sensible heat and heat of fusion. The latter has been estimated to about 4×10^4 J kg^{-1} at 773 K, which represents only 3.6% of the heat required to heat the wood from 373 to 773 K. Thence:

$$\phi = h(T_w - T_d) = v\,\rho C_p(T_d - T_o) \qquad 3)$$

Thanks to 1) with $\beta = 1$ and 3) it can be deduced that h is proportional to P:

$$h = KP \qquad 4)$$

3) and 4) show that $\frac{v}{P}$ is a linear function of T_w, allowing the calculation of T_d and K :

$$\frac{v}{P} = \frac{K}{\rho C_p}\left(\frac{T_w}{T_d - T_o} - \frac{T_d}{T_d - T_o}\right) \qquad 5)$$

As expected, Fig. 4 shows that the variation is linear. With $T_o = 373$ K, $\rho = 700$ kg s^{-1} and $C_p = 2800$ J kg^{-1} K^{-1} the following values are deduced:

$$K = 0.02 \text{ W m}^{-2} \text{ K}^{-1} \text{ Pa}^{-1} \quad \text{and} \quad T_d = 753 \pm 30 \text{ K}$$

4.2. Discussion

4.2.1. About the heat transfer coefficient h

The variations of h deduced from relation 3) and from experimental measurements are reported in Fig. 5. It appears that h is independant of d and T_w and is only a function of P. Of course, a best fitted straight line leads to the same values of K (0.02 W m^{-2} K^{-1} Pa^{-1}) and β (0,998) as previously optimized.

The three significant modes of heat transfer are convection, radiation and more or less direct contact with the disk. There are few chances that convection may occur significantly because of transpirational cooling effect. The radiation heat transfer coefficient can be defined as: $h_R = \sigma\varepsilon(T_w^2 + T_d^2)(T_w + T_d)$. Assuming ε = 0.5 and T_d = 753 K, h_R(W m^{-2} K^{-1}) has the following values:: 62 (873 K), 74 (973 K), 89 (1073 K), 106 (1173K). These are much lower than the experimental values of h, especially at high pressure (Fig. 5).

Direct heat transfer by interface contact between the disk and the rod can take place by combined mechanisms of conduction across true contact points and conduction across entrapped interstitial fluid. The prediction of theoretical h values is difficult: they depend on the thermal conductivity of fluid and solids, surface finish, and hardness, contact pressure, etc. Extreme values of h compiled by Rohsenow et al. [8] have been reported in Fig. 5 (dashed lines). In spite of very different experimental conditions (contact materials are metals, gap materials are metals or gases). The order of magnitude is correct. However, it is difficult to find a physical justification to the linear variation of h with P. For explaining this, theories of lubrication might be invoked if the whole heat transfer was supposed to take place across a continuous layer of insulating fluid between the two solid surfaces.

In anyway, the coefficient h is very high, showing that the mechanisms of heat transfer by contact must not be underestimated in the study of reactors where solid particles are pyrolysed by contact on the hot walls of the vessel (cyclone reactor for instance [3,8,10]).

4.2.2. About the surface temperature T_d

T_d has been assumed independent of T_w and P. The good linearity observed in Fig. 4 is a first confirmation of this. Fig. 4 also shows that v = 0 for T_w = 753 K, in good agreement with the experimental observation that no fast reaction significantly occurs when T_w < 753 K. These observations are also in agreement with thermogravimetric measurements showing that pyrolysis of dry wood is essentially complete at 773 K [4]. Let us also remind the model proposed in [2] assimilating fast pyrolysis to a three phases reaction: heating to 773 K, melting at 773 K, vaporization of tars.

Thus it seems fairly reasonable to assume that the temperature of the wood surface is of the order of 753 K whatever T_w and P. According to this mechanism, it could be wrong to say that wood is heated at the temperature of the walls of a reactor before decomposing.

4.3. Relationship between v and e

There are three differents ways for establishing a simple relationship between v and e.

. Let us suppose that e is the distance between the two isothermal surfaces T = 473 K, T_d = 773 K, and that the heat transferred is used to increase the wood temperature:

$$v\rho C_p(T_d - T) = \frac{\lambda}{e}(T_d - T) \quad \text{or} \quad ve = \frac{\lambda}{\rho C_p} = \alpha \qquad 6)$$

where α is the thermal diffusivity of wood.

. Assuming that penetration of heat into the rod takes place by simple one-dimension conduction, the expression giving T as a function of depth z in the solid at steady state is [8]:

$$\frac{T - T_o}{T_d - T_o} = \exp\left(-\frac{vz}{\alpha}\right) \qquad 7)$$

Taking T = 437 K, T_o = 373 K and T_d = 773 K, z is considered to be equal to e and then:

$$ve = 1.39\ \alpha \qquad 8)$$

. A model has been proposed [5] for representing the thermal volatilization of solid particles, where the equations of simultaneous heat and mass balances are numerically solved. Assuming a constant surface temperature, this model yields:

$$v = \frac{1}{b\rho}\left(\frac{\lambda r}{C_p}\right)^{1/2} \quad \text{and} \quad e = \frac{5}{b}\left(\frac{\lambda r}{rC_p}\right)^{1/2} \qquad 9)$$

b is a constant number close to 2.6 when $\Delta H = 0$, r is the chemical rate of reaction and e is the thickness of the solid layer where 99 % of the reaction occurs. From expressions 9) we obtain:

$$ve = \frac{5}{b^2}\frac{\lambda}{\rho\ C_p} \simeq 0.74\ \alpha \qquad 10)$$

. From the three methods above it can be deduced that

$$0.7\ \alpha < ve < 1.4\ \alpha \qquad 11)$$

Several values of α have been proposed in the litterature: 10^{-7} m^2 s^{-1} [6], 0.82 x 10^{-7} m^2 s^{-1} [2], 0.6 to 1.5 x 10^{-7} m^2 s^{-1} [11], 1.4 x 10^{-7} to 3.4 x 10^{-7} m^2 s^{-1} [12]. These different estimations lead to: 0.4 x 10^{-7} < ve ($m^2 s^{-1}$) < 5 x 10^{-7}.

Fig. 2 shows that the experimental results (mean value ve = 0.8 x 10^{-7} $m^2 s^{-1}$) are in agreement with this rough estimation (dashed lines).

As an illustration, for the highest ablation rate measured (fig. 3): 32.5 x 10^{-3} m s^{-1}, the thickness of the ablation layer e is predicted to be about 3 x 10^{-6} m.

5. CONDITIONS REQUIRED FOR THE OBSERVATION OF ABLATION

Relation 3) shows that fast pyrolysis in ablation regime (high value of v and small value of e) is expected when high heat fluxes are available as for example in solar concentrators or image furnaces. A few experiments have been done with an image furnace (mean flux density:: 5 x 10^5 W m^{-2}) focused on the end of a beech wood rod (d = 8 x 10^{-3} m), automatically adjusted as the reaction proceeds. The rod is placed inside a transparent glass vessel in steam atmosphere.

The apparent rate of reaction is measured to about 2 x 10^{-4} m s^{-1} while the theoretical value is 8.5 x 10^{-3} m s^{-1} (calculated on the basis of 3) with ρ = 700 kg m^{-3}, C_p = 2800 J kg^{-1} s^{-1}, $T_d - T_o$ = 400 K). The reaction produces also large amounts of char. How can this discrepancy be explained? The primary products remain for some time at the surface (there is no mechanical elimination) until they disappear by partial decomposition under the effect of high local temperature and by gasification with steam. This relatively thick layer of products partially prevents the radiation to reach fresh parts of wood and a part of the flux is consumed by the endothermal reaction of char gasification. Consequently, the overall reaction takes place in slow pyrolysis regime.

As a conclusion, it appears that fast pyrolysis of wood in ablation regime is observed if two conditions are fulfilled: high available heat flux density and efficient elimination of primary products from the surface of wood.

REFERENCES

[1] J.P. DIEBOLD. Proceedings of Specialists' Workshop on Fast Pyrolysis of Biomass

Copper Mountain Co (USA), October 19-22 (1980), p. 237
[2] T.B. REED, J.P. DIEBOLD and R. DESROSIERS. Ibid., p. 7
[3] J. LEDE, F. VERZARO, B. ANTOINE and J. VILLERMAUX. Ibid. p. 327
[4] F. SHAFIZADEH. Ibid. p. 79
[5] J. VILLERMAUX and B. ANTOINE. Rev. Gen. Therm. Fr. 227 (1980), 851
[6] J. VILLERMAUX, J. LEDE and F. VERZARO. Rev. Gén. Therm. Fr. 227 (1980), 861
[7] A. ROLIN. Thesis. Centre agréé régional CNAM, Nancy (F) (1981)
[8] W.R. ROHSENOW and J.P. HARTNETT. Handbook of Heat Transfer. McGraw Hill (1973)
[9] J. LEDE et J. VILLERMAUX. La Recherche 134 (1982) 787
[10] J.P. DIEBOLD and J. SCAHILL. Fundamentals of Thermochemical Biomass Conversion YMCA of the Rockies, Estes Park Co (USA) October 18-22 (1982)
[11] G. LESGOURGUES and J.L. HOUZELOT. Private communication. Laboratoire des Sciences du Génie Chimique. Nancy (F) (1981)
[12] R. CHARUEL, J.C. ROSSELET and J.M. SERRA-TOSIO. Colloque Sciences et Industries du Bois. Grenoble 20-22 Septembre (1982)

NOMENCLATURE

a,b,k Constants
C_p Heat capacity of wood
d Rod diameter
e Thickness of ablation layer
h, h_R Heat transfer coefficient: Experimental, by pure radiation
P Pressure
r Chemical rate of reaction
T_o, T_d, T_w Temperatures: initial (373 K), of the surface of pyrolysing wood, of the disk
v Ablation rate
z Depth in the rod
α Thermal diffusivity of wood
β Exponent
ΔH Enthalpy of the reaction
ε Emissivity
ϕ Density of flux
λ Thermal conductivity of wood
ρ Mass density of wood
σ Boltzmann constant (5.67×10^{-8} W m^{-2} K^{-4})

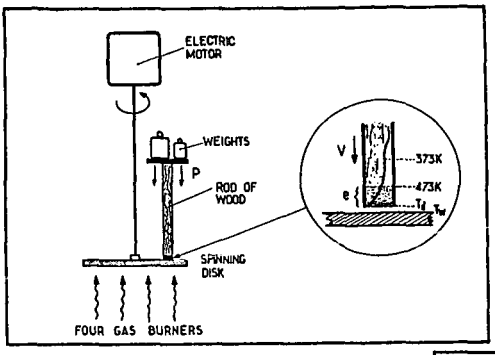

Figure 1. Scheme of experimental set-up

Figure 2. Variations of the thickness of ablation layer e as a function of ablation rate v.

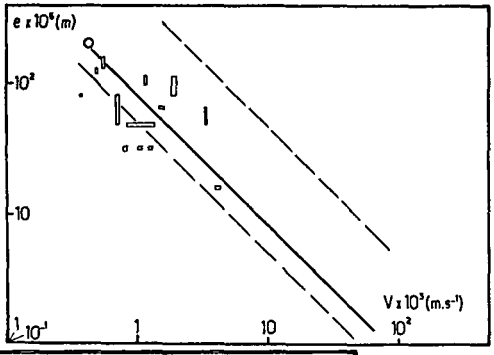

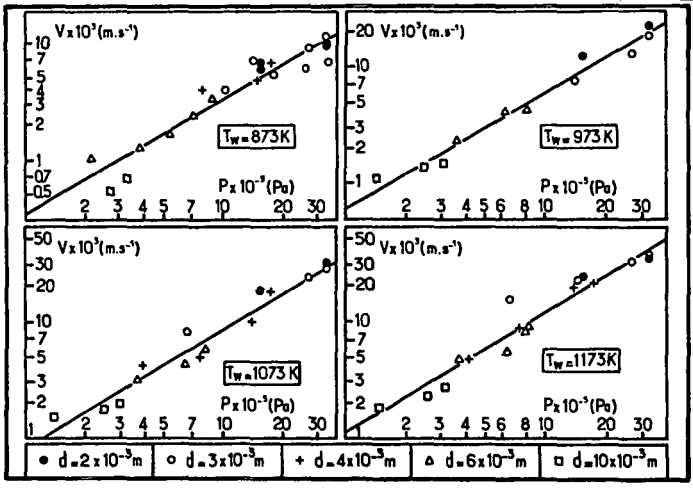

Figure 3. Experimental variations of ablation rate v as a function of pressure P for four values of disk temperature T_w.

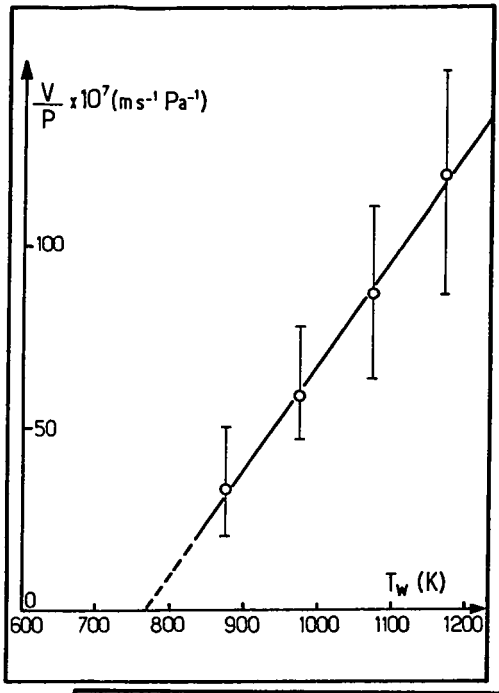

Figure 4. Variations of the ratio $\frac{\text{Ablation rate v}}{\text{Pressure P}}$ as a function of disk temperature T_w.

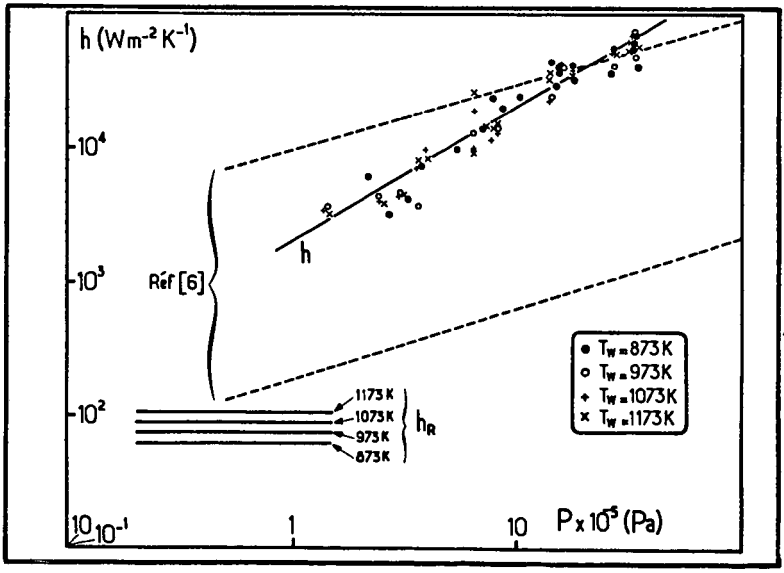

Figure 5. Variations of heat transfer coefficient h as a function of pressure p.

A NEW MODEL FOR THERMAL VOLATILIZATION OF SOLID PARTICLES UNDERGOING FLASH-PYROLYSIS

J. Villermaux, B. Antoine, J. Lédé and F. Soulignac

Laboratoire des Sciences du Génie Chimique, CNRS-ENSIC Nancy-France

Many industrial processes involve the consumption of solid particles immersed in a reacting medium. Among these, the gasification of coal and biomass in fixed, fluidized or moving beds is of special interest. A great number of models describing gas-solid reactions can be found in the literature [1] [2] [3] [4] [5]. Models dealing with the thermal volatilization of a solid controlled by heat transfer between the surrounding medium and the inner volume of the particle are more scarce. In addition, existing models often rely on the concept of a "surface reaction", which is questionable, because deeper layers also contribute to the reaction as heat penetrates into the solid.

We propose below a new model describing the volatilization of a solid by thermal penetration (VTP model). This model was initially imagined for interpreting flash-pyrolysis of sawdust particles. Actually, it could be applied to any kind of solid reactions where volatilization is controlled by heat conduction from the outer surface. Only a few preliminary but significant results are presented in this paper. More extensive and accurate simulations will be published later.

1. Assumptions and model equations

The basic assumptions of the model are :

- The solid is homogeneous and its mean density ρ is constant and independent of temperature.

- Heat transfer takes place by conduction in the solid, heat conductivity λ and heat capacity c_p are assumed to be constant.

- The rate of volatilization of the solid is $\mathcal{R}$. $\mathcal{R}$ is the mass of solid transformed into gas per unit time and per unit solid volume. $\mathcal{R}$ increases with temperature according to Arrhenius law $\mathcal{R} = k_o \exp(-E/R_g T)$.

- The reaction is endothermic, the reaction enthalpy per unit mass of solid is $\Delta H > 0$ (the case of $\Delta H < 0$ can also be treated by this model, but it will not be discussed here). It is assumed that $\Delta H = \Delta H_1 + \Delta c_p (T - T_1)$ where T_1 is a reference temperature.

- The gaseous products escape freely towards the surface without any diffusional resistance (this is possible if the remaining solid has a porous structure allowing free gas permeation).

- However, it is assumed that the remaining solid shrinks so that it conserves a constant density. The result is that, seen from the center, all the points in the solid seem to move nearer to each other. Conversely, seen from the surface, it is the center which seems to come nearer. This linear shrinking velocity will be denoted as u.

- The solid particle is initially at constant temperature T_o where the reaction is negligible. It is suddenly immersed in a hot medium. Four kinds of boundary conditions can be imagined :

a) Constant surface temperature $T_s = T_p$ (Cauchy condition).

b) Constant surface heat flux q_o

c) Convective heat transfer from a gas at constant temperature T_p (Fourier condition)

d) Radiative heat transfer from a wall at constant temperature T_p.

Only conditions a) and c) will be considered here.

- The particles may have different initial shapes. The case of infinite slabs and spheres will be treated below but this is not a limitation of the model. Actually, a unified treatment valid for any shape can be developed, especially in the so-called "ablation regime". The situation is very similar to that encountered in the study of diffusion-controlled reactions in catalyst pellets.

- Volatilization thus causes shrinking along one single dimension. One wants to calculate the decay of thickness L as a function of time and the time t_F for total consumption of the particle.

Depending on the problem, coordinate axis may be attached to the outer surface of the particle (Oz normal to the surface, directed towards the center and thus moving as volatilization proceeds). This is especially convenient for a slab and for the study of the "ablation regime". This will be referred to below as convention I. Conversely, the axis may be attached to the center of the particle (Or normal to the outer surface); this is more convenient for a sphere and a cylinder, and will be referred to below as convention II.

At any time, there exist a temperature profile T (z,t) or T (r,t) and a shrinking velocity profile u (z,t) or u (r,t). The mass and energy balances are easily written as follows:

Dimensional units, infinite slab, convention I:

Mass balance:

$$\rho \frac{\partial u}{\partial z} + \mathfrak{R} = 0 \qquad (1)$$

$$\mathfrak{R} = k_o \exp(-E/R_g T) \qquad (2)$$

Initial and boundary conditions:

$$\left.\begin{array}{l} t = 0,\ u = 0,\ L = L_o \\ z = 0,\ u = 0 \\ z = L,\ u_L = \dfrac{dL}{dt} < 0 \end{array}\right\} \qquad (3)$$

Heat balance:

$$\lambda \frac{\partial^2 T}{\partial z^2} = \mathfrak{R}\Delta H + \rho u\, c_p \frac{\partial T}{\partial z} + \rho c_p \frac{\partial T}{\partial t} \qquad (4)$$

Initial and boundary conditions:

$$\left.\begin{array}{l} t = 0,\ T = T_o \\ z = 0, \quad \text{a) } T = T_p \qquad \text{b) } -\lambda \dfrac{\partial T}{\partial z} = q_o \\ \text{c) } -\lambda \dfrac{\partial T}{\partial z} = h(T_p - T) \qquad \text{d) } -\lambda \dfrac{\partial T}{\partial z} = \varepsilon\sigma(T_p^4 - T^4) \\ z = L \quad \dfrac{\partial T}{\partial z} = 0 \end{array}\right\} \qquad (5)$$

Infinite slab (p = 0), infinite cylinder (p = 1), sphere (p = 2), convention II:

$$\frac{1}{r^p} \frac{\partial}{\partial r} (r^p \rho u) + \mathfrak{R} = 0 \ , \ \mathfrak{R} \text{ given by (2)} \qquad (1')$$

Initial and boundary conditions :

$$\left.\begin{array}{l} t = 0,\ u = 0,\ r = R_o \\ r = 0,\ u = 0 \\ r = R,\ u_R = \dfrac{dR}{dt} < 0 \end{array}\right\} \qquad (3')$$

Heat balance:

$$\frac{\lambda}{r^p}\frac{\partial}{\partial r}\left(r^p\frac{\partial T}{\partial r}\right) = \mathfrak{R}\,\Delta H + \rho u c_p\frac{\partial T}{\partial r} + \rho c_p\frac{\partial T}{\partial t} \qquad (4')$$

Initial and boundary conditions:

$$\left.\begin{array}{l} t = 0,\ T = T_o;\ r = 0,\ \dfrac{\partial T}{\partial r} = 0 \\ r = R \quad a)\ T = T_p \qquad\qquad b)\ \lambda\dfrac{\partial T}{\partial r} = q_o \\ c)\ \lambda\dfrac{\partial T}{\partial r} = h(T_p - T) \qquad d)\ \lambda\dfrac{\partial T}{\partial r} = \varepsilon\sigma(T_p^4 - T) \end{array}\right\} \qquad (5')$$

It is interesting to write the model equations in reduced form. For the slab case, convention I, dimensionless quantities are defined as follows: $x = z/L_o$, $\theta = t\mathfrak{R}^*/\rho$, $v = \rho u/(L_o\mathfrak{R}^*)$, $Y = T/T^*$, $W = \mathfrak{R}/\mathfrak{R}^*$, $A = E/(R_gT^*)$, $M = \mathfrak{R}^*L_o^2c_p/\lambda$, $\ell = L/L_o$, $H = \Delta H_1/(c_pT^*)$, $K = \Delta c_p/c_p$, $B = hL_o/\lambda$, $Q_o = q_oL_o/(\lambda T^*)$, $S = \varepsilon\sigma L_oT^{*3}/\lambda$. ($R_g$ is the gas constant).

T^* is a reference temperature (in the numerical examples treated here $T^* = T_1 = T_p$), and $\mathfrak{R}^*$ is the rate of reaction at T^*.

Equations (1) to (5) are then written:

$$\frac{\partial v}{\partial x} + W = 0 \qquad (6)$$

$$W = \exp\left(-A\left(\frac{1 - Y}{Y}\right)\right) \qquad (7)$$

$$\theta = 0,\ v = 0;\quad x = 0,\ v = 0;\quad x = \ell,\ v = \frac{d\ell}{d\theta} \qquad (8)$$

$$\frac{1}{M}\frac{\partial^2 Y}{\partial x^2} = (H + K(Y - Y_1))W + v\frac{\partial Y}{\partial x} + \frac{\partial Y}{\partial \theta} \qquad (9)$$

$$\left.\begin{array}{l} \theta = 0,\ Y = Y_o \\ x = 0 \quad a)\ Y = Y_o \qquad\qquad b)\ -\dfrac{\partial Y}{\partial x} = Q_o \\ \qquad c)\ -\dfrac{\partial Y}{\partial x} = B(Y_p - Y) \qquad d)\ -\dfrac{\partial Y}{\partial x} = S(Y_p^4 - Y^4) \end{array}\right\} \qquad (10)$$

A similar reduction can be performed on equations (1') to (5'), the characteristic length R_o replacing L_o. The important parameters are the activation criterion A, the thermicity criterion H, the thermal BIOT number B, and especially M, which appears as a THERMAL THIELE MODULUS

$$M = \frac{\mathfrak{R}^* L_o^2}{\alpha\rho} = \frac{t_T}{t_R} \qquad (11)$$

where $\alpha = \lambda/(\rho c_p)$ is the thermal diffusivity

$t_R = \rho/\mathfrak{R}^*$ is a characteristic reaction time and $t_T = L_o^2/\alpha$ is a characteristic heat penetration time. If $M \ll 1$, $t_T \ll t_R$ so that heat has the time to penetrate into the particle before it volatilizes. Volatilization is thus controlled by the chemical reaction, this is the so-called CHEMICAL REGIME. If $M \gg 1$, $t_T \gg t_R$, heat has not the time to reach the particle core and volatilization takes place in a thin layer close to the surface. The rate of volatilization is controlled by an irreducible coupling between reaction and heat diffusion: this is the so-called ABLATION REGIME. We shall see below that shrinking then proceeds at a constant linear velocity.

2. Examples of simulations

Equations (6) to (10) and their equivalent for a sphere were solved numerically, yielding internal velocity and temperature profiles and time θ_F for total consumption as a function of physical parameters.

In the simulations reported here, the following values were selected:

$Y_p = Y_i = 1$, $Y_o = 0.25$ (for instance $T_o = 300$ K and $T_p = T^* = 1200$ K)

H = 0.5, A variable (1, 10, 100)

M and B variable.

Figure 1 shows internal temperature profiles, mainly for a 50 % linear size reduction (e.g. $\ell = 0.5$) in the case of Fourier (c) and Cauchy (a) conditions. The influence of M is obvious. When M is small, the temperature tends to become uniform whereas when M is large (M > 100), a steep temperature profile exists close to the surface. This is especially clear for constant surface temperature (Cauchy condition, B = ∞). In this case, a comparison between curves drawn for $\ell = 0.75$ and $\ell = 0.5$ shows that the temperature profile is simply translated as a function of time when volatilization proceeds, the core of the particle remaining cold. The influence of the Biot number B is also interesting: it appears that the ablation regime is more difficult to reach (even for large M) if the rate of heat transfer at the surface is slow (small B). Figures 2 to 4 show the reduction of size of particles (L/L_o or R/R_o) as a function of reduced time θ. Starting from the chemical regime (M = 0), where $L/L_o = \exp(-\theta)$, the decay curves tend to become straight lines in frankly established ablation regime (M > 100, B = ∞): $L/L_o = 1 - \theta/\theta_F$. Times for total consumption θ_F are reported as a function of M in figures 5 and 6. Several interesting remarks can be made by inspection of these figures:

- θ_F increases when M augments and when B diminishes (Fourier condition).

- Curves for different shapes are very close to each other for equal values of the Biot number B.

- As B → ∞, the Fourier condition tends to the Cauchy condition. In ablation regime, θ_F then tends to be proportional to $\sqrt{M}$.

For A = 10 and H = 0.5, one finds approximately

$$\theta_F \approx 3 \sqrt{M} \tag{12}$$

In dimensional variables,

$$t_F \approx 3 \sqrt{t_R t_T} = 3 L_o \frac{\overline{t_R}}{\alpha} \tag{13}$$

This means that the time for total consumption is proportional to the initial size and that the shrinking velocity is constant (a clue for the ablation regime). This also makes it possible to determine the true value of the reaction time t_R even in the presence of a severe heat transfer control. A value for the thickness of the reaction zone may be obtained as the ratio $e = \alpha/|u| \approx \alpha t_F/L_o$ of the heat diffusivity to the shrinking velocity. Then,

$$e \approx 3 \sqrt{\alpha t_R} \tag{14}$$

and

$$e/L_o \approx 3 L_o/\sqrt{M} \tag{15}$$

For instance, if M = 10 000, $e \approx 0.03 L_o$

- Coefficient 3 in relationships (12), (13), (14), (15) obviously depends on the numerical values of A, H and Y_o selected for simulations. Figure 6 shows that the absolute value of θ_F depends on A but that the curves are roughly parallel. It can be expected that in ablation regime, the $\sqrt{M}$ dependency still holds whatever the value of A.

In a previous paper [6], an empirical expression for θ_F in ablation regime and variable H has been established:

$$\theta_F \approx 1.13 (H + 2.3) \sqrt{M} \tag{16}$$

(A = 10, $Y_o = 0.25$, Cauchy condition)

However, this relationship should be checked by more careful numerical studies.

3. Conclusion

Although relying on very simple assumptions, the VTP model makes it possible to estimate the rate of consumption of solid particles as a function of physico-chemical parameters. Evidence for the existence of two volatilization regimes is provided, depending on the value of the thermal Thiele Modulus M and the thermal Biot number B. The ablation regime is achieved if both $M = t_T/t_R$ and $B = hL_o/\lambda$ are large (M, B > 100). In this regime, the shrinking velocity is constant and the reaction takes place only in a thin layer at the solid surface. Experimental data on wood pyrolysis obtained with sawdust or with massive rods confirm the existence of these two regimes (see companion paper). Total consumption times estimated in a cyclone reactor or direct measurement of ablation velocities are in agreement with theoretical predictions of the VPT model.

Example: For wood particles, $\lambda = 0.2\ W\ m^{-1}\ K^{-1}$, $c_p = 2800\ J.kg^{-1}.K^{-1}$, $\rho = 500\ kg.m^{-3}$, $\alpha = 1.4 \times 10^{-7} m^2\ s^{-1}$, $H = 0.5$ corresponds to $\Delta H = 1680\ kJ.kg^{-1}$ at $T^* = 1200$ K. Then, $t_T = L_o^2/\alpha \approx 7 \times 10^{-2}$ s. For particles of $L_o = 10^{-4}$ s, the ablation regime requires that (M > 100) $t_R < 7 \times 10^{-4}$ s. If $t_R = 7 \times 10^{-4}$ s, then $t_F = 3\ t_R \sqrt{M} = 30\ t_R = 21 \times 10^{-3}$ s.

These preliminary results have been obtained with very simple numerical methods which are not best adapted to the "stiff" conditions encountered in the ablation regime (M and B both large). Further improvements are in progress, which will make it possible to perform more accurate simulations in a broader range of variation of parameters.

Literature cited

[1] Szekelly J., Evans J.W. and John H.Y. Gas Solid Reactions, Academic Press, 1976

[2] Levenspiel O. The Chemical Reactor Omnibook O.S.U., Corvallis, Oregon USA, 1979

[3] Hicks B.L. Theory of ignition considered as a thermal reaction. J. Chem. Phys. 22, (1954), 414

[4] Kindelan M., and Williams F.A. Theory for endothermic gasification of a solid by a constant energy flux. Comb. Sci. Technology, 10 (1975), 1

[5] Bradley H.H. Jr. Theory of ignition of a reactive solid by constant energy flux. Comb. Sci. Technol. 2 (1970), 11

[6] Villermaux J. and Antoine B. Pyrolyse éclair de solides divisés dans un réacteur continu. 1. Un nouveau modèle de volatilisation thermique de particules solides. Rev. Gen. Therm. Fr. n° 227, Nov. 1980, 851

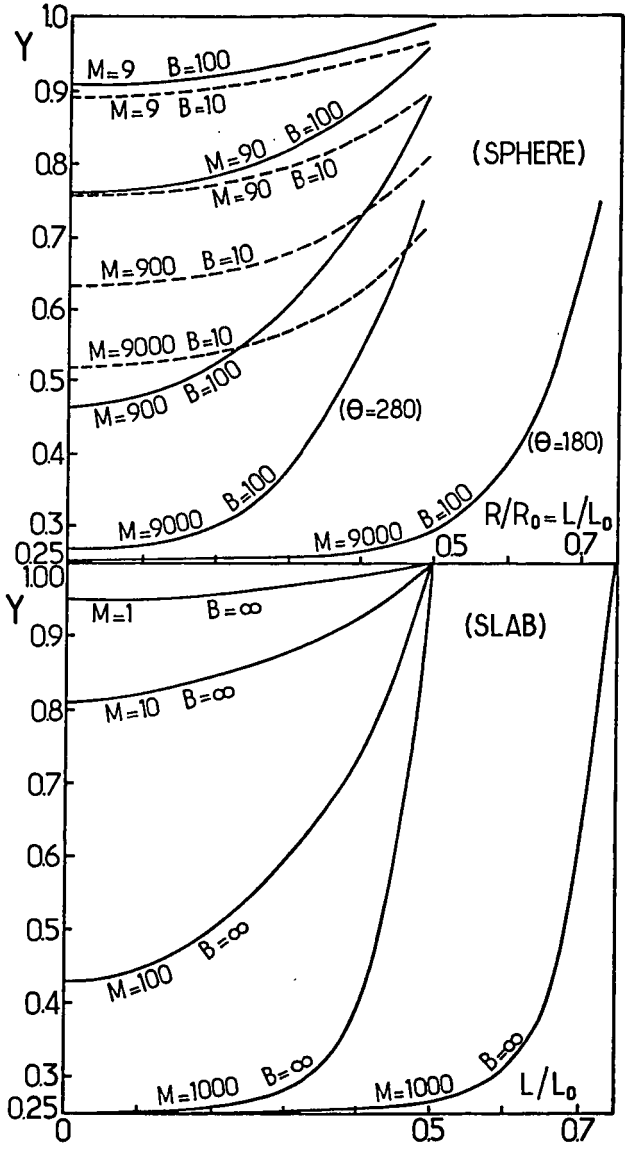

Fig. 1. Internal temperature profiles as a function of M and B (sphere and slab), mainly for $L/L_o \gtrsim 0.5$. Notice the translation of the profile in ablation regime ($L/L_o = 0.75 \rightarrow L/L_o = 0.5$). A = 10, H = 0.5, $Y_o = 0.25$

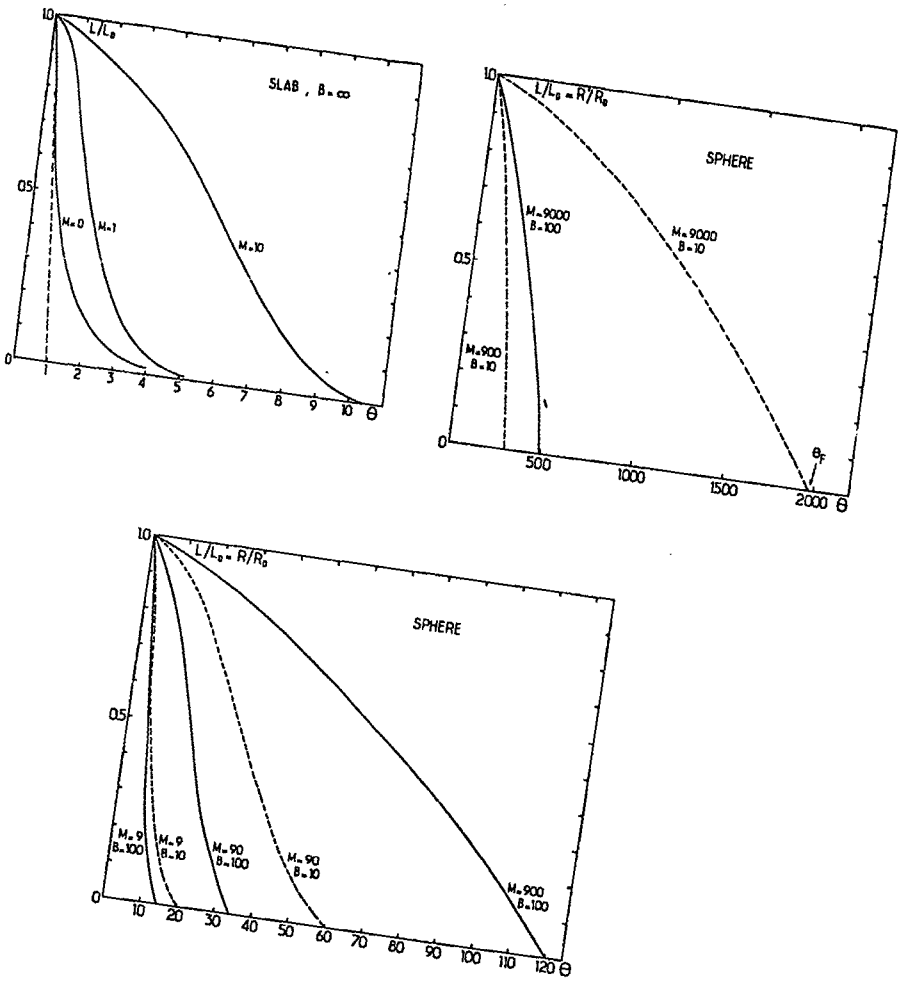

Fig. 2,3,4. Decrease of the particle size (L/L_o) as a function of time θ. Various shapes and conditions. A = 10, H = 0.5, Y_o = 0.25.

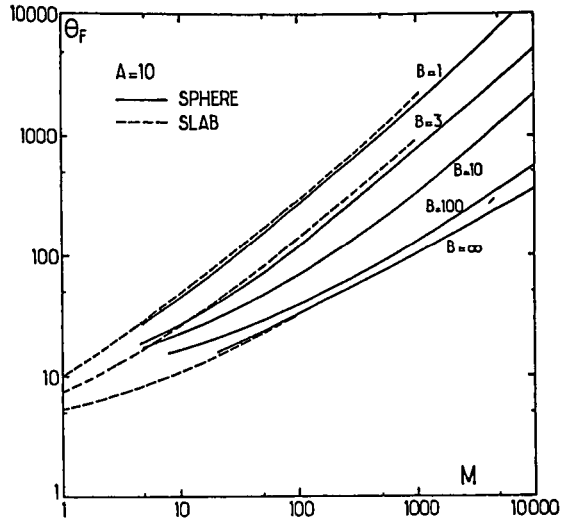

Fig. 5. Time for total consumption θ_F as a function of thermal Thiele modulus M. Various shapes and Biot numbers B (Fourier and Cauchy conditions). Notice the $\sqrt{M}$ dependency in ablation regime. A = 10, H = 0.5, Y_o = 0.25.

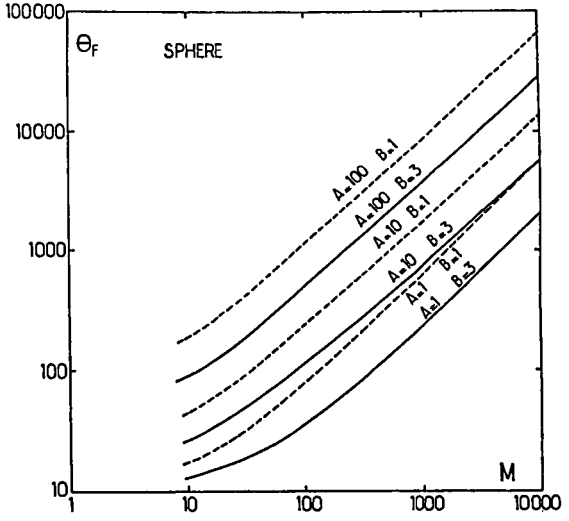

Fig. 6. Time for total consumption $_F$ as a function of thermal Thiele modulus M. Influence of activation parameter A. H = 0.5, Y_o = 0.25.

Numerical Studies of the Radiant Flash Pyrolysis of Cellulose

Virendra Kothari and Michael J. Antal, Jr.*

Department of Mechanical & Aerospace Engineering
Princeton University
Princeton, New Jersey 08544

INTRODUCTION

When biomass particles are heated very rapidly (>1000°C/s) in an oxygen free environment, they undergo pyrolysis with the formation of little or no char (1,2). If concentrated solar energy is used to rapidly heat the particles (3), their temperature may exceed that of the surrounding gaseous environment by several hundred degrees Celsius when pyrolysis occurs (4,5). This "two temperature" effect gives rise to the formation of high yields of sirups from the pyrolyzing biomass (6-8). Our interest in the selective formation of sirups during the radiative flash pyrolysis of biomass caused us to initiate numerical explorations of the combined effects of heat and mass transfer on the radiative flash pyrolysis phenomena. These explorations are described in this paper.

An earlier work (9) presented the derivation of the general equations governing chemical reaction, species, energy, and momentum conservation, as well as the appropriate boundary conditions, for a spherical particle of cellulose undergoing rapid pyrolysis in an intense radiative flux. The following section discusses three simplified sets of equations, which represent three different levels of physical complexity, and offer some insight into the more complex problem.

SIMPLIFIED PYROLYSIS MODELS

The general pyrolysis model (9) is specified by a coupled set of two ordinary and three partial differential equations, as well as the appropriate boundary conditions. The three "level" problems discussed in this section simplify the general problem by representing only the effects of: (1) chemical reaction and external heat transfer, (2) chemical reaction, external and internal heat transfer, and (3) chemical reaction, external heat transfer and internal mass transfer.

The major assumptions underlying the Level 1 problem are that the resistances to heat and mass transfer within the particle are negligible. Hence the particle is assumed to sustain no temperature or pressure gradients within it. We also assume that only a single vapor phase species (levoglucosan) is present within the particle, and we neglect the kinetic energy of the vapor as well as the rate of change of its enthalpy relative to that of the cellulose. Integrating over the volume of the particle, the energy conservation equation becomes

$$V_p(\rho_s c_{ps}+\rho_c c_{pc})\frac{dT}{dt} = V_p\Delta H(-W_s) + A_p\alpha FI + A_p\bar{h}(T_f-T) + A_p\varepsilon\sigma(T_w^4-T^4) \qquad 1)$$

The reaction rate W_s is given by

$$W_s = \frac{-d\rho_s}{dt} = A' e^{-E/R_g T}\left(\frac{V^*}{\rho_{so}}\right)^{n-1}\rho_s^n \qquad 2)$$

*Author to whom correspondence should be sent.
Present address: Department of Mechanical Engineering
University of Hawaii
Honolulu, Hawaii 96822

where

$$\rho_c = a(\rho_{so} - \rho_s) \qquad 3)$$

with $\rho_{so}, \rho_c = 0$ and $T = T_i$ at $t = o$. In previous studies, a constant value for the heat transfer coefficient $\bar{h}$ was assumed. As discussed in Reference 7, the outward bulk flow of voltatiles generated by pyrolysis effectively reduces the rate at which heat is transferred from the surrounding gaseous environment to the particle. The corrected heat transfer coefficient $\bar{h}$ is related to the uncorrected value h by

$$\frac{\bar{h}}{h} = \frac{\phi_h}{e\phi_{h-1}} \qquad 4)$$

To nondimensionalize equations 1 -4 we take as a reference temperature T_p the temperature at which the devolatilization rate is maximum. A reference time is chosen to be $(T_p - T_i)/\beta$ where β is a characteristic average heating rate. Table 1 summarizes the six dimensionless parameters Θ_1-Θ_6 which result from a nondimensionalization of Eq. 1. A further discussion of the significance of these parameters is given in the following section.

The Level 2 problem accounts for the existence of temperature gradients within "large" particles undergoing rapid heating, or particles with a low thermal diffusivity. The resistance to mass transfer is still presumed to be negligible; pyrolytic vapors exit the particle without holdup. With these assumptions, the energy equation becomes

$$(\rho_s c_{ps} + \rho_c c_{pc})\frac{\partial T}{\partial t} = \Delta H(-\dot{w}_s) + \frac{1}{r^2}\frac{\partial}{\partial r}\left(r^2 k_e \frac{\partial T}{\partial r}\right) - N\frac{\partial}{\partial r}(c_p T) \qquad 5)$$

wherein the molar flux of volatiles N is given by the species continuity equation

$$\frac{1}{r^2}\frac{\partial}{\partial r}(r^2 WN) = bw_s \qquad 6)$$

The initial and boundary conditions associated with Eqs. 2, 3, 5, and 6, which specify the Level 2 problem, are given by

$$\begin{aligned} &t = 0 \qquad \rho_s = \rho_{so}, \rho_c = 0,\ T = T_i,\ N = 0 \\ &r = 0 \qquad \frac{\partial T}{\partial r} = 0 \\ &r = R \qquad k_e \frac{\partial T}{\partial r} = \alpha F I + \bar{h}(T_f - T) + \sigma\varepsilon(T_w^4 - T^4) \end{aligned} \qquad 7)$$

The nondimensionalization of Eqs. 2, 3, and 5-7 introduces the two new dimensionless parameters Θ_7 and Θ_8 given in Table 1.

The Level 3 problem attempts to account for the effects of mass transfer on the Level 1 problem. Two major assumptions are made: (1) the resistance to heat transfer within the particle is negligible; hence the particle is considered to be isothermal, and (2) the mass flux is given by the hydrodynamic flow expression

$$N_i = (-p_i \frac{B_o}{\mu})\frac{dc_i}{dr} \qquad 8)$$

Equation 8 presumes viscous flow to be much greater than the diffusive flow, which would be the case if the permeability B_o is large compared to the diffusivity of the gas within the solid. An evaluation of the mass transfer peclet number $\frac{pB_o}{\mu D}$

for this problem results in a value exceeding 4000 (7), justifying assumption (2). With these assumptions, the equation governing the concentration of volatiles within the particle becomes

$$\frac{\partial}{\partial t}(\varepsilon_p cW) - \frac{1}{r^2}\frac{\partial}{\partial r}\left(r^2 pW \frac{Bo}{\mu}\frac{\partial c}{\partial r}\right) = bw_s \qquad 9)$$

with $p = cR_gT$. The initial and boundary conditions are given by

$$t = 0 \qquad \rho_s = \rho_{so},\ \rho_c = 0,\ T = T_i, c = p_o/R_gT_i$$

$$r = 0 \qquad \frac{\partial T}{\partial r} = 0 \quad , \quad \frac{\partial c}{\partial r} = 0 \qquad 10)$$

$$r = R \qquad k_e \frac{\partial T}{\partial r} = \alpha FI + \bar{h}\,(T_f - T) + \varepsilon\sigma(T_W^4 - T^4)$$

$$N = \bar{K}\,(c - c_\infty)$$

where $\bar{K}$ is the corrected mass transfer coefficient given by

$$\frac{\bar{K}}{K} = \frac{\phi_m}{e^{\phi_m} - 1} \qquad 11)$$

Thus the Level 3 problem is specified by Eqs. 1-3 and 9-11, whose nondimensionalization introduces the new parameter θ_g (see Table 1). The reader should note that the Level 3 problem is more mathematically complex then its predecessors due to the coupled boundary conditions in Eq. 10, reflected in the dependence of $\bar{h}$ and $\bar{K}$ on ϕ_h and ϕ_m, which are both functions of the unknown flux of volatiles N at the surface of the particle.

RESULTS

The coupled set of ODE's and PDE's making up the Level 1-3 problems were solved using the method of lines (10) as implemented in a modified form (9) of the algorithm PDEONE developed by Sincovec and Madsen (11). The coupled system of ODE's obtained from the method of lines was integrated using the GEARB package developed by Hindmarsh (12). Numerous tests were performed to ensure the integrity (accuracy and precision) of the results, as described in detail in Reference 9.

The influence of the particle diameter, the incident intensity of solar radiation, and the freestream fluid temperature on the time dependent volatilization of the cellulose particle was studied in a variety of numerical simulations. Table 2 catalogues values of the parameters selected for study. Due to space limitations, only a small fraction of the results will be discussed here. The interested reader is referred to Reference 9 for a more complete presentation.

Figures 1 and 2 display the weight loss of a particle as a function of time (as would be measured using a TGA) for particles with diameters of 100 and 500 μm surrounded by steam at 500°C, when exposed to flux densities of 50, 100, 200, 400 and 1600 W/cm^2. Figure 3 shows the temperature histories of a 100 μm diameter subjected to a variety of flux densities with a freestream temperature of 800°C. It is seen that the pyrolysis of the particle can be considered to take place in two stages - a heatup stage and a devolatilization stage. In the heatup stage, the particle heats up rapidly without a significant loss of weight. As the temperature of the particle increases, the reaction rate increases considerably and the devolatilization stage sets in. As a general trend, it is observed that the time taken for complete devolatilization of the particle decreases with increasing solar flux, increasing fluid temperature and decreasing particle size. However, as evidenced in Figure 3, smaller particles subject to lower flux densities reach a stagnation temperature slightly above the freestream temperature after which little temperature change occurs until pyrolysis is complete. This causes the time for volatilization of the smaller particles subject to lower flux densities in cooler environments to increase considerably.

To calculate the values of the dimensionless numbers θ_1-θ_6 associated with the Level 1 problem, T_p and β must be evaluated. An estimate of T_p (1) may be obtained using

$$T_p \cong E/(R_g \ln(A' R_g T_p^2/\beta E)) \qquad 12)$$

where the value β can be estimated using the following formulae for the initial values of the heating rate due to radiation and convection

$$\beta_r = \frac{4\pi R^2 \alpha F I}{\frac{4\pi R^3}{3} \rho_{so} c_{pso}} \qquad 13)$$

$$\beta_c = 4\pi R^2 \frac{h}{2}(T_f - T_i)/\frac{4\pi R^3}{3} \rho_{so} c_{pso} \qquad 14)$$

with $\beta = \beta_r + \beta_c$. As discussed earlier, the value of β decreases during heatup and volatilization. This penomena is illustrated in Figure 4. If the value of β estimated above is reduced by 50%, values for T_p estimated using Eq. 12 usually differ from the exact values by less than 50°C. Larger errors are encountered for small particles and low fluxes, when a stagnation temperature is reached. For these cases, the value $T_p = T_f$ would be more appropriate.

Tables 3 and 4 present representative values of the nondimensional numbers θ_1-θ_6 based on values for T_p and β calculated using the above procedure. Increasing values of θ_1 and θ_2 reflect the decreasing ability of solar radiation to provide both the sensible heat and the endothermic heat of reaction requirements. The anomalous behavior of θ_3 reflects errors associated with our method for approximating the value of β used to calculate T_p. Negative values of θ_4 occur when $T_p > T_f$. For $\theta_4 < -1$ the particle should reach a stagnation temperature, in which case $T_p \cong T_f$ and θ_4 is artificially assigned the value $\theta_4 = 0$. As expected, values of θ_5 and θ_6 are influenced by β and T_p.

If heat transfer to the particle during devolatilization is rate limiting, then a characteristic time t_{dh} for devolatilization can be estimated using

$$t_{dh} = \frac{\Delta H \rho_{so} R}{\alpha F I + h(T_f - T_p)/2} \qquad 15)$$

Similarly, a characteristic heatup time t_{hh} can be defined based on the sensible heat requirement:

$$t_{hh} = \frac{\rho_{so} C_{pso} (T_p - T_i) R}{\alpha F I + h\left(\frac{(T_f - T_i) + (T_f - T_p)}{2}\right)} \qquad 16)$$

Figures 5 and 6 display the relationship between the actual values for t_h and t_d and the estimated values t_{hh} and t_{dh} using Eqs. 15 and 16 above. The evident linear relationship between the estimated and actual values of t_h and t_d provides an algorithm (using Eqs. 15 and 16, and Figures 5 and 6) which accurately estimates t_h, t_d and the total time $t_t = t_h + t_d$ required for pyrolysis without resort to numerical integration of the Level 1 ODE's.

For all of the cases studied in this work $t_h \leq t_d$; consequently chemical kinetics control the total time required for the pyrolysis of the particle. Only for extremely high heating rates does $t_h \leq t_d$.

Figure 7 displays representative results for the Level 2 problem. In general, internal conduction and convection increase the time required for devolatilization, but have little effect on heatup. The increase in t_d is more prominent for larger particles, and higher heating rates. The fact that t_h is not dependent on internal conduction and convection may be understood in terms of the characteristic time for conduction $t_c = R^2/\alpha_s$, which takes on values 4.17, 16.7 and 417 ms for particles with diameters of 50, 100 and 500 μm (respectively). These values of t_c are comparable to the heatup times t_h for the Level 1 problem; hence the value of Θ_7 is close to unity for all the cases studied. Consequently, pyrolysis does not occur at the same time throughout the particle; rather the particle's surface rapidly heats and undergoes pyrolysis while the inside remains "cool." Thus pyrolysis occurs by ablation in all the cases studied, and t_h is unaffected by internal conduction and convection.

Table 5 displays values of Θ_8 calculated using the approximate characteristic temperature T_p defined earlier for the Level 1 problem. Values of Θ_8 indicate that for large particles and higher heating rates the internal convective heat flux (which tends to cool the particle) becomes comparable in magnitude to the conductive heat flux. This effect tends to increase t_d by counteracting heat flow into the particle during pyrolysis. Figure 8 displays the dependence of t_d (Level 2)/t_d (Level 1) vs. Θ_8. The observed linear dependence permits one to correct the estimated value of t_d (obtained by methods discussed earlier for the Level 1 problem) by simply evaluating Θ_8 and multiplying t_d (Level 1) by the appropriate correction factor obtained from Figure 8.

Values of Θ_9 were estimated for the range of parameters studied in this work. In almost all cases $\Theta_9 \geq 10$ (in the worst case $\Theta_9 \approx 1$); consequently for the cases studied volatiles do not accumulate within the particle and no pressure gradients are generated. For this reason, no attempt was made to solve the Level 3 problem.

CONCLUSIONS

For all the cases treated in this work, chemical kinetics control the time required to achieve devolatilization of the particle. Because of ablation, the time required for intraparticle heat transfer plays a less significant role. Mass transfer limitations were not significant for any of the cases studied.

Simple formulae were derived which facilitate rapid accurate estimates of t_h, t_d and t_t for many problems of interest. Evaluation of the nondimensional parameters Θ_1 - Θ_9 should enable other workers to apply the specific results of this work to their own problems.

Table 1

Dimensionless Parameters

Parameter	Expression	Significance
θ_1	$\frac{\rho_{so} c_{pso} R B}{\alpha F I}$	$\frac{\text{sensible heat requirement}}{\text{heat supplied by incident solar radiation}}$
θ_2	$\frac{\Delta H_o}{c_{pso}(T_p - T_i)}$	$\frac{\text{heat of reaction}}{\text{sensible heat}}$
θ_3	$\left(\frac{T_p - T_i}{B}\right) / \frac{1}{(V^*)^{n-1} A' \exp(-E/R_g T_p)}$	$\frac{\text{heatup time}}{\text{pyrolysis time}}$
θ_4	$\frac{h(T_f - T_p)}{\alpha F I}$	$\frac{\text{convective heat transfer}}{\text{incident solar radiation}}$
θ_5	$\frac{\epsilon \sigma T_w^4}{\alpha F I}$	$\frac{\text{wall radiation}}{\text{incident solar radiation}}$
θ_6	$\frac{\epsilon \sigma T_p^4}{\alpha F I}$	$\frac{\text{particle radiation}}{\text{incident solar radiation}}$
θ_7	$\frac{T_p - T_i}{B} / \frac{R^2 \rho_{so} c_{pso}}{k_{eo}}$	$\frac{\text{Heatup time}}{\text{conduction time}}$
θ_8	$R^2 \left(\frac{\rho_{so}}{W}\right) V^{*n-1} A' \exp(-E/R_g T_p) c_{po} / k_{eo}$	$\frac{\text{internal convection}}{\text{conduction}}$
θ_9	$\frac{p_o^2 W B_o}{R^2 R_g T_p \mu} \Big/ b \rho_{so} (V^*)^{n-1} A' \exp(-E/R_g T_p)$	$\frac{\text{volatiles flow rate}}{\text{volatiles generation rate}}$

Table 2

Selected Values of Parameters
Used in the Simulations

Particle diameter	=	50, 100 and 500 μm
Flux density	=	50, 100 200, 400 and 1600 W/cm^2
Freestream temperature	=	500° and 800°C

Table 3

Values of dimensionless parameters
100 μ diameter, T_f = 500°C

I (W/cm^2)	θ_1	θ_2	θ_3	θ_4	θ_5	θ_6
1600	1.635	-0.0245	10.282	-0.275	0.003	0.051
400	2.041	-0.0273	10.651	-0.877	0.036	0.153
200	2.583	-0.0285	11.046	-1.598	0.072	0.274
100	3.667	-0.0510	?	?	0.144	0.144
50	5.834	-0.0510	?	?	0.288	0.288

Table 4

Values of dimensionless parameters
500 μ diameter, T_f = 500°C

I (W/cm^2)	θ1	θ2	θ3	θ4	θ5	θ6
1600	1.526	-0.0285	10.434	-0.004	0.009	0.034
400	1.607	-0.0318	11.372	-0.122	0.036	0.104
200	1.715	-0.0336	11.532	-0.210	0.072	0.182
100	1.931	-0.0354	11.451	-0.358	0.144	0.321
50	2.363	-0.0370	11.419	-0.612	0.288	0.578

Table 5

Values of the dimensionless parameter, θ_8

T_f = 800°C

I	Particle diameter		
(W/cm^2)	50 μ	100 μ	500 μ
1600	0.252	0.531	2.78
200	0.084	0.155	0.54
50	0.063	0.108	0.232

T_f = 500°C

I	Particle diameter		
(W/cm^2)	50 μ	100 μ	500 μ
1600	0.236	0.488	2.74
200		0.108	0.485
50			0.169

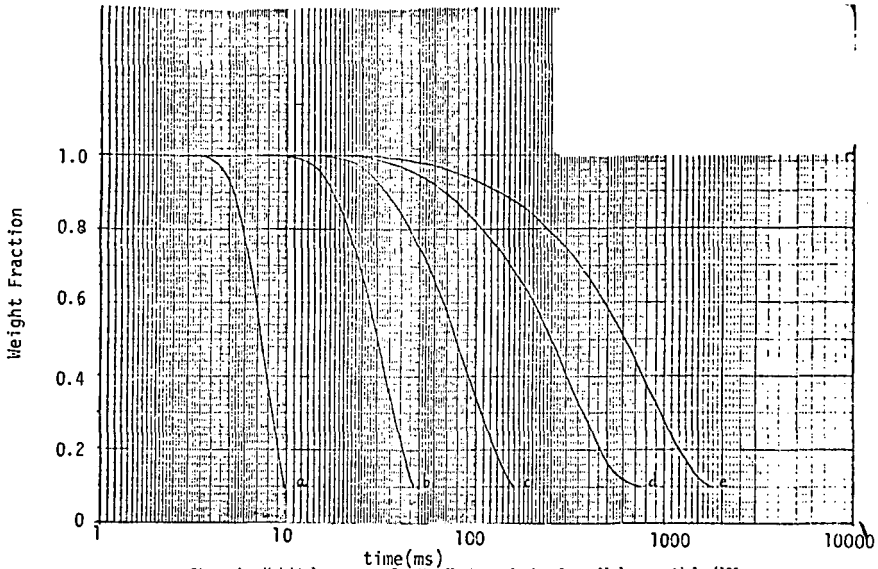

Figure 1. Weight loss curves for the flash pyrolysis of a cellulose particle (100μ diameter) in steam (T_f=500°C) at varying flux levels.

Curve	a	b	c	d	e
Flux(W/cm^2)	1600	400	200	100	50

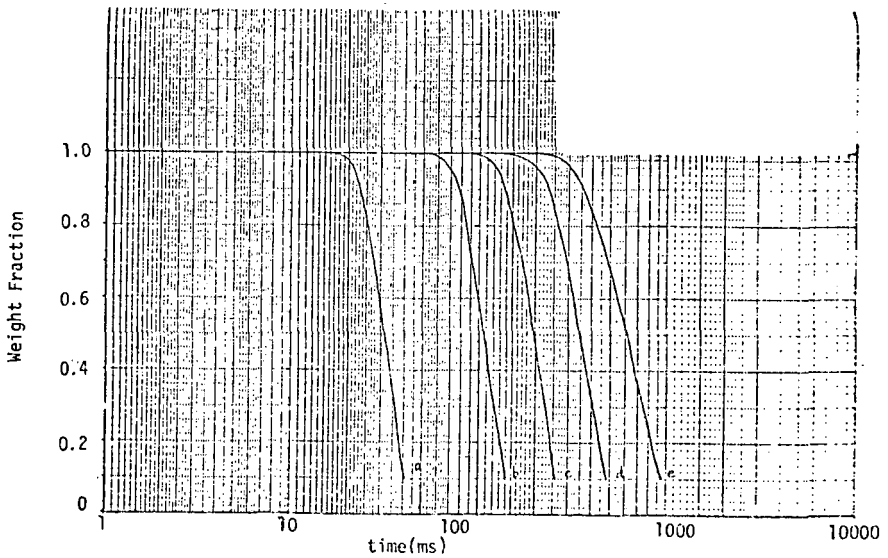

Figure 2. Weight loss curves for the flash pyrolysis of a cellulose particle (500μ diameter) in steam (T_f=500°C) at varying flux levels.

Curve	a	b	c	d	e
Flux(W/cm^2)	1600	400	200	100	50

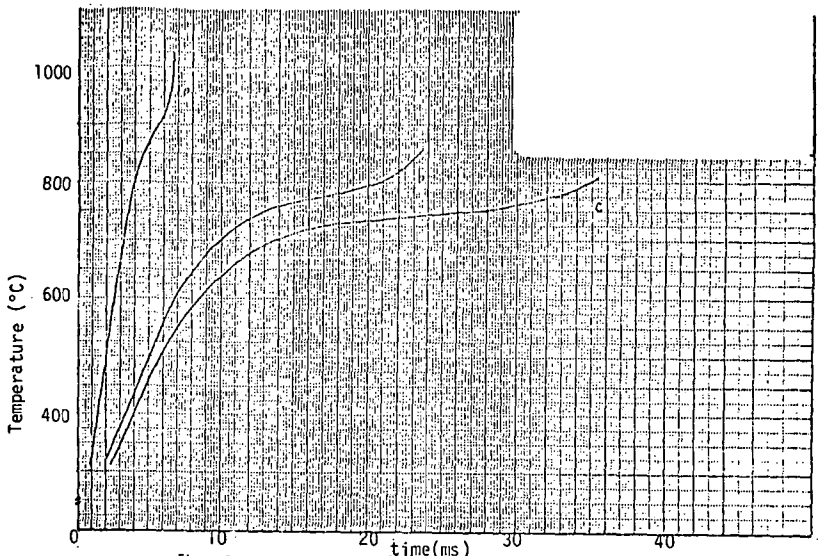

Figure 3. Temperature histories of a 190μ diameter particle at low, intermediate and high fluxes. T_f=800°C

Curve	a	b	c
Flux(W/cm^2)	1600	200	50

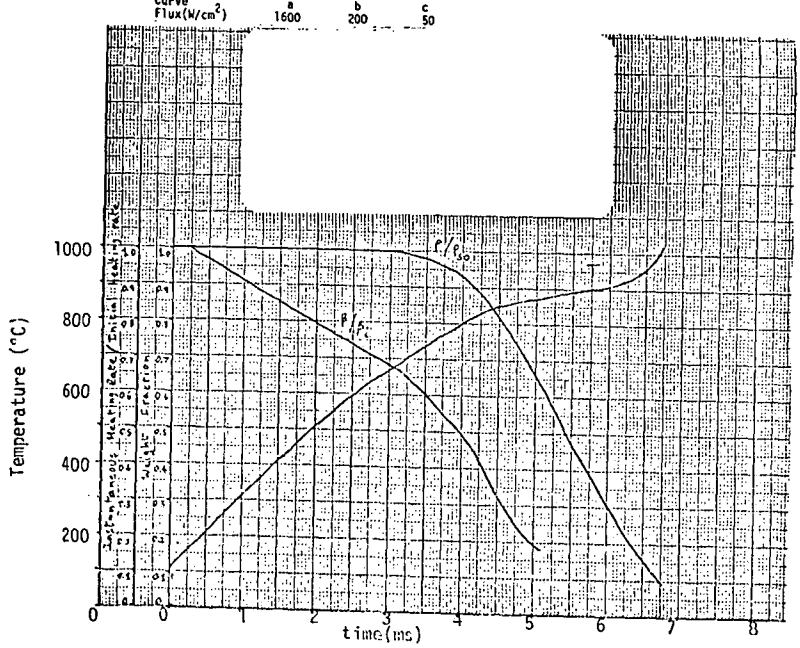

Figure 4. Weight loss, Temperature and heating rate for a 100μ diameter particle, T_f=800°C, I=1600W/cm^2

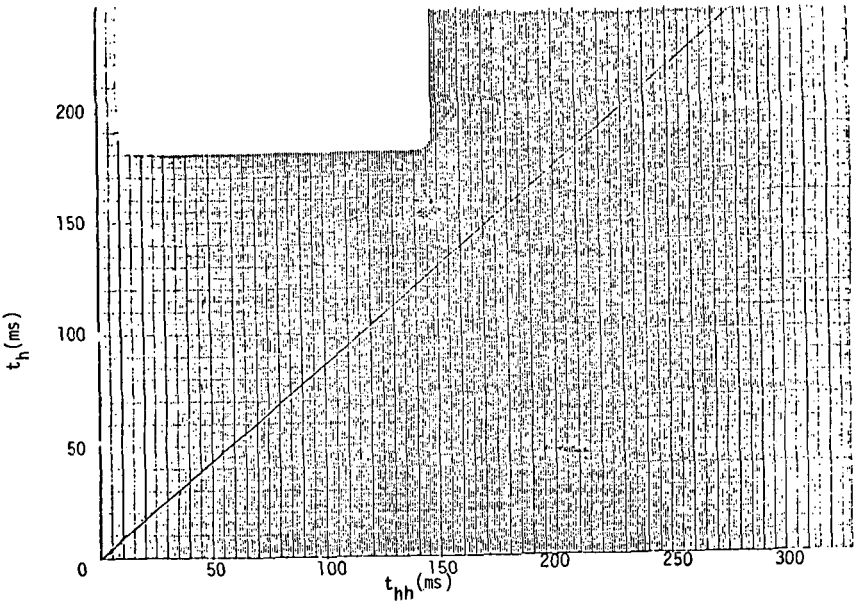

Figure 5. Plot of numerically computed heatup time, t_h, vs. characteristic heatup time, t_{hh}

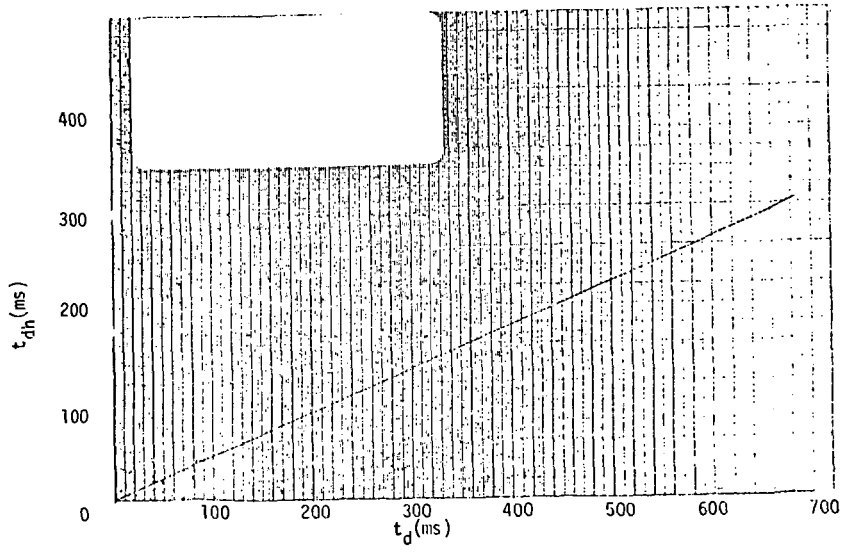

Figure 6. Plot of numerically computed devolatilization time, t_d, vs. characteristic devolatilization time, t_{dh}

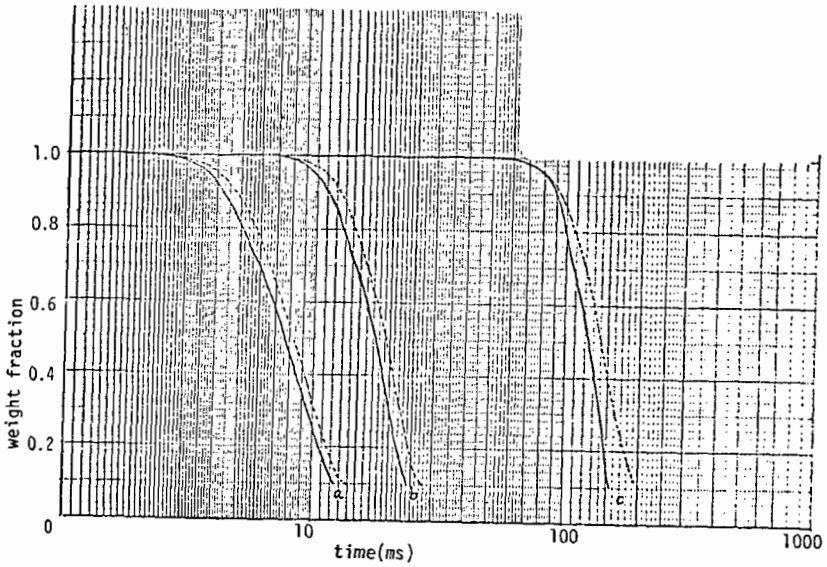

Figure 7. Plot of numerically computed heatup time, t_h, vs. characteristic heatup time, t_{hh}

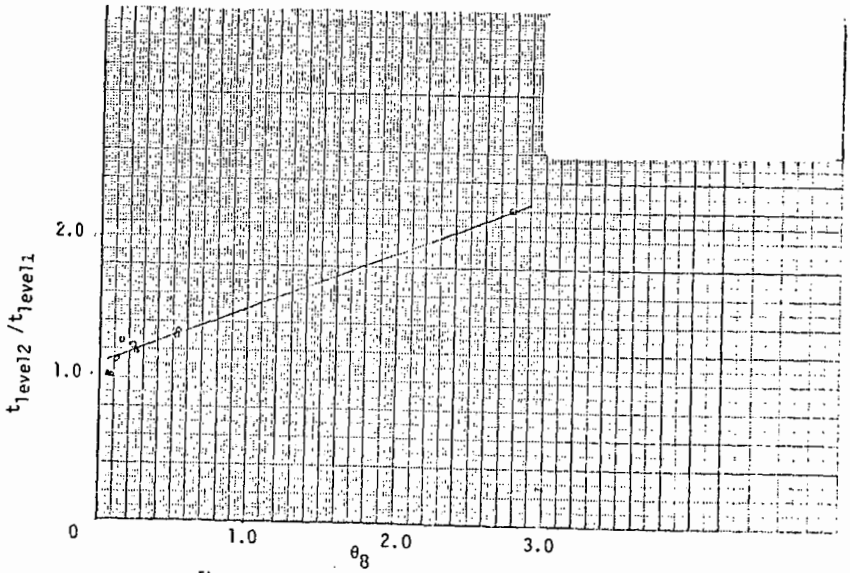

Figure 8. Plot of numerically computed devolatilization time, t_d, vs. characteristic devolatilization time, t_{dh}

REFERENCES

1. M.J. Antal, Jr. "The Effects of Residence Time, Temperature and Pressure on the Steam Gasification of Biomass" in "Biomass as a Non Fossil Fuel Source" D.E. Klass ed. A.C.S. Symposium Series No. 144, American Chemical Society, Washington, D.C. 1981 pp 313-334.

2. M.W. Hopkins, M.J. Antal, Jr., and J.G. Kay, "Radiant Flash Pyrolysis of Biomass Using a Xenon Flashtube", J. Applied Polym. Scie., in press.

3. M.J. Antal, L. Hofmann, J.R. Moreira, C.T. Brown, and R. Steenblick, "Design and Operation of a Solar Fired Biomass Flash Pyrolysis Reactor", Solar Energy, 30, pp 299-312, 1983.

4. L. Hofmann, "Experimental and Theoretical Simulations of Solar Powered Biomass Pyrolysis Reactors", MSE thesis, Princeton University, Princeton, N.J. 1981.

5. L. Hofmann and M.J. Antal, Jr., "Numerical Simulations of Solar Fired Biomass Pyrolysis Reactors", submitted for publication in Solar Energy.

6. C.I. DeJenga, M.J. Antal and M. Jones, "Yields and Composition of Sirups Resulting from the Flash Pyrolysis of Cellulosic Materials Using Radiant Energy", J. Applied Polym. Scie., 27, pp 4313-4322 (1982).

7. M.W. Hopkins, "Investigations of the Flash Pyrolysis of Biomass Using Simulated Solar Radiation", MSE thesis, Princeton University, Princeton, N.J. 1982.

8. M.W. Hopkins, C.I. DeJenga, and M.J. Antal, "The Flash Pyrolysis of Cellulosic Materials Using Concentrated Visible Light", Solar Energy, in press.

9. V.S. Kothari, "Numerical Studies of the Flash Pyrolysis of Cellulose", MSE thesis, Princeton University, Princeton, N.J. 1980.

10. O.A. Liskovets, "The method of Lines (review)." Differential Equations, 1, 1308. (English Translation). (1965).

11. R.F. Sincovec and N.K. Madesen, "Software for nonlinear partial differential equations." ACM Trans. Math. Software 1, 232. (1975).

12. A.C. Hindmarsh, "GEAR: Ordinary differential equation system solver." Report UCID-30001 Rev. 2, Lawrence Livermore Lab., Livermore, California. (1974).

A MATHEMATICAL MODEL FOR STRATIFIED DOWNDRAFT GASIFIERS

Thomas B. Reed, Benjamin Levie, and Michael L. Markson
Solar Energy Research Institute, Golden, CO 80401

Michael S. Graboski
Colorado School of Mines, Golden, CO 80401

INTRODUCTION

The downdraft gasifier originating from World War II Swedish designs has proven to be successful in generating a clean product gas when operated in an air blown mode. Such gas producers are useful for generating an essentially tar free boiler gas or engine fuel from renewable resources such as wood and agricultural waste. Recently, a new generation of stratified downdraft gasifiers (1, 2) has been studied. A successful model of this type of gasification process should be able to clearly show the interdependency of operating variables in order to optimize both cost of gasifier and performance. Such a process model would be useful in determining the proper gasification conditions when input conditions or design parameters change.

Figure 1 shows the important features of the gasifier. Biomass fuel and oxidizer are fed cocurrently to the top of the gas generator where pyrolysis of the fuel takes place. The pyrolysis reaction is driven by heat transfer from the gas and hot char bed below. As the fresh solid is heated it dries and devolatilizes. The volatiles evolved contain combustible species which react with oxygen/air to produce heat, CO, CO_2, H_2, H_2O and light hydrocarbons. During pyrolysis, the gas and solid are at vastly different temperatures because pyrolysis cools the solid while oxidation heats the gas. (At the end of pyrolysis the gas may be more than 500K hotter than the solid.) In this zone of the reactor, about 80% to 90% of the solid weight loss occurs.

Once oxygen is consumed and pyrolysis is completed, reduction of char by CO_2 and H_2O can occur in the gasification zone. The reactions occurring are endothermic so that the gas and solid temperatures fall as carbon conversion proceeds. The reactions tend to quit at about 1000K due to kinetic limitations.

In the steady-state operation of the downdraft gasifier, a specific oxygen to fuel ratio exists for a given feedstock and carbon conversion level. In practice it is found that gasifier throughput does not affect the required O_2/fuel ratio and the product gas composition for a sufficiently deep char bed. Also, it is found that the majority of hydrocarbons are destroyed in the pyrolysis zone. These data suggest that the pyrolysis and gasification zones are to a good approximation separate and that the whole char bed in downdraft gasifiers is not truly active.

In the char gasification zone three reactions dominate (neglecting the cracking of residual tars and hydrocarbon gases from the pyrolysis zone):

Boudouard Reaction

$$\text{Char} + CO_2 \rightarrow 2CO \quad \Delta H = +40{,}778 \text{ kcal/mol}$$

Water Gas Reaction

$$\text{Char} + H_2O \rightarrow CO + H_2 \quad \Delta H = +32{,}472 \text{ kcal/mol}$$

Water Gas Shift Reaction

$$H_2O + CO \rightleftharpoons H_2 + CO_2 \quad \Delta H = -8306 \text{ kcal/mol}$$

The kinetics and thermodynamics of these reactions determine the conversion of char to gas and the subsequent gas composition at any point in the char gasification zone.

In the reaction scheme, the water-gas and Boudouard reactions are coupled by the shift reaction. Therefore, only two of these reactions can be considered to be truly independent. The water-gas shift reaction is fairly rapid over carbon surfaces at gasification temperatures and is assumed to be in equilibrium in this investigation. In our model we have assumed that Edrich et al. (3) kinetics for the Boudouard reaction over ponderosa pine charcoal approximates the carbon reduction reaction occurring in the gasifier. Since the activation energy for carbon reduction by CO_2 is about 35 kcal, kinetics in error by a factor of 2 will be equivalent to a 50°C offset. This offset is within the accuracy of data available for bed temperature. At atmospheric pressure, this reaction sequence should adequately describe the kinetic processes. At elevated pressure, methane forming kinetics should probably be considered. For char particles with minor dimensions up to 3/4 inch, Edrich et al. (3) also show that intraparticle mass transfer is not important. Therefore, the same rate expression for char gasification applies regardless of particle size (if less than 3/4 inch).

The reactor design conditions which affect the char gasification zone include initial conditions, such as char and gas temperatures, flow rate and composition of the incoming gas, and gasifier parameters, such as char gasification kinetics, cross-sectional area of reactor, heat transfer from the gas to the solids, and the density and void fraction of the char. An adequate model must account for changes in these initial conditions and parameters.

To date the most extensive modelling of the char zone of the stratified downdraft gasifier has been developed by Reed (1). Reed's model of the char gasification zone assumes equal molar feed rates of CO_2 and carbon (char). This zone is assumed to be adiabatic, yielding a change in temperature of about 24°K per 1% of reaction of carbon. Coupling the temperature change to the kinetics of the Boudouard reaction then yields the conversion of carbon and temperature of the reaction versus time and position (depending on feed rate). The model gives a good first approximation of the gasifier behavior leading the way towards the use of theory for practical predictions.

MODEL FORMULATION

The overall gasifier model consists of two parts; these are a pyrolysis model and a gasification model. The pyrolysis model is used to provide a starting gas composition, flow rate, and temperature for the char gasification zone. To initiate the modelling, the air/fuel or O_2/fuel ratio, feed ultimate and proximate analysis and a methane leakage from the gasifier are specified. The model generates pyrolysis gas composition and temperature along with carbon conversion gas composition and temperature along the char bed length.

Pyrolysis Model

Biomass is assumed to be artificially composed of fixed carbon (char) and volatile matter. Upon pyrolysis, for biomass under downdraft gasifier conditions, the char yield is assumed to be equal to that from the proximate yield. The char is treated as pure carbon. With the specification of an air or O_2/fuel ratio and feed composition, an adiabatic reaction calculation around the pyrolysis zone will yield temperature, gas composition and flow rate. It is further assumed that any methane escaping pyrolysis is not cracked in the char bed. Therefore, the mass and energy balance around the pyrolysis zone allows for the methane leakage specified as a model input.

In order to calculate the adiabatic flame temperature of the pyrolysis gas, when it is oxidized by the air or oxygen, first the energy released by the combustion is determined.

$$\Delta H_{298} = HHV - \Delta H_{combustion}$$

where ΔH_{298} is the energy released from the pyrolysis and partial combustion assuming N_2, CO, CO_2, H_2, H_2O, CH_4, and char are the only products, HHV is the high heating value of the biomass (calculated by the ITG method), and $\Delta H_{combustion}$ is the sum of the moles of the products of pyrolysis times their heats of combustion. In the model predictions presented below, a typical biomass composition of 51 percent carbon, 6 percent hydrogen and 43 percent oxygen by weight was assumed for the material balance calculation.

The adiabatic flame temperature can then be determined by the following equation

$$\int_{T_{298}}^{T_{flame}} \Sigma m_i Cp_i = \Delta H_{298}$$

In this model an integral average value of C_{Pi} for each of the gas constituents is utilized. The calculated adiabatic flame temperature is then used to determine the correct K_p and gas composition in a second iteration. Since the flame temperature varies little with changes in K_p, only two iterations are necessary for accurate gas composition and adiabatic flame temperature predictions. Specifying the amount of fixed carbon yielded from the biomass and the oxygen to fuel ratio gives a unique gas composition and temperature.

Char Gasification Model

The char gasification model described below assumes that the char gasification zone is adiabatic and, as in the pyrolysis zone, the water gas shift reaction is at equilibrium. Char gasification kinetics are employed to compute the conversion/length profile. Heat balances on the gas and solid are used to determine temperature profiles. Material balances written for gas and char in the reactor assume plug flow; however, the gas and char move at different rates down the reactor. The fractional conversion of the char, X, is defined as follows:

$$X = (\dot{m}_c(0) - \dot{m}_c(z))/\dot{m}_c(0)$$

where $\dot{m}_c(0)$ = molar flow rate of carbon at top of gasification zone, and $\dot{m}_c(z)$ = molar flow rate of carbon at position "z" in the gasification zone. The carbon mass balance is then:

$$\dot{m}_c(0)dX/dz = r_c S$$

where X is the fractional conversion of the char, z is the distance down the reactor, r_c is the rate of conversion of in moles char/min, S is the cross sectional area of the reactor, and $\dot{m}_c(0)$ is the char feed rate in moles char/min. The rate is computed from kinetic data.

For the Boudouard reaction:

$$-r_c = (k_1 \cdot PCO_2)/(1 + k_2 \cdot PCO)$$

$$k_1 = \exp(-E_1/RT + 12.3091)$$

$$k_2 = \exp(-E_2/RT - 28.4295)$$

where r_c is in units of 1/min, E_1 = 43870 - 19811/T_p (pretreatment) cal/mol, E_2 = -67,300 cal/mol and PCO and PCO_2 are partial pressures of CO and CO_2 respectively. The pretreatment temperature is the temperature at which the biomass is pyrolyzed. In this model it is assumed to be 1000K. For the purpose of this model, the bed voidage and particle size are assumed constant. Shift kinetics are assumed to be rapid. Thus, the gas composition is brought to a water gas shift equilibrium at each position in the reactor. To account for kinetics the equilibrium constant is displaced from the gas temperature by 50°C.

The energy balance includes individual equations for the char, and one for the gas phase. In the gas phase:

$$\Sigma m_g cp_g \frac{dT_g}{dz} = h \cdot A_p (T_s - T_g) \rho (1-\epsilon) S$$

where m_g is the mass flow rate of the gas, cp_g is the heat capacity of the gas, T_g is the gas temperature, h is the heat transfer coefficient between the gas and the char, A_p is the surface area per gram char, T_s is the char temperature. ρ is the char density and ϵ is the void fraction in the bed.

For the solid phase

$$\Sigma m_s cp_s \frac{dT_s}{dz} = - \Sigma m_g cp_g \frac{dT_g}{dz} - \left(\dot{m}_c(0) \cdot \frac{dX}{dz} \cdot \Delta H_B + \dot{m}_{H_2O}(0) \frac{dY}{dz} \cdot \Delta H_{WGS}\right)$$

where X is the conversion of char, H_B is the heat of reaction for the Boudouard, Y is the conversion of steam to hydrogen, and H_{WGS} is the heat of reaction for the water gas shift reaction. The mass and energy balances are coupled and solved using a Runge Kutta integration routine in an interactive mode.

The model results are very dependent on initial conditions, including the input from the pyrolysis model calculations of temperature and composition of the gas. The average temperature of the solid is not known exactly but is assumed to be somewhere between the flame temperature and the pyrolysis front temperature. The solid temperature is not critical, since the heat transfer coefficient is large and the heat capacity of the solid phase is small relative to the gas phase.

The heat transfer coefficient in the energy balance has been calculated by an empirical correlation of Satterfield (4) for fixed bed reactors. The model needs the area to volume ratio of the feedstock to calculate the heat transfer coefficient, h, and the particle area to weight ratio, A_p.

EXPERIMENTAL DATA

To compare the prediction of the model with experimental gasifier results, a quartz tube gasifier 54 mm outer diameter, shown in Fig. 2, was employed. A type K 1/16-in. thermocouple was used for temperature measurement through the pyrolysis and gasification zones. A 1/16-in. 304 SS tube was placed directly alongside the thermocouple, through which gas samples were pulled. A 10 cc syringe (+ needle) was used to evacuate the tube and to take the sample. Gas analysis was done with a Carle #111H gas chromatograph, with a hydrogen transfer tube and a ten ft Carbosieve column. Integration of analysis was performed with a Varian # CDS111 integrator.

Two samples were taken for each level measured. Once a steady state conditon in the gasifier was achieved, the probes were inserted to the specified level and the gas sampling temperature recording procedure begun. The probes were then moved at 2 cm intervals up through the bed until the temperature read below gasification pyrolysis temperatures (100°C). The time interval in between each sample was approximately 1 minute.

RESULTS

Table 1 presents results of the pyrolysis material and energy balance model. The adiabatic flame temperatures of the pyrolysis products, assuming fractions of fixed carbon from 0.05 to 0.20 when burned with various ratios of O_2/fuel has been calculated. The model also yields the gas composition at the end of pyrolysis for each fixed carbon and O_2/fuel ratio. The gas temperature and composition is then input into the gasification model. For predictions of the laboratory data, the fixed carbon is assumed to be 15% and the O_2/fuel ratio is set at 0.45. For the oxygen runs the O_2/fuel ratio is assumed to be 0.40. The results presented yield varying char loss through the grate. An alternate calculation is to iterate on the air/fuel ratio to consume a specified amount of fixed carbon.

Table 1. Pyrolysis Model Calculations

Feed Gas	O_2/Fuel	Fraction Fixed Carbon	Adiabatic Flame Temperature (K)
Air	0.4	0.05	575
(O_2)			(888)
		0.10	764
			(1182)
		0.15	955
			(1475)
		0.20	1146
			(1765)
	0.45	0.05	745
			(1201)
		0.10	924
			(1490)
		0.15	1104
			(1775)
		0.20	1282
			(2055)
	0.50	0.05	897
			(1504)
		0.10	1067
			(1785)
		0.15	1236
			(2061)
		0.20	1403
			(2330)

Figure 3 shows the model predictions of the char and gas phase temperature profiles through the gasifiction zone for air gasification. The solid phase is represented by the solid line, the gaseous phase is represented by the dotted line and the experimental data are represented by stars. Excellent agreement with the data is observed throughout the char gasification zone, with the exception of the data point at the grate. This discrepancy is caused by heat loss (conduction and radiation) at the grate, resulting in lower temperature measurements than expected. In a reactor with a layer of ceramic balls above the grate it would be expected that heat loss would not be important.

Figure 4 shows predictions and experimental data of the CO/CO_2 ratio down the reactor. The agreement between model predictions and experimental data is good

confirmation of the model. Since no adjustable parameters were input into the model to make the temperature profile and CO/CO_2 ratio predictions, the model appears successful at simulating laboratory conditions.

The effect of varying throughput on char conversion is shown in Fig. 5. In this figure, the result of inputting into the model ten times normal, normal, and one tenth normal air thorughput is illustrated. Quantitatively, after the solid and gas have come to the same temperature, the conversion of char for a given distance is linearly dependent on the throughtput. Although an increase in throughput increases the heat transfer from the gas to the solid, the net effect on char conversion, as yielded by model calculations, is the same char conversion for equivalent residence times, regardless of throughput. Increasing the surface area/volume ratio for the feedstock also increases heat transfer from gas to char, but again no significant difference in conversion occurs for various ratios, after the gas and solid temperatures approach the same point.

Figure 5 also shows the char conversion for a throughput consisting of oxygen instead of air. An interesting outcome from using oxygen in the model calculations is that the temperature of the char only rises about 50K above the peak temperature of the air gasification case, as depicted in Fig. 6. This is in spite of the initial gas temperature of the oxygen run of 1750K, compared to 1400K for the air case. Similar results have been observed in the laboratory for the oxygen gasifier. The reason for this phenomenon is the buffering effect of the endothermic gasification reactions which increase their rates at higher temperatures, thus converting greater amounts of sensible heat to chemical energy. The end result then is not higher temperatures in the reactor but higher conversion of the char in the gasification zone.

CONCLUSIONS

(1) A pyrolysis model has been developed which yields gas temperature and composition for both air and oxygen gasification. The results of this model are then input into a separate char gasification model.

(2) A char gasification model has been developed which utilizes no adjustable parameters to predict design parameters and gasifier process conditons.

(3) The two models yield realistic temperature profiles of the solid and gas phases down the reactor. Predictions compare very well with laboratory data.

(4) The CO/CO_2 ratio predicted agree well with laboratory data.

(5) The model shows an essentially linear correlation between throughput and char conversion for a given reactor length.

(6) The model predicts equivalent conversions of char for various surface to volume ratios of the same feedstock.

(7) The model demonstrates the buffering effect of the endothermic gasification reactions in keeping down the char temerpature in an oxygen gasifier.

RECOMMENDATIONS

(1) A model should be incorporated to give the residence time and integral average temperature of the char after pyrolysis. This addition would allow determinations of the appropriate reactor length for complete gasification, and remove the estimation of initial particle temperature in the char gasification zone.

(2) Experimental data shold be taken with various gasifier conditions and designs to check model predictions and assumptions.

ACKNOWLEDGEMENTS

Support for this project from the Office of Alcohol fuels of the United States Department of Energy is gratefully acknowledged. Review of this paper by J. Diebold and T. Milne is sincerely appreciated.

REFERENCES

1. Reed, T.B., M. Markson, "A Predictive Model for Stratified Downdraft Gasification of Biomass," Proceedings of the 14th Biomass Thermochemical conversion contractors Meeting. Atlanta, GA, 1982.

2. Walawender, Walter P., S. M. Chern and L. T. Fan, "Wood Chip Gasification in a Commercial Downdraft Gasifier," Presented at the International Conference on Fundamentals of Thermochemical Biomass Conversion. Estes Park, CO, 18-22 October 1982.

3. Edrich, R., T. Bradley, and M. S. Graboski, "The Gasification Kinetics of Ponderosa Pine Charcoal," Presented at the International Conference on Fundamentals of Thermochemical Biomass Conversion. Estes Park, CO, 18-22 October 1982.

4. Satterfield, C. N. Mass Transfer in Heterogeneous Catalysis. MA: MIT Press, 1970.

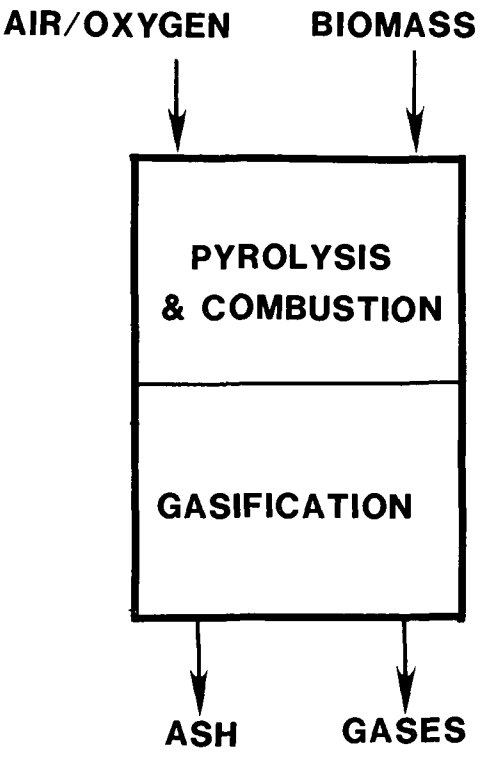

Figure 1. Stratified Downdraft Gasifier.

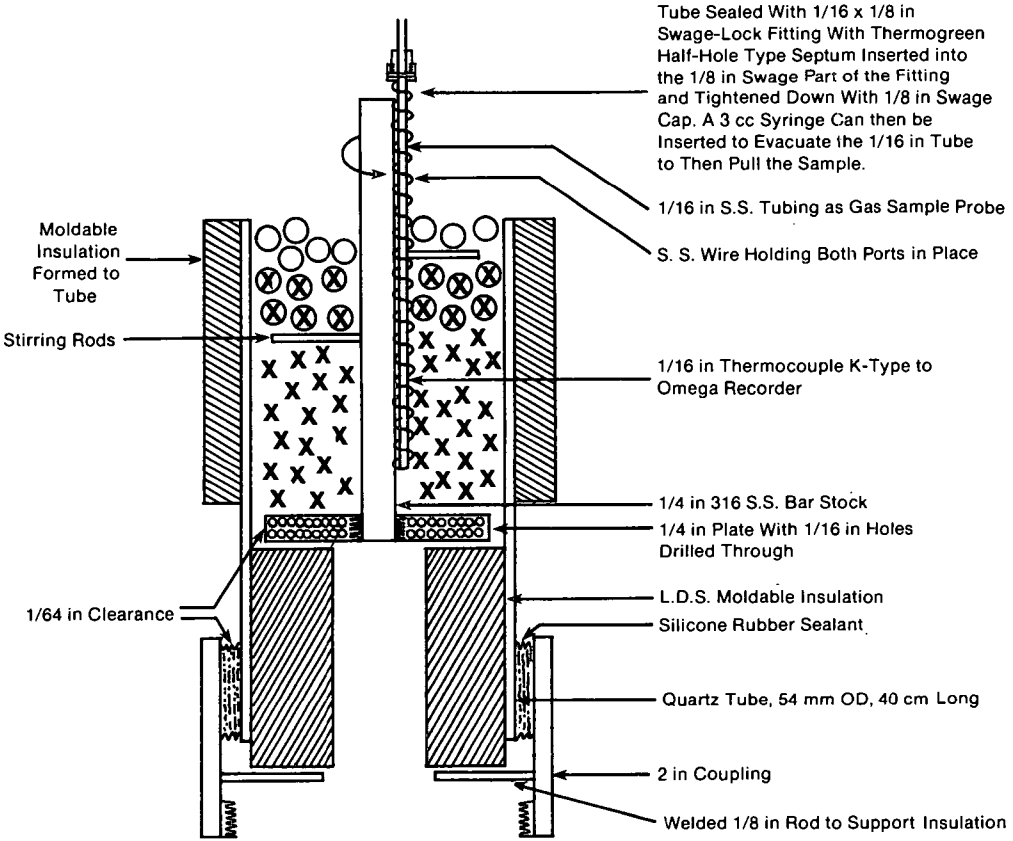

Figure 2. Quartz Tube Gasifier and Measurement Apparatus.

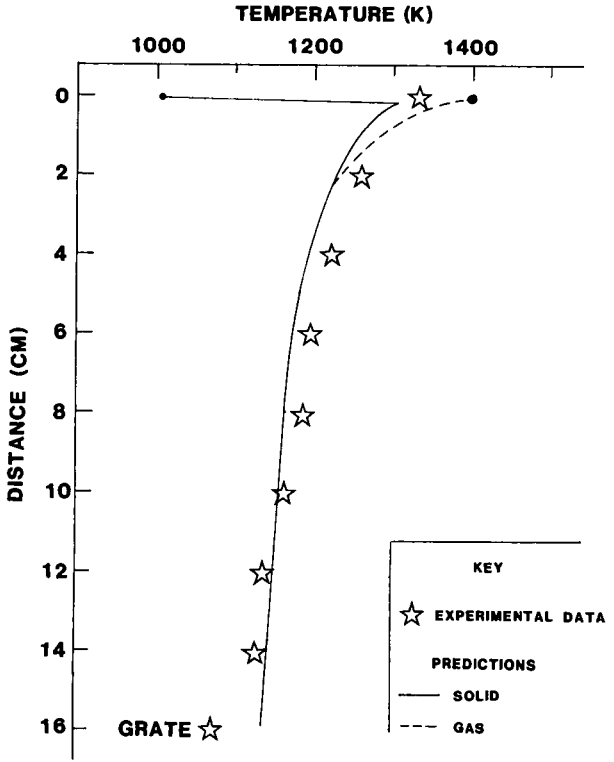

Figure 3. Char Gasification Zone Solid and Gas Temperature Predictions and Experimental Data for Air Gasifier with 1/4-in. Wood Chips.

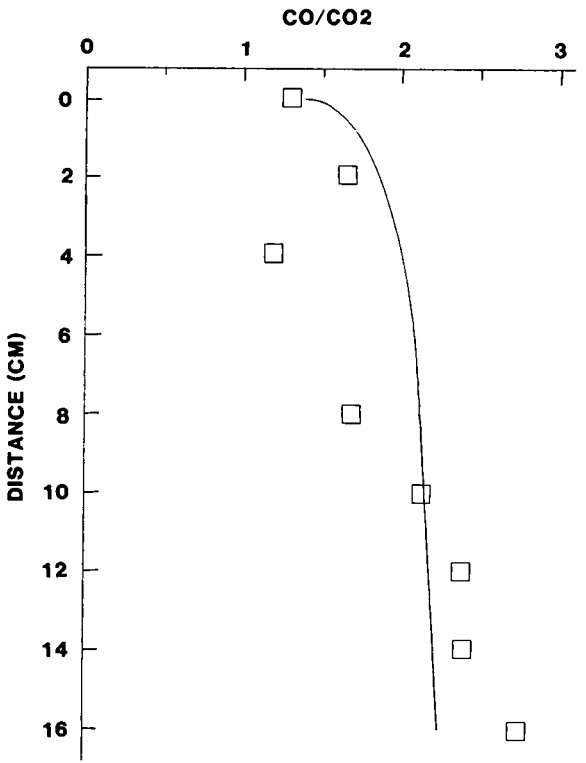

Figure 4. Char Gasification Zone CO/CO_2 Prediction and Experimental Data for Air Gasifier with 1/4-in. Wood Chips.

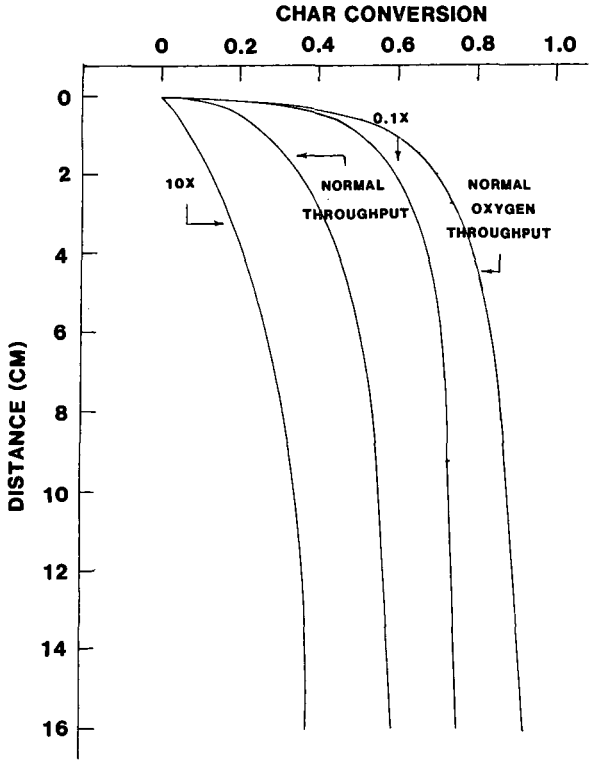

Figure 5. Char Gasification Zone Fractional Char Conversion for Various Air and Oxygen Throughputs.

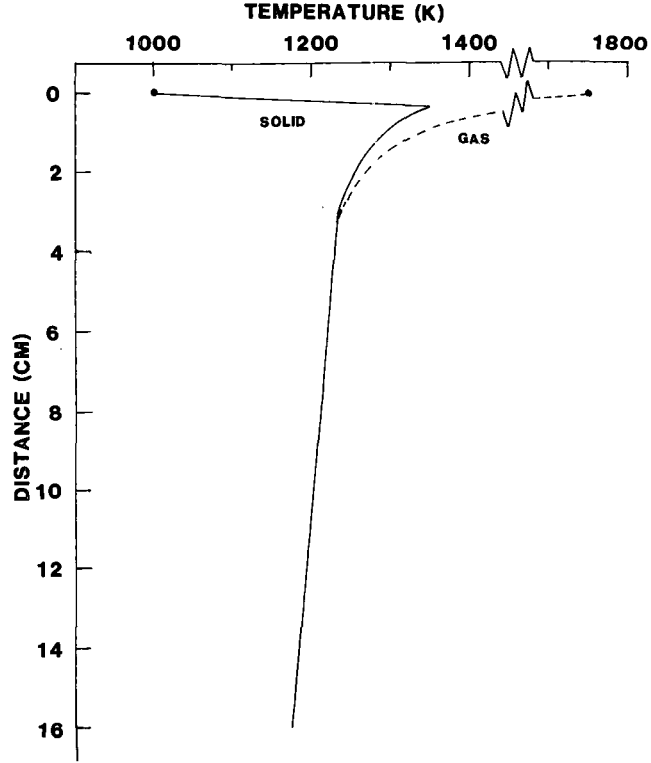

Figure 6. Char Gasification Zone Solid and Gas Temperature Predictions for Oxygen Gasifier with 1/4-in. Wood Chips.